

The Role of the Deleted in Liver Cancer Protein Family in Breast Epithelial Cell Transformation

Von der Fakultät Energie-, Verfahrens- und Biotechnik der Universität Stuttgart zur Erlangung der Würde eines Doktors der Naturwissenschaften (Dr. rer. nat.) genehmigte Abhandlung

Vorgelegt von:

Gerlinde Holeiter

aus Sathmar

Hauptberichter: Prof. Dr. Klaus Pfizenmaier
Mitberichter: Prof. Dr. Roland Kontermann
Tag der mündlichen Prüfung: 26. Juni 2009

Institut für Zellbiologie und Immunologie
Universität Stuttgart
2009

Table of contents

ABBREVIATIONS	5
SUMMARY	9
ZUSAMMENFASSUNG	10
1 INTRODUCTION	11
1.1 Tumorigenesis	11
1.2 Cell migration	11
1.3 Rho GTPases	13
1.4 The large RhoGAP family of proteins	15
1.5 The deleted in liver cancer (DLC) proteins	16
1.5.1 DLC proteins are multidomain proteins	17
1.5.2 Isoforms of the DLC family members	19
1.5.3 Subcellular localization of DLC proteins	21
1.5.4 Exogenous expression of DLC proteins	22
2 MATERIALS AND METHODS	23
2.1 Materials	23
2.1.1 Chemicals and solvents	23
2.1.2 Reagents	24
2.1.3 Transfection reagents	24
2.1.4 Protein inhibitors	24
2.1.5 Protein and DNA standards	25
2.1.6 Buffers and solutions	25
2.1.7 Cell culture reagents and media	26
2.1.8 Kits	26
2.1.9 Plasmids and vectors	27
2.1.10 Primers	28
2.1.11 Short interfering RNAs (siRNAs)	28
2.1.12 Antibodies	29
2.1.13 Bacterial strain	30
2.1.14 Human cell lines	30
2.1.15 Equipment	31
2.1.16 Consumables	31
2.2 Methods	33
2.2.1 DNA cloning	33
2.2.2 Cell culture	34
2.2.3 Preparation of collagen-coated glass coverslips	34
2.2.4 Transient transfection of HEK293T cells using TransIt® 293	34
2.2.5 Transient transfection of MCF7 cells using Lipofectamine™ 2000	34
2.2.6 Transient transfection of breast cancer cell lines using Oligofectamine™	35
2.2.7 RNA isolation	35

2.2.8	Complementary DNA (cDNA) synthesis.....	36
2.2.9	Semi-quantitative RT-PCR	36
2.2.10	Generation of antibodies against human DLC2 and human DLC3	37
2.2.11	Protein extraction for immunoblotting	37
2.2.12	Quantification of protein amounts in RiPA lysates	37
2.2.13	SDS polyacrylamide gel electrophoresis (SDS-PAGE)	37
2.2.14	Western blotting	38
2.2.15	Rho binding domain (RBD) pull-downs	38
2.2.16	RhoA and Cdc42 biosensor assays (Raichu assays).....	38
2.2.17	Luciferase reporter assays	39
2.2.18	Transwell cell migration assays	39
2.2.19	Wound-healing assays.....	40
2.2.20	Invasion assays.....	40
2.2.21	G-LISA Rho GTPase activation assays.....	40
2.2.22	Cell cycle analysis.....	41
2.2.23	Immunofluorescence microscopy.....	41
3	RESULTS.....	42
3.1	Chapter 1	42
3.1.1	DLC1 and DLC2 inhibit Rho signaling in intact cells	42
3.1.2	Selective and efficient silencing of DLC1 and DLC2.....	44
3.1.3	DLC1 and DLC2 knock-down increases cellular RhoA-GTP levels	45
3.1.4	DLC1 depletion enhances stress fiber formation and focal adhesion assembly.....	46
3.1.5	Subcellular distribution of DLC1 and DLC2 in MCF7 cells	47
3.1.6	Down-regulation of DLC1 enhances cell migration	48
3.1.7	DLC1 knock-down cells does not increase the invasive behavior of breast cancer cells.....	52
3.1.8	DLC1 controls cell migration by modulation of Dial1 signaling.....	53
3.2	Chapter 2	57
3.2.1	Exogenously expressed DLC3 shows GAP activity for RhoA	57
3.2.2	DLC3 is located in focal adhesions and disrupts actin stress fibers	58
3.2.3	DLC3 expression in breast cancer cell lines	60
3.2.4	Efficient and specific silencing of DLC3	61
3.2.5	DLC3 depletion increases chemotactic migration but not migration in wounding assays	61
3.2.6	DLC3 knock-down does not stimulate random migration	63
3.2.7	DLC3 down-regulation does not increase cell invasion.....	64
3.2.8	DLC3 knock-down attenuates RhoA activity	65
3.2.9	DLC3 depletion impacts on cell morphology	67
4	DISCUSSION	68
4.1	Investigating DLC1 and DLC3 functions by RNA interference	68
4.2	Investigating DLC2 functions by RNA interference.....	74
4.3	Conclusions and future directions.....	76
5	REFERENCE LIST.....	78
6	ACKNOWLEDGEMENTS	87

Abbreviations

Abbreviations

°C	degree celsius
aa	amino acids
APS	ammonium persulfate
BCC	breast cancer cell
BME	basement membrane extract
BSA	bovine serum albumin
Cas	Crk-associated substrate
Cdc42	cell division cycle 42 protein
cDNA	complementary DNA
CERT	ceramide transfer (protein)
CFP	cyan fluorescent protein
CHO	chinese hamster ovary (cells)
c-Src	cellular homologue of the transforming gene of <i>Rous sarcoma virus</i> (v-Src)
CTEN	C-terminal tensin like (protein)
ddH ₂ O	bidistilled water
Dia1	mammalian ortholog of <i>Drosophila melanogaster</i> diaphanous protein 1
DLC	deleted in liver cancer
DLC1	deleted in liver cancer protein 1
DLC1	deleted in liver cancer protein 1
DLC2	deleted in liver cancer protein 2
DLC3	deleted in liver cancer protein 3
DMEM	Dulbecco's Modified Eagle Medium
DMSO	dimethyl sulfoxide
DNA	deoxyribonucleic acid
dNTP	deoxynucleotide triphosphate
DTT	dithiothreitol
ECL	enhanced chemiluminescence
EDTA	ethylene diamine tetraacetic acid
EF1A1	elongation factor 1A1
EGFP	enhanced green fluorescent protein
EtBr	ethidium bromide
FA	focal adhesion
FACS	fluorescence activated cell sorting
FAK	focal adhesion kinase
FAT	focal adhesion targeting (region)
FCS	fetal calf serum
FRET	fluorescence resonance energy transfer
g	gram
g	gravity, 9.81 m/s ²
G1 (phase)	gap 1 (phase)
G2/M (phase)	gap 2 (phase) / mitosis (phase)
GAP	GTPase-activating protein
GAPDH	glyceraldehyde-3-phosphate dehydrogenase

Abbreviations

GDI	guanine nucleotide-dissociation inhibitor
GDP	guanosine diphosphate
GEF	guanine nucleotide exchange factor
GFP	green fluorescent protein
G-LISA	enzyme-linked immunosorbent assay for GTPases
GST	glutathione-S-transferase
GTP	guanosine triphosphate
h	hour
HCC	hepatocellular carcinoma
HEK	human embryonic kidney (cells)
HMG-CoA	HMG coenzyme A
HMG	hydroxymethylglutaryl
HRP	horseradish peroxidase
IgG	immunoglobulin G
IPTG	sopropyl-beta-D-thiogalactopyranoside
Kd	saturation affinity constant
kDa	kilo Dalton
l	liter
LacZ	beta-galactosidase gene in <i>E. coli</i>
LIM	an acronym of the three gene products Lin-11, Isl-1 and Mec-3
LOH	loss of heterozygosity
M	molar; mol/l
mA	milliampere
mAb	monoclonal antibody
mRNA	messenger RNA
MALDI-TOF	MALDI - Time Of Flight (mass spectrometry)
MALDI	Matrix Assisted Laser Desorption/Ionisation
MEF	mouse embryonic fibroblast
mg	milligram
min	minute
ml	milliliter
MLC	myosine light chain
mM	millimolar
MMP	matrix metalloprotease
M-MuLV	Moloney Murine Leukemia Virus
mRNA	messenger RNA
MT	microtubule
MTT	methylthiazolyldiphenyl-tetrazolium bromide
NADPH	nicotinamide adenine dinucleotide phosphate
NLS	nuclear localization sequence
ns	not significant
ORF	open reading frame
pAb	polyclonal antibody
PAGE	polyacrylamide gel electrophoresis
PBS	phosphate buffered saline
PBS-T	PBS with Tween-20
PC	polycarbonate

Abbreviations

PCR	polymerase chain reaction
PFA	paraformaldehyde
PGP	phosphatidyl-glycerol-phosphate
pH	potential of hydrogen
PH	pleckstrin homology (domain)
PI	propidium iodide
PIP ₂	phosphatidylinositol 4,5-bisphosphate
PKD	protein kinase D
PKN	protein kinase N
PLC-delta1	phospholipase C-delta 1
PMSF	phenylmethylsulfonyl fluoride
PTB	phosphotyrosine-binding (domain)
PTEN	phosphatase and tensin homologue
PVDF	polyvinylidene difluoride
Rac1	Ras-related C3 botulinum toxin substrate 1 ; a Rho GTPase protein
Ras	abbreviation that originated from rat sarcoma; a GTPase protein
RBD	Rho binding domain
Rho	Ras homology protein
Rho proteins	Rho GTPase proteins (e.g. RhoA, Rac1 and Cdc42)
RhoA	Ras homology protein A
RhoB	Ras homology protein B
RhoC	Ras homology protein C
RhoGAP	GTPase-activating protein for Rho proteins
RiPA	radioimmunoprecipitation assay (buffer)
RNA	ribonucleic acid
RNAi	RNA interference
RNase	ribonuclease
ROCK	Rho-associated coiled-coil kinase; Rho kinase
rpm	rotations per minute
RPMI	medium named after Roswell Park Memorial Institute
RT	room temperature
RU	relative (fluorescent) unit
S phase	synthesis phase
SAM	sterile alpha motif
SDS	sodium dodecyl sulfate
sec	second
SEM	standard error of the mean
Ser	serine
SF	stress fiber
SH2	Src homology 2 domain
SH3	Src homology 3 domain
shRNA	short hairpin RNA
siRNA	short interfering RNA
SRF	serum response factor
StAR	steroidogenic acute regulatory (protein)
START	StAR-related lipid transfer (domain)
TAE	tris-acetate-EDTA

Abbreviations

TEMED	N,N,N',N'-tetramethylethyl-diamine
Temp.	temperature
TK	thymidine kinase
Tris	tris-hydroxymethyl-amino-methane
Tyr	tyrosine
UTR	untranslated region
UV	ultra violet
VEGF	vascular endothelial growth factor
v/v	volume per volume
w/v	weight per volume
YFP	yellow fluorescent protein
µg	microgram
µl	microliter
µm	micrometer
µM	micromolar
DLC1-3	DLC1 and DLC2 and DLC3
2D	two dimensional
3D	three dimensional

Summary

Three genes of the human genome encode for a subfamily of Rho GTPase-activating proteins (RhoGAPs) termed 'deleted in liver cancer' (DLC) proteins. Rho GTPases participate in a complex set of intracellular signaling pathways including the regulation of cytoskeleton dynamics and cell motility. Since RhoGAPs accelerate the transfer of active GTP-bound Rho proteins to the inactive state, they are able to attenuate signal transduction activities of Rho GTPases. *In vitro* the DLC proteins show GAP activity towards the Rho proteins RhoA and Cdc42 but not for Rac1. DLC proteins have furthermore been identified as binding partners for tensin proteins and localize to focal adhesions. As the name implicates, loss of DLC protein expression has been first observed in hepatocellular carcinomas. Meanwhile, their down-regulation has also been found in a variety of other human cancers, indicating a possible role for the three DLC family members as tumor suppressors. Studies with overexpressed DLC1-3 suggest that they share common cellular functions. Ectopic expression of DLC1, for example, has been shown to inhibit cell migration, proliferation, anchorage independent growth and even metastasis. However, whether the loss of DLC family members is the cause of aberrant Rho signaling in transformed cells has not been investigated. To elucidate the functions of endogenous DLC proteins we silenced DLC1-3 expression in breast cancer cell lines using a RNA interference (RNAi) approach and compared the cellular alterations. We demonstrate that the loss of each DLC family member leads to a distinct cellular phenotype. For instance, knockdown of DLC1 and DLC3 enhanced cell motility in transwell assays, but had a differential impact on random cell migration and RhoA activity. By contrast, DLC2 down-regulation failed to affect cell locomotion, although it led to an enhanced level of active RhoA. Furthermore, we provide data supporting the involvement of DLC1 in the control of directed cell migration through a Dia1- and not Rho kinase (ROCK)-dependent pathway. In summary, we show that despite their overlapping substrate specificity towards RhoA *in vitro*, DLC family members have non-redundant cellular functions. We assume that this is most likely due to their multimodular structures, distinct spatial distributions and interaction with different signaling proteins in intact cells.

Zusammenfassung

Drei Gene des humanen Genoms kodieren für eine Unterklasse der Rho GTPase-aktivierenden Proteine (RhoGAPs), die man als 'deleted in liver cancer' (DLC) Proteine bezeichnet. Rho GTPasen sind an einer Reihe komplexer intrazellulärer Signalwege beteiligt, welche auch die Regulation von Zytoskelettveränderungen und die Zellmigration miteinschließen. Da RhoGAPs die Überführung aktiver GTP-gebundener Rho-Proteine in den inaktiven Zustand vermitteln, können sie die Signalgebung der Rho GTPasen vermindern. DLC-Proteine weisen *in vitro* GAP-Aktivität hinsichtlich der Rho-Proteine RhoA und Cdc42 auf, aber nicht für Rac1. Außerdem sind sie als Bindungspartner für Tensin-Proteine identifiziert worden und in fokalen Adhensionspunkten lokalisiert. Wie der Name impliziert, wurde der DLC-Expressionsverlust zuerst in Leberkarzinomen beobachtet. Mittlerweile wurde ihre reduzierte Expression auch in einer Vielzahl anderer humaner Krebsarten gefunden. Dies deutet auf eine mögliche Rolle der drei DLC-Familienmitglieder als Tumorsuppressoren hin. Studien mit überexprimierten DLC1-3 lassen vermuten, dass sie überlappende zelluläre Funktionen aufweisen. Es wurde gezeigt, dass die Expression von DLC1 die Zellmigration, die Proliferation, das Wachstum unabhängig von Matrixkontakten und selbst die Metastasenbildung unterdrücken kann. Ob allerdings der Verlust der DLC-Familienmitglieder eine veränderte Rho-Signalgebung in transformierten Zellen bewirkt, wurde noch nicht untersucht. Um die Funktionen von endogenen DLC-Proteinen zu untersuchen, haben wir die DLC1-3 Expression in Brustkrebszelllinien mit Hilfe von RNA-Interferenz ausgeschaltet und die zellulären Veränderungen verglichen. Wir konnten zeigen, dass der Verlust der einzelnen DLC-Familienmitglieder zu unterschiedlichen zellulären Phänotypen führt. So erhöhte sowohl der Verlust von DLC1 als auch von DLC3 die Zellmigration in Transwell Assays, allerdings ließen sich im Falle von ungerichteter Zellmigration und RhoA-Aktivität Unterschiede feststellen. Dem gegenüber steht DLC2, dessen Expressionsverlust nicht die Zellmigration beeinflusste, obwohl eine erhöhte RhoA-Aktivität zu beobachten war. Außerdem beweisen wir durch unsere Daten, dass DLC1 durch einen Dia1-abhängigen und ROCK-unabhängigen Signalweg an der gerichteten Zellmigration beteiligt ist. Zusammenfassend kann man sagen, dass DLC-Familienmitglieder, abgesehen von ihrer überlappenden Substratspezifität hinsichtlich RhoA *in vitro*, individuelle zelluläre Funktionen aufweisen. Wir vermuten, dass dies auf ihren mehrmoduligen strukturellen Aufbau, ihre unterschiedliche subzelluläre Lokalisation und die Interaktion mit spezifischen Signalmolekülen zurückzuführen ist.

1 Introduction

1.1 Tumorigenesis

Cancer is a major public health problem in Germany, the United States and many other parts of the world. Although much progress has been made in reducing mortality rates, cancer still accounts for more deaths than heart disease in persons under the age of 85 years. Currently, one in four deaths in the United States is due to cancer (1). In Germany, breast cancer represents with 18% the leading cause of female cancer death (2).

The growth of normal human mammary epithelial cells is tightly controlled. These cells proliferate for a limited life span and finally senesce (3). A critical initial step in tumorigenesis involves the loss of senescence checkpoints and immortalization, which allows a cell to grow indefinitely and to go through further oncogenic stages (4). Cell transformation is a highly complex multi-step process in which genetic and environmental factors together are thought to alter critical cell regulatory pathways (5) and lead to new cellular characteristics. Transformed cells are able to proliferate independently of exogenous growth-promoting or growth-inhibitory signals, penetrate surrounding tissues and metastasize to distant sites, trigger an angiogenic response, and avoid mechanisms that limit cell proliferation, for instance apoptosis. These properties reflect changes in cellular signaling pathways that in normal cells control cell proliferation, survival and motility.

1.2 Cell migration

The basic cell migration machinery of cancer cells is similar to that of normal cells. Cell movement results from a complex interplay of numerous signaling proteins and adaptor molecules. In a simplified view, cell migration represents a persisting cycle of several steps (6) including cell matrix extension at the leading edge as the first event (Figure 1). The formed membrane protrusions trigger recognition of the surrounding extracellular matrix (ECM) and are described to be quite diverse in morphology and dynamics. The most common protrusions observed in migrating cells are filopodia, thin finger-like dynamic cell membrane extensions composed of long parallel actin filament bundles, and lamellipodia, flat broad sheets of membrane and polymerized actin filaments (7). Furthermore, the edge of a lamellipodium can roll back to form small, actin filament-containing and highly dynamic membrane protrusions termed ruffles. The driving force for the formation of cell extensions is mediated by actin polymerization (8). In a second step, growing cell protrusions attach to the adjacent ECM and initiate binding via transmembrane receptors of the integrin family (9).

Introduction

Adaptor proteins couple the actin cytoskeleton to integrins, which then become locally enriched, cluster and develop into an initial small and transient focal complex. When focal complexes grow and stabilize they are thought to form a mature focal contact, also known as focal adhesion (FA) (10). The number and size of focal contacts can vary from cell to cell and in response to different environmental conditions. Focal adhesions contain integrins, signaling molecules such as the focal adhesion kinase (FAK), adaptor proteins like vinculin and paxillin and proteins that are directly coupled to the actin filament. Moreover, FAs serve as insertion places of highly organized parallel bundles of actin filaments termed stress fibers (SFs) which typically display a periodic α -actinin-myosin II pattern (8). Myosin II is the main motor protein in eukaryotic non-muscle cells [reviewed in (11), (12)] and promotes the actomyosin contraction of stress fibers. Finally, shortening of the cell body generates inward tension towards focal contacts and the breakdown of cell-substrate linkages in the back of the cell (13). Focal adhesion disassembly at the cell rear together with the elongation and attachment at the leading edge results in a successive forward gliding of the cell body. Therefore, the speed of migrating cells is limited by the turnover rates of adhesion and de-adhesion events (6).

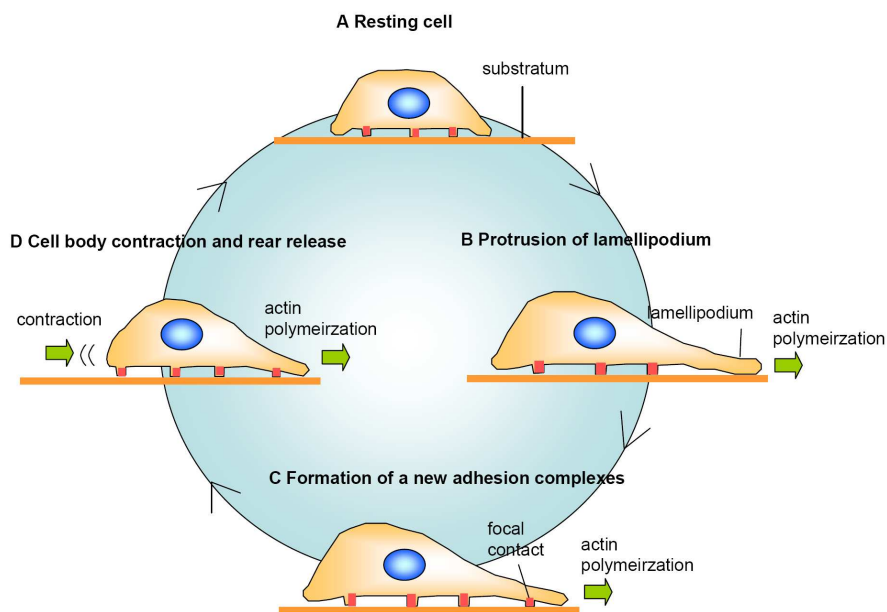


Figure 1: Schematic representation of cell movement. Cell migration displays a multistep cycle: driven by actin polymerization, resting cells (A) start to form membrane protrusions at the leading edge, such as lamellipodia (B). Next, integrin receptors anchor the cellular extensions to the extracellular matrix and form focal adhesions (C). Subsequently, actomyosin-driven contraction of the cell body and disassembly of focal adhesions at the cell rear (D) results in a successive forward gliding of the cell body.

Cell motility involves signaling pathways such as the rearrangement of actin cytoskeleton, focal contact formation and actomyosin-dependent contractility which are regulated by the family members of Rho GTPases [reviewed in (14; 15)].

1.3 Rho GTPases

The small GTPases of the Rho family represent a subgroup of the Ras superfamily and include more than 20 proteins, of which the prototypic members RhoA, Rac1, and Cdc42 have been best characterized. Rho family proteins are targeted to cell membranes by lipid modification (either a geranyl-geranyl or less frequently a farnesyl anchor) at the so-called 'CAAX box'. Rho proteins act as molecular switches that connect changes of the external environment to intracellular signaling pathways. Activation of growth-factor receptors as well as tyrosine kinase receptors, G protein-coupled receptors and integrins are thought to result in Rho GTPase-mediated alterations of cellular processes. For instance, Rho GTPases are critical regulators of the actin cytoskeleton and microtubules (MT) and are involved in cell migration, focal adhesion assembly and disassembly, cell cycle progression, gene expression, tumorigenesis, apoptosis, vesicle trafficking, morphogenesis, neutrophil activation, phagocytosis and activation of the NADPH oxidase [reviewed in (14-16)]. Since Rho GTPases play an important role in such a variety of signaling events they have to be highly regulated. Rho proteins cycle between an active GTP-bound state and an inactive GDP-bound state, a process that is controlled by three sets of regulatory proteins (Figure 2). GEFs (guanine nucleotide exchange factors) promote the exchange of GDP for GTP thereby activating Rho proteins (17). GAPs (GTPase activating proteins) accelerate the intrinsic rate at which Rho hydrolyzes bound GTP to GDP and hence becomes inactivated (18). Additionally, GDIs (guanine nucleotide-dissociation inhibitors) have been described to keep Rho in its GDP-bound state and allow the cycle between cytosol and membranes (19). Exclusively in their active state Rho GTPases are able to interact with a large number of effector proteins such as kinases and scaffold proteins, which control cellular functions by phosphorylation of targets and through protein-protein interactions, respectively (20).

To regulate the actin cytoskeleton RhoA interacts with two major downstream effector proteins, the serine/threonine kinase ROCK (Rho-associated coiled-coil forming kinase; Rho kinase) and the formin molecule mDia1 (mammalian ortholog of *Drosophila* diaphanous; also termed Dia1) (20). It is assumed that ROCK and Dia1 cooperate with their actions on actin and myosin to induce actomyosin bundles, also known as stress fibers. For instance, Dia1 is described to mediate actin filament assembly by nucleation and polymerization (21) and

Introduction

ROCK mediates cross-linking of myosin by two different mechanisms. On the one hand, ROCK phosphorylates and inactivates the myosin phosphatase which leads to an increased myosin light chain (MLC) phosphorylation, and on the other hand ROCK can even directly phosphorylate myosin light chain (22). MLC phosphorylation leads to cross-linking of actin by myosin and enhanced actomyosin contractility. Furthermore, ROCK is found to stabilize existing actin filaments by phosphorylation and activation of the LIM-kinase, which in turn phosphorylates and inactivates the actin-depolymerizing factor cofilin (23). Of note, opposing actions of Dia1 and ROCK were also reported. Dia1 is potentially linked to Rac activation and membrane ruffle formation through c-Src-induced phosphorylation of focal adhesion proteins (24; 25). ROCK antagonizes this Dia1 action (24). Furthermore, Dia1 facilitates and ROCK disrupts cell-cell adhesion in epithelial cells (26). Thus, the balance between the two pathways appears to determine cell morphology, adhesion, and motility.

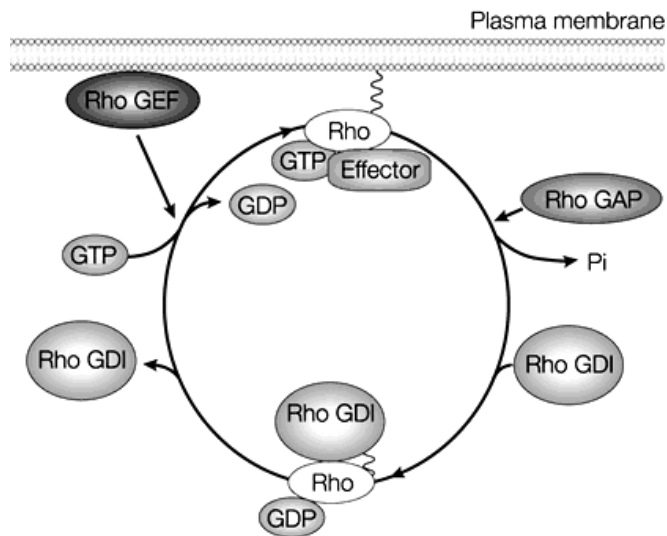


Figure 2: Rho GTPases are highly regulated molecular switches. Rho family proteins shuttle between the active GTP-bound and the inactive GDP-bound state. Activation is supported by guanine nucleotide exchange factors (GEFs) which promote exchange of GDP for GTP. GTPase activating proteins (GAPs) promote the hydrolysis of GTP to GDP, while guanine nucleotide dissociation inhibitors (GDIs) prevent nucleotide exchange and preclude Rho from membranes. Activated GTP-bound Rho proteins bind to effectors which mediate downstream signaling pathways. The figure was taken from: *Nature Reviews Molecular Cell Biology* 2; 887-897 (2001) [see referece (27)]

Rho proteins are involved in the regulation of proliferation, motility and apoptosis; cellular events that are typically altered during oncogenesis. Furthermore, analyses of both the RNA and protein level have correlated their increased expression with tumor progression (28; 29). Along with this observation, studies with constitutive active mutants of Rho proteins showed that they appear to act downstream of oncogenic Ras molecules (30). *In vivo* studies using recombinant mice lacking or overexpressing Rho signaling proteins have confirmed the involvement of Rho GTPases in cancer (31; 32). In the last few years, especially RhoC has attracted growing interest since its expression correlates with metastasis of several cancer types, including breast cancer (33). In contrast to Ras, the transforming ability of Rho proteins has not been associated with the appearance of activating mutations (34), but rather

due to deregulation of Rho protein activity. Many Rho GEFs (such as Dbl and Ect2) were identified as oncogenes and their overexpression can induce malignant transformation (35). In addition, a few RhoGAPs have been suggested to potentially serve as tumor suppressors, if their loss results in a hyperactivation of Rho proteins and facilitates the growth and metastasis of cancer cells.

1.4 The large RhoGAP family of proteins

The RhoGAP family is defined by the presence of a conserved RhoGAP domain that accelerates the low intrinsic GTPase activity of Rho proteins. So far, more than 70 RhoGAPs have been identified in different species ranging from yeast to human (36). The RhoGAP domain is built up by nine alpha helices and contains a highly conserved arginine residue in a loop structure (37). This positive charged arginine is essential for the GAP activity since it is introduced into the catalytic site of Rho GTPases and stabilizes the proper position of the hydrolytic water molecule. Thus, the freedom of the water molecule is limited and the energy barrier for GTP hydrolysis is reduced (38). Some GAPs display a broad specificity whereas others are specific to a single Rho GTPase. How the substrate specificity of RhoGAPs is achieved in RhoGAP-Rho GTPase pairwise interactions is a still open question. Although the exact molecular mechanisms remain to be resolved, mutagenesis studies have shown that residues outside the catalytic region of Rho GTPases are involved in directing RhoGAP specificity (39).

RhoGAP family members typically contain aside from their GAP domain other functional motifs, including catalytic domains (protein kinase, Rho GEF and Arf GAP domains) as well as protein-protein (SH2 and SH3 domains) and protein-lipid adaptor modules (e.g. PH domain). The most common motifs among RhoGAPs are Src homology domain 3 (SH3) domains that bind proline-containing peptides, and phosphoinositide-binding pleckstrin homology (PH) domains (40). This begs the assumption whether the additional motifs may serve as regulatory modules of RhoGAP activities. Numerous regulatory mechanisms are possible, including lipid binding (α 1-chimaerin), protein-protein interaction (MgcRacGAP, ARAP3), phosphorylation (p190RhoGAP, MgcRasGAP), phosphorylation-mediated subcellular translocation (CdGAP) and proteolytic degradation (p190-A) (40). Another explanation for the several additional domains could be that some GAP domains may simply serve as Rho GTPase interaction modules, and therefore RhoGAP proteins could act as effectors or scaffold proteins mediating cross-talk between Rho GTPases and other signaling pathways. For example, full-length α 1-chimaerin lacks GAP activity but retains the ability to bind GTPases and seems to co-operate with Rac1 and Cdc42 to promote formation of

lamellipodia and filopodia (41). Furthermore, given that Rho GTPases are implicated in a large number of biological responses, each RhoGAP protein may selectively regulate a specific Rho GTPase-mediated biological function and might accelerate reactions other than the stimulation of GTP hydrolysis of Rho proteins (38).

1.5 The deleted in liver cancer (DLC) proteins

Three genes of the human genome encode for a RhoGAP subfamily termed 'deleted in liver cancer' (DLC) proteins. The DLC1-3 genes appear to be paralogues that arose through duplication of chromosomal segments (42). DLC1 is the founding member of this family and was originally identified by Yuan and colleagues (43) as a gene under-represented in human hepatocellular carcinoma (HCC). Orthologues of each of the three DLC family proteins have been identified in other vertebrates and even in invertebrates. For example, p122RhoGAP, the rat ortholog of human DLC1 (93% amino acid sequence identity) was originally identified as an interacting partner of PLC-delta1 (phospholipase C-delta1) and is thought to enhance the hydrolysis of phosphatidylinositol 4,5-bisphosphate (PIP₂) by PLC-delta1 (44). While the DLC mRNAs are widely expressed in human tissues and at various stages of development, they are absent or down-regulated in a significant number of carcinomas, including HCC, breast and colon, and have been shown to act as tumor suppressors (42). Several mechanisms exist which lead to the decreased expression of DLC proteins in human cancers. First, human DLC genes are mapped to regions (DLC1: 8p22; DLC2: 13q13; DLC3: Xq13) which are frequently lost in cancers (43). The DLC1 locus on the short arm of chromosome 8 (8p22) for example is a frequent site of allelic deletions in epithelial tumors and breast tumors (45). The DLC3 locus on chromosome Xq13 is near a site of LOH (loss of heterozygosity) in ovarian cancers, but this region has not been reported to be frequently deleted in other cancer types (46). Nevertheless, reduced DLC3 mRNA levels were observed in a majority of human prostate, kidney, lung, breast, uterine and ovarian cancer tissues (42). Secondly, DLC1-3 expression can be decreased through epigenetic mechanisms. The promoter region of the DLC1 gene is GC-rich with characteristic CpG islands that serve as methylation sites. Promoter hypermethylation is thought to be the principal mechanism responsible for inactivation of the DLC1 gene in a number of solid tumors (47). Furthermore, transcriptional inhibition has been linked with histone hypoacetylation by the recruitment of histone deacetylases to chromatin (48). Since DLC1 expression was increased after treatment with a histone deacetylase inhibitor in several human cancer cell lines, alterations

in histone modifications seems to contribute to the third mechanism which can lead to repressed DLC1 expression (49; 50).

1.5.1 DLC proteins are multidomain proteins

DLC1-3 are structurally related multimodular proteins composed of an N-terminal SAM domain, followed by an unstructured region, a RhoGAP domain and a C-terminal START domain (Figure 3).

The sterile alpha motif (SAM) domain has been described originally as a sequence domain present in a few sexual differentiation proteins in yeast (51) and is a common protein-protein interaction motif found in numerous human signaling proteins. SAM domains are typically arranged in five helices but distinct from this, DLC1 and DLC2 SAM motifs form four-alpha-helical bundles (52; 53). SAM modules have been described to possess diverse binding properties and form homo- and hetero-oligomers with other SAM domain-containing proteins and even bind to non-SAM-containing proteins. By the use of protein precipitation and MALDI-TOF mass spectrometry analyses it has been shown that DLC1 SAM, but not DLC2 SAM, directly interacts with the eukaryotic elongation factor 1A1 (EF1A1) and facilitates its recruitment to the membrane periphery upon growth factor stimulation (54). Some SAM domains even possess the ability to bind RNA [reviewed in (55)] and in case of the DLC2 SAM domain, interaction with a lipid ligand has been discussed (52-54).

Immediately next to the SAM domain a region follows that lacks a secondary structure and shows hardly sequence identity to known conserved protein motifs. This unstructured middle region is an important feature since the open and extended conformation enables the interactions with other proteins as well as the attachment of post-translational modifications such as a phosphate group (56). Multiple serine-threonine kinase phosphorylation sites have been identified in DLC proteins, most of them are located in this middle region [reviewed in (42)]. Protein phosphorylation is thought to serve as a reversible mean to regulate the interaction with other proteins as well as the activity and/or subcellular localization of many signaling proteins. For instance, work from our own lab has shown that DLC1 is phosphorylated by protein kinase D (PKD) at serines 327 and 431 (57). This phosphorylation is important for the interaction with 14-3-3 proteins and was found to prevent DLC1-mediated stimulation of Rho-GTP hydrolysis (57). 14-3-3 proteins are adaptor proteins which are described to form homo- and heterodimers and bind to their target proteins in a phosphorylation dependent manner (58; 59). Moreover, the unstructured region of DLC

Introduction

proteins harbors several proline-rich segments that could bind to proline recognition domains, such as the SH3 module that is present in many signaling proteins (60).

The around 200 amino acid long RhoGAP domain of DLC1-3 is the most highly conserved region among the three proteins. GAP domains enhance the low hydrolytic rate of Rho GTPases to convert bound GTP to GDP (38). All DLC proteins contain a conserved arginine residue that is essential for their RhoGAP activity. DLC1-3 were found to have highest GAP activities towards the Rho isoforms (RhoA, RhoB and RhoC), only moderately increase hydrolysis of Cdc42-GTP and have almost no effect on GTPase activity of Rac1 [reviewed in (42)]. Several cellular functions of the DLC proteins have been attributed to the RhoGAP domain. DLC proteins suppress Ras signaling, prevent cellular transformation and inhibit Rho-mediated cytoskeleton remodeling in a GAP-dependent manner [reviewed in (42)].

The START (steroidogenic acute regulatory protein (StAR)-related lipid transfer) domain is described as a protein module that binds lipids (61) and sterols. Fifteen human START domain-containing proteins have been identified (62; 63) which are involved in lipid transfer between intracellular compartments, lipid metabolism and regulation of cell signaling [reviewed in (62; 64)]. START domains form a deep lipid-binding pocket (62) covered by a lid that protects the bound hydrophobic ligand from the external environment. The identity of the bound lipids is known for only a few members of the START family. For instance, CERT (ceramide transfer protein) was shown to mediate the specific exchange of ceramide from donor to acceptor membranes (65) and the StAR (steroidogenic acute regulatory) protein transfers cholesterol from the outer to the inner mitochondrial membrane (66). The cellular functions as well as the ligands of DLC1-3 START domains are not well characterized. In case of DLC2 it has been reported that the START domain is targeted to mitochondria and lipid droplets (67). The functional role of this subcellular localization is not well understood. Probably START domains simply function in lipid sensing rather than in lipid transfer or membrane targeting, since the ligand-binding region lies in a hidden pocket. Further, it remains open whether START domains regulate Rho-GAP activity upon binding with lipids.

Introduction

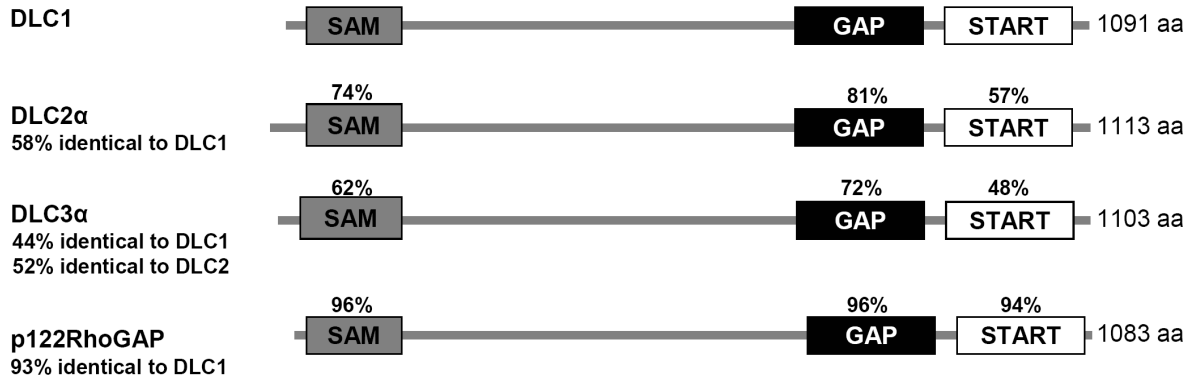


Figure 3: Comparison of the mammalian DLC family proteins. Domain organization of human DLC1, DLC2 alpha, DLC3 alpha and the rat DLC1 ortholog p122RhoGAP. Following regions are indicated: SAM domain, RhoGAP motif and START domain. Numbers above each conserved region indicates the percent identity to the corresponding domain of human DLC1. Amino acid (aa) lengths of the indicated proteins are given at the right and the percent identity of the full-length polypeptides are given beneath the protein name.

1.5.2 Isoforms of the DLC family members

The DLC genes appear to have more than one transcription start site, potentially yielding DLC isoforms with different N-termini (Figure 4-6). However, for most DLC transcription variants the existence has not been verified experimentally. The DLC1 gene potentially yields a larger isoform of 1528 aa, termed KIAA1723 (68). Furthermore, translation initiation at an in-frame downstream AUG codon would yield a DLC1 variant of 1083 aa, termed AK025544 (42).

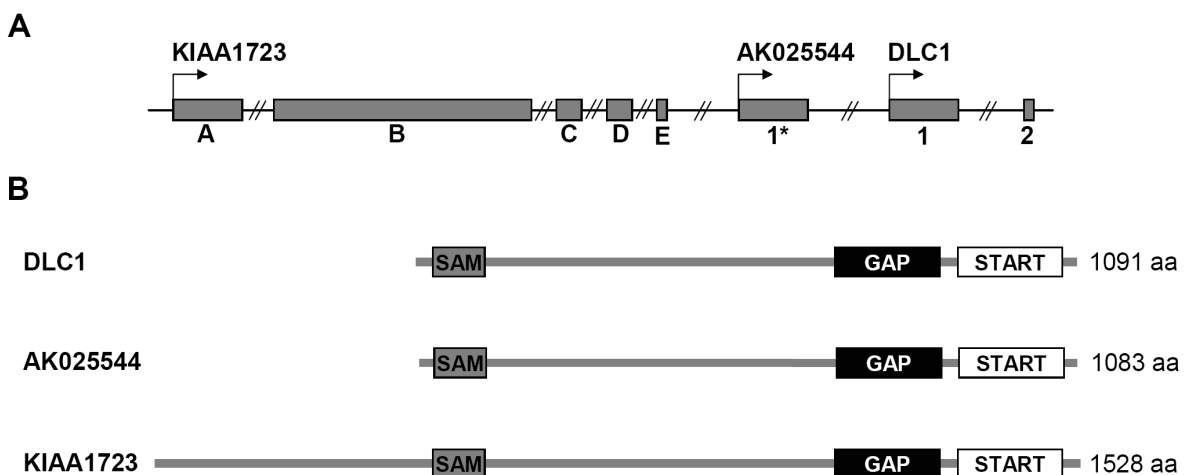


Figure 4: Exon organization of the human DLC1 gene and domain structures of predicted DLC1 variants. (A) Exon structure of the DLC1 gene (5' end) on chromosome 8p22. Boxes represent exons and arrows indicate the potential transcription start sites. (B) Functional domains of the predicted DLC1 isoforms. The SAM domain, RhoGAP motif and START domain are indicated. Amino acid (aa) lengths of the proteins are given at the right.

Introduction

A bioinformatic search performed by Leung and colleagues (69) identified four isoforms of DLC2: alpha, beta, gamma and delta (Figure 5). The DLC2 alpha isoform is the full-length protein of DLC2. The beta isoform differs from DLC2 alpha by only a few amino acids at the N-terminus. DLC2 gamma contains a RhoGAP and a START domain but lacks the N-terminal SAM domain, whereas DLC2 delta contains only the SAM domain.

The heterogeneity at the 5' ends of the DLC3 transcripts (Figure 6) seems to arise by the use of alternative promoters (DLC3 alpha/beta) and exon skipping (DLC3 gamma) (42). The alpha isoform represents the full-length DLC3 protein, whereas DLC3-beta was predicted to encode a 1023-aa protein that lacks the SAM domain. DLC3 gamma appears to use the same transcription start site as DLC3 alpha but lacks exon 3, causing a reading frame shift that would result in premature translation termination after 52 aa. RT-PCR analysis of normal human liver, prostate and mammary gland RNA indicated that DLC3 alpha and beta but not DLC3 gamma are present in these tissues (42). Moreover, the mouse transcripts of DLC3 correspond to the alpha and beta variants (42).

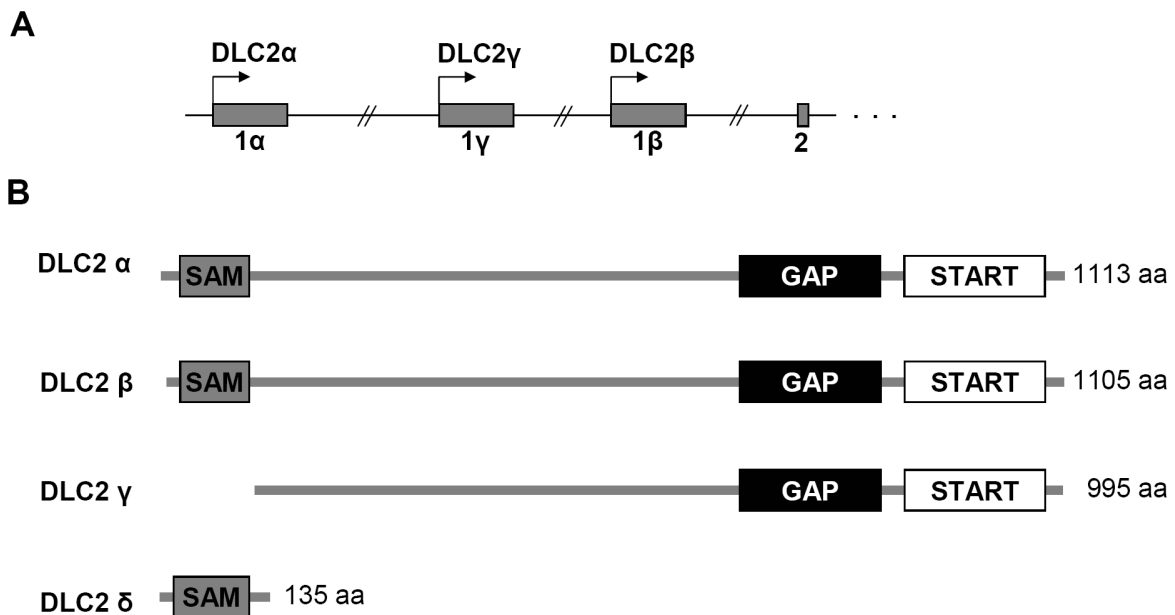


Figure 5: Exon organization of the human DLC2 gene and the domain structures of the predicted DLC2 isoforms. (A) Schematic representation of the DLC2 gene (5' end) on chromosome 13q13. Boxes represent exons and arrows indicate the potential transcription start sites. Exons 2-14 are common among the DLC2 isoforms alpha, beta and gamma. (B) Functional domains of the predicted DLC2 isoforms. The SAM domain, RhoGAP motif and START domain are indicated. Amino acid (aa) lengths of the indicated proteins are given at the right.

Introduction

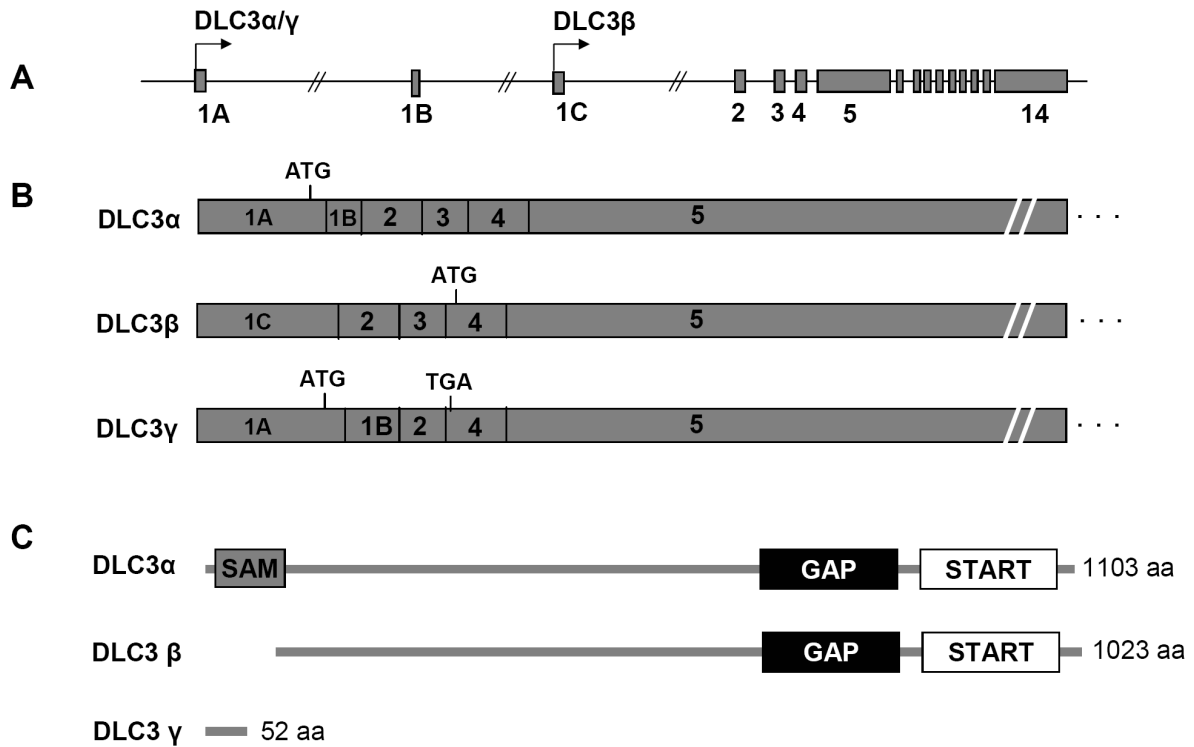


Figure 6: Exon organization of the human DLC3 gene and domain structures of the corresponding DLC3 isoforms. (A) Diagram of the exon structure of the human DLC3 gene on chromosome Xq13. Boxes represent exons, arrows indicate the potential transcription start sites upstream of exons 1A and 1C. (B) Schematic representation of the exon sequences present at the 5' ends of the three DLC3 transcripts. The localization of the putative ATG translation start codons in the three transcripts and the premature TGA stop codon in the DLC3 gamma isoform are marked. (C) Domain organization of the three DLC3 isoforms alpha, beta and gamma. The SAM domain, RhoGAP motif and START domain are indicated and the amino acid (aa) lengths of the proteins are given at the right.

1.5.3 Subcellular localization of DLC proteins

Yeast-two-hybrid screenings and colocalization studies have revealed that in certain cell types (e.g. fibroblasts) DLC1 and DLC3 are present in focal adhesions, due to their interaction with tensin family proteins (70-74). Full-length DLC1 and DLC3 were found to interact with SH2 (Src homology 2) and phosphotyrosine-binding (PTB) domains of the focal adhesion protein tensin1 (for DLC1: in addition CTEN and tensin2). The binding site to the SH2 domain was mapped to the amino acid stretch ⁴⁴⁰SIYD⁴⁴⁵ of DLC1 and ³⁵³STYDNL³⁵⁸ of DLC3, respectively. In the case of DLC1, Tyr442 plays an important role for the interaction, since mutation of this amino acid abolished SH2 domain binding. But unlike most ligands for SH2 domains, phosphorylation of the Tyr residue was not required for interaction. In contrast to DLC1 and DLC3, DLC2 seem to localize to mitochondria. When recombinant DLC2 was expressed in the human hepatoma cell line Huh-7, the protein was found to

colocalize with mitochondrial markers and was further detected in structures that resembled lipid droplets (67). Furthermore, our group identified a novel nuclear localization sequence (NLS) within DLC1, adjacent to the PKD phosphorylation site serine 431 (57). Upon phosphorylation of Ser431 14-3-3 adaptor proteins bind to DLC1, thereby masking the NLS motif, inhibiting nucleocytoplasmic shuttling and leading to DLC1 trapping in the cytoplasm. Thus, 14-3-3 binding provides a regulatory tool for DLC1 activity and compartmentalization.

1.5.4 Exogenous expression of DLC proteins

In order to investigate the cellular functions of DLC proteins several groups re-expressed the family members in a variety of cultured cell lines and analyzed the alterations in morphology and signaling events. For instance, overexpression of DLC proteins resulted in a GAP-dependent disruption of actin stress fibers and focal adhesions leading to a collapse of the cytoskeleton and a rounded morphology (75). A possible molecular mechanism by which DLC proteins interfere with focal adhesion assembly came from a study with DLC1 overexpression in the hepatocellular carcinoma cell line SNU-368. Kim and colleagues showed, that exogenous expression of DLC1 led to dephosphorylation of focal adhesion proteins such as the focal adhesion kinase (FAK), paxillin and the Crk-associated substrate (Cas) (75). Beside these effects on cell morphology, DLC1-3 have been associated with inhibition of cell proliferation, reduction of anchorage-independent growth and even tumor growth suppression in nude mouse xenograft models (76; 77). Furthermore, DLC1 is thought to regulate the motility and invasiveness of several cancer cell lines, including HCC and breast cancer cell lines (75; 77; 78).

2 Materials and Methods

2.1 Materials

2.1.1 Chemicals and solvents

All solvents and chemicals were of analytical grade.

Table 1: List of chemicals and solvents that were used in this work

Chemical / Solvent	Company
Acrylamide, Rotiphorese Gel 30	Carl Roth GmbH & Co, Karlsruhe
Ammonium persulfate (APS)	Carl Roth GmbH & Co, Karlsruhe
Bromphenol blue	Serva, Heidelberg
Calcium chloride (CaCl ₂)	Merck, Darmstadt
Crystal violet	Merck, Darmstadt
Dimethylsulfoxide (DMSO)	Carl Roth GmbH & Co, Karlsruhe
Disodium hydrogen phosphate (Na ₂ HPO ₄)	Carl Roth GmbH & Co, Karlsruhe
Dithiothreitol (DTT)	Carl Roth GmbH & Co, Karlsruhe
Ethanol (EtOH)	Carl Roth GmbH & Co, Karlsruhe
Ethidium bromide (EtBr)	Roche Diagnostics, Mannheim
Ethylene diamine tetraacetic acid (EDTA)	Carl Roth GmbH & Co, Karlsruhe
Glycerol	Carl Roth GmbH & Co, Karlsruhe
Glycine	Carl Roth GmbH & Co, Karlsruhe
Isopropyl-beta-D-thiogalactopyranoside (IPTG)	MBI Fermentas, St. Leon-Rot
Magnesium chloride (MgCl ₂)	Carl Roth GmbH & Co, Karlsruhe
Magnesium sulphate (MgSO ₄)	Carl Roth GmbH & Co, Karlsruhe
Methanol (MeOH)	Carl Roth GmbH & Co, Karlsruhe
N,N,N,N-Tetramethylethyldiamine (TEMED)	Carl Roth GmbH & Co, Karlsruhe
Paraformaldehyde (PFA)	Carl Roth GmbH & Co, Karlsruhe
Phenylmethylsulphonyl fluoride (PMSF)	Sigma-Aldrich, München
Potassium chloride (KCl)	Carl Roth GmbH & Co, Karlsruhe
Potassium dihydrogen phosphate (KH ₂ PO ₄)	Carl Roth GmbH & Co, Karlsruhe
Propidium iodide (PI)	Invitrogen, Carlsbad, USA
Sodium azide (NaN ₃)	Sigma-Aldrich, München
Sodium chloride (NaCl)	Carl Roth GmbH & Co, Karlsruhe
Sodium dodecyl sulfate (SDS)	Carl Roth GmbH & Co, Karlsruhe
Sodium fluoride (NaF)	Carl Roth GmbH & Co, Karlsruhe
Sodium orthovanadate (Na ₃ VO ₄)	Sigma-Aldrich, München
Thimerosal	Carl Roth GmbH & Co, Karlsruhe

Materials and Methods

Tris-hydroxymethyl-aminomethane (Tris)	Carl Roth GmbH & Co, Karlsruhe
Triton X-100	Carl Roth GmbH & Co, Karlsruhe
Tween 20	Carl Roth GmbH & Co, Karlsruhe
β -Glycerophosphate	Sigma-Aldrich, München
β -Mercaptoethanol	Carl Roth GmbH & Co, Karlsruhe

2.1.2 Reagents

Table 2: List of reagents that were used in this work

Reagent	Company
Agarose	Carl Roth GmbH & Co, Karlsruhe
Alexa Fluor 546® -labeled phalloidin	Molecular Probes /Invitrogen, Carlsbad, USA
Blocking reagent	Roche Diagnostics, Mannheim
Bovine Serum Albumin (BSA)	Sigma-Aldrich, München
Collagen R	Serva, Heidelberg
Complete Protease Inhibitor Cocktail	Roche Diagnostics, Mannheim
Complete Protease Inhibitor Cocktail (EDTA-free)	Roche Diagnostics, Mannheim
Fluoromount-G	Southern Biotech, Birmingham, USA
Goat Serum	Gibco / Invitrogen, Carlsbad, USA
Keyhole Limpet Hemocyanin	Pineda, Berlin
MitoTracker® Red CMXRos	Molecular Probes / Invitrogen, Carlsbad, USA
RNase A stock solution (20 mg/ml)	Invitrogen, Carlsbad, USA

2.1.3 Transfection reagents

Table 3: List of transfection reagents that were used in this work

Transfection reagent	Company
Lipofectamine™ 2000	Invitrogen, Carlsbad, USA
Oligofectamine™	Invitrogen, Carlsbad, USA
TransIT® 293	Mirus, Madison, USA

2.1.4 Protein inhibitors

Table 4: List of protein inhibitors that were used in this work

Protein inhibitor	Company
Y27632 (ROCK inhibitor)	Calbiochem, San Francisco, USA
H1152 (ROCK inhibitor)	Calbiochem, San Francisco, USA

Materials and Methods

2.1.5 Protein and DNA standards

Table 5: List of protein and DNA standards that were used in this work

Protein and DNA standard	Company
GeneRuler 1 kb DNA ladder	MBI Fermentas, St. Leon-Rot
PageRuler prestained protein ladder	MBI Fermentas, St. Leon-Rot

2.1.6 Buffers and solutions

Table 6: List of buffers and solutions that were used in this work

Buffer / Solution	Content
Acrylamide running gel solution	8% and 15% (v/v) acrylamide, 375 mM Tris pH 8.8, 0.1% SDS, 0.1% ammonium persulfate, 0.06% N,N,N,N-tetramethylethylenediamine
Acrylamide stacking gel solution	5% (v/v) acrylamide, 130 mM Tris pH 6.8, 0.1% (w/v) SDS, 0.1% ammonium persulfate, 0.1% N,N,N,N-tetramethylethylenediamine
Blocking solution for Western blotting	0.5% (v/v) blocking reagent, 0.05% (v/v) Tween 20, 0.01% (v/v) Thimerosal in PBS
Blocking solution for microscopy	5% (v/v) goat serum, 0.1% (v/v) Tween 20 in PBS
Blotting buffer	200 mM glycine, 25 mM Tris base, 20% (v/v) methanol
Laemmli protein sample buffer (5 x stock)	400 mM Tris, pH 6.8, 500 mM dithiothreitol, 50% (v/v) glycerol, 10% (w/v) SDS, 0.2% (w/v) bromophenol blue
Raichu lysis buffer	50 mM Tris (pH 7.5), 0.5% (v/v) Triton X-100, 5 mM β -glycerolphosphate, 5 mM sodium fluoride
PBS	140 mM NaCl, 2.7 mM KCl, 8 mM Na_2HPO_4 , 1.5 mM KH_2PO_4
PBS-Tween (PBS-T)	0.05 % (v/v) Tween 20 in PBS
PFA fixing solution	4% PFA in PBS
Propidium iodide (PI) staining solution	PI (50 $\mu\text{g}/\mu\text{l}$), RNaseA (20 $\mu\text{g}/\mu\text{l}$) in PBS
Passive lysis buffer (for Luciferase reporter assays)	Promega, Mannheim
SDS running buffer	25 mM Tris pH 8.8, 192 mM glycine, 0.1% SDS
TAE buffer	40 mM Tris-acetate, 1 mM EDTA, pH 8.3
RBD extraction buffer	50 mM Tris (pH 7.5), 500 mM NaCl, 10 mM MgCl_2 , 1% Triton X-100, 1 mM sodium orthovanadate, 10 mM sodium fluoride, 20 mM β -glycerophosphate, 0.5 mM phenylmethylsulfonyl fluoride plus Complete Protease inhibitor Cocktail (EDTA-free) (1:25)
Firefly substrate solution	470 μM D-luciferin, 530 μM ATP, 270 μM CoA, 33 mM DTT, 20 mM tricine, 2.67 mM MgSO_4 , 0.1 mM EDTA (pH 7.8)
<i>Renilla</i> substrate solution	0.7 coelenterazine, 2.2 mM Na_2EDTA , 0.44 mg/ml bovine serum albumin, 1.1 M NaCl, 1.3 mM NaN_3 , 0.22 M potassium phosphate buffer (pH 5.0)
RiPA lysis buffer	50 mM Tris (pH 7.5), 150 mM NaCl, 1% NP ₄₀ , 0.5% sodium deoxycholate, 0.1% SDS, 1 mM sodium

Materials and Methods

	orthovanadate, 10 mM sodium fluoride, 20 mM β -glycerophosphate plus Complete Protease Inhibitor Cocktail (1:25)
--	--

2.1.7 Cell culture reagents and media

Table 7: List of cell culture reagents and media that were used in this work

Cell culture reagent / Medium	Company
Trypsin-EDTA (10 x stock)	Invitrogen, Carlsbad, USA
OptiMEM [®]	Invitrogen, Carlsbad, USA
Fetal calf serum (FCS)	PAA Laboratories, Pasching, Österreich
RPMI 1640 + L-glutamine (= RPMI 1640)	Gibco / Invitrogen, Carlsbad, USA
RPMI 1640 + L-glutamine, phenol red-free	Gibco / Invitrogen, Carlsbad, USA
DMEM	Gibco / Invitrogen, Carlsbad, USA
Cell culture medium	Contents
cell freezing medium	90% (v/v) FCS, 10% (v/v) DMSO
cell culture medium for breast cancer cell lines	DMEM / RPMI 1640 + 10% (v/v) FCS
cell culture medium for HEK293T cells	RPMI 1640 + 10% (v/v) FCS

2.1.8 Kits

Table 8: List of kits that were used in this work

Kit	Company
G-LISA [™] RhoA Activation Assay Biochem Kit [™] (Absorbance Based)	Cytoskeleton, Denver, USA
G-LISA [™] Rac1 Activation Assay Biochem Kit [™] (Absorbance Based)	Cytoskeleton, Denver, USA
G-LISA [™] Cdc42 Activation Assay Biochem Kit [™] (Absorbance Based)	Cytoskeleton, Denver, USA
PureLink [™] Micro-to-Midi Total RNA Purification System	Invitrogen, Carlsbad, USA
First Strand cDNA Synthesis Kit with random hexamer primers	MBI Fermentas, St. Leon-Rot
HRP SuperSignal [®] West substrate pico	Pierce/Thermo, Rockford, USA
HRP SuperSignal [®] West substrate dura	Pierce/Thermo, Rockford, USA
DC Protein Assay	Bio-Rad, Hercules, USA
QuikChange site-directed PCR mutagenesis Kit	Stratagene, La Jolla, CA, USA
SulfoLink Immobilization Kit	Thermo, Rockford, USA
REDTaq PCR Master Mix	Sigma-Aldrich, München

Materials and Methods

2.1.9 Plasmids and vectors

Table 9: List of plasmids and vectors that were used in this work

Vector / Plasmid	Source
pEGFPC1 and pEGFPN1 vector	Clontech, Mountain View, CA, USA
pmCherryC1 and pmCherryN1 vector	Clontech, Mountain View, CA, USA
pcDNA3 vector	Invitrogen, Carlsbad, USA
pRaichu 1298x (Raichu-RhoA biosensor)	kindly provided by Michiyuki Matsuda (Osaka University, Japan)
pRaichu 1026x (Raichu-Cdc42 biosensor)	kindly provided by Michiyuki Matsuda (Osaka University, Japan)
p3DA-Luc (firefly luciferase reporter)	kindly provided by Guido Posern (MPI of Biochemistry, Martinsried, Germany)
pRL-TK (<i>Renilla</i> luciferase plasmid)	Promega, Mannheim
pEGFP and pmCherry plasmids encoding DLC variants	DNA cloning: see section 2.2.1

The pRaichu-1298x and pRaichu-1026x plasmids (see section 2.2.16) encode for FRET (fluorescence resonance energy transfer)-based RhoA and Cdc42 biosensors (Raichu biosensors), respectively, and were kindly provided by Michiyuki Matsuda (Osaka University, Japan). The Raichu biosensors developed by Matsuda's group are composed of the respective Rho GTPase, a flexible linker, and the Rho binding domain (RBD) of a specific substrate molecule, concatenated between a cyan and a yellow fluorescent protein (CFP and YFP) (79). The firefly luciferase reporter p3DA-Luc used for luciferase reporter assays (see section 2.2.17) contains three serum response factor (SRF) binding elements and was kindly provided by Guido Posern (MPI of Biochemistry, Martinsried, Germany). The *Renilla* luciferase plasmid pRL-TK was from Promega and encodes the luciferase gene from the marine organism *Renilla reniformis* under the control of a thymidine kinase (TK) promoter. It was used as an internal control for transfection efficiency in luciferase reporter assays (see section 2.2.17).

Materials and Methods

2.1.10 Primers

All primers were purchased from MWG Biotech AG (Ebersberg, Germany).

Table 10: List of primers that were used in this work

Primers used for verifying silencing efficiency		Sequence
DLC1	forward	5'-TGG TCA AGA GAG AGC ATG AT-3'
	reverse	5'-TGA AGC TGA AGC TGG ACA GT-3'
DLC2	forward	5'-CAA AGG AAA AAG GGT GAC GA-3'
	reverse	5'-TCC TCC AAT TAA CCC CAT TG-3'
DLC3	forward	5'-CTG GAC CAA GTA GGC ATC TTC C-3'
	reverse	5'-CTC TTC CAT GTA GAG GCT CAG G-3'
GAPDH	forward	5'-CCC CTT CAT TGA CCT CAA CTA-3'
	reverse	5'-CGC TCC TGG AAG ATG GTG AT-3'

Primers used for evaluation of DLC expression levels in BCC cell lines		Sequence
DLC1	forward	5'-TGG TCA AGA GAG AGC ATG AT-3'
	reverse	5'-TGA AGC TGA AGC TGG ACA GT-3'
DLC2	forward	5'-AGC CCC TGC CTC AAA GTA TT-3'
	reverse	5'-ATG GGC GTC ATC TGA TTC TC-3'
DLC3	forward	5'-CCC CTT CAT TGA CCT CAA CTA-3'
	reverse	5'-CGC TCC TGG AAG ATG GTG AT-3'

2.1.11 Short interfering RNAs (siRNAs)

All short interfering RNAs (siRNAs) were purchased from MWG Biotech AG (Ebersberg, Germany). RhoA-, RhoC-, Cdc42- and Dia1-specific siRNAs have been described previously (25; 80; 81).

Table 11: List of siRNAs that were used in this work

siRNAs		Sequence
siLacZ	sense	5'-GCG GCU GCC GGA AUU UAC C dTdT-3'
	antisense	5'-GGU AAA UUC CGG CAG CCG C dTdT-3'
siDLC1-I	sense	5'-GGA CAC GGU GUU CUA CAU C dTdT-3'
	antisense	5'-GAU GUA GAA CAC CGU GUC C dTdT-3'
siDLC1-II	sense	5'-UUA AGA ACC UGG AGG ACU A dTdT-3'

Materials and Methods

	antisense	5'-UAG UCC UCC AGG UUC UUA A dTdT-3'
siDLC2-I	sense	5'-CCA AGG CAC UUU CUA UUG A dTdT-3'
	antisense	5'-UCA AUA GAA AGU GCC UUG G dTdT-3'
siDLC2-II	sense	5'-GCU CUC CAC GAG UCA UAC A dTdT-3'
	antisense	5'-UGU AUG ACU CGU GGA GAG C dTdT-3'
siDLC3-I	sense	5'-UAG CCA CAG UUG AGG UCA A dTdT-3'
	antisense	5'-UUG ACC UCA ACU GUG GCU A dTdT-3'
siDLC3-II	sense	5'-UCU CUG AGG CGG AAG GAA A dTdT-3'
	antisense	5'-UUU CCU UCC GCC UCA GAG A dTdT-3'
siDia1-I	sense	5'-GCU GGU CAG AGC CAU GGA U dTdT-3'
	antisense	5'-AUC CAU GGC UCU GAC CAG C dTdT-3'
siDia1-II	sense	5'-GAA GUU GUC UGU UGA AGA A dTdT-3'
	antisense	5'-UUC UUC AAC AGA CAA CUU C dTdT-3'
siRhoA	sense	5'-GCA GGU AGA GUU GGC UUU G dTdT-3'
	antisense	5'-CAA AGC CAA CUC UAC CUG C dTdT-3'
siRhoC	sense	5'-GAC UAU GAU CGA CUG CGG T dTdT-3'
	antisense	5'-GCC GCA GUC GAU CAU AGU C dTdT-3'
siCdc42	sense	5'-AAA GAC UCC UUU CUU GCU UGU dTdT-3'
	antisense	5'-ACA AGC AAG AAA GGA GUC UUU dTdT-3'

2.1.12 Antibodies

Table 12: List of primary and secondary antibodies that were used in this work

Primary antibody			
Antibody	Species		Company
anti-DLC1	mouse	mAb	BD Biosciences, Franklin Lakes, USA
anti-DLC2 antiserum	rabbit	pAb	Pineda, Germany: raised by immunizing rabbits with the DLC2-specific peptide ³⁷³ TALPDAGDQSRMHEFH ³⁸⁸
anti-DLC3 antiserum	rabbit	pAb	Pineda, Germany: raised by immunizing rabbits with the DLC3-specific peptide ¹⁹⁸ WEAWPVASFRHPQWTHRGC ²¹⁷
anti-paxillin	mouse	mAb	BD Biosciences, Franklin Lakes, USA
anti-RhoA (26C4)	mouse	mAb	Santa Cruz Biotechnology, Santa Cruz, USA
anti-RhoA (119) for RhoA/C detection	rabbit	pAb	Santa Cruz Biotechnology, Santa Cruz, USA
anti-Rac1 (clone 23A8)	mouse	mAb	Upstate/Millipore, Billerica, USA
anti-Cdc42	rabbit	pAb	Santa Cruz Biotechnology, Santa Cruz, USA
anti-Dia1 (V-20) for immunoblotting	goat	pAb	Santa Cruz Biotechnology, Santa Cruz, USA

Materials and Methods

anti-Dia1 for microscopy	mouse	mAb	BD Biosciences, Franclin Lakes, USA
anti-tubulin	mouse	mAb	Sigma-Aldrich, München

Secondary Antibody			
Label	recognized IgG	from	Company
Horseradish peroxidase (HRP)	anti-mouse	sheep	GE Healthcare, München
Horseradish peroxidase (HRP)	anti-rabbit	donkey	GE Healthcare, München
Horseradish peroxidase (HRP)	anti-goat	donkey	Santa Cruz Biotechnology, Santa Cruz, USA
Alexa Fluor® 488	anti-mouse	goat	Molecular Probes/Invitrogen, Carlsbad, USA
Alexa Fluor® 546	anti-mouse	goat	Molecular Probes/Invitrogen, Carlsbad, USA

2.1.13 Bacterial strain

BL21 bacteria transformed with a pGEX vector encoding the Rho binding domain (RBD) of rhotekin fused to GST (glutathione-S-transferase) was kindly provided by John Collard (The Netherlands Cancer Institute, Amsterdam, The Netherlands).

2.1.14 Human cell lines

Fresh cultures of the human cell lines were established every three months from frozen stocks stored in liquid nitrogen.

Table 13: List of human cell lines that were used in this work

Zell lines		Originally obtained form
HEK293T	human embryonic kidney cells that contain the SV40 large T antigen	Angelika Hauser, IZI, University of Stuttgart, Germany
MCF7	human breast cancer cell line (poorly invasive)	Institute of Clinical Pharmacology, Robert Bosch Hospital, Stuttgart, Germany
MDA-MB 231	human breast cancer cell line (highly invasive)	Institute of Clinical Pharmacology, Robert Bosch Hospital, Stuttgart, Germany
MDA-MB 436	human breast cancer cell line (poorly invasive)	Institute of Clinical Pharmacology, Robert Bosch Hospital, Stuttgart, Germany
MDA-MB 468	human breast cancer cell line (poorly invasive)	Institute of Clinical Pharmacology, Robert Bosch Hospital, Stuttgart, Germany

All breast cancer cell (BCC) lines used in this work were kindly provided by the Institute of Clinical Pharmacology, Robert Bosch Hospital, Stuttgart, Germany.

Materials and Methods

2.1.15 Equipment

Table 14: List of equipment that were used in this work

Equipment	Company
Autoflow CO ₂ Water-Jacketed Incubator (cell culture incubator)	NUAIRE™ IR
CASY® (cell counter)	Schärfe System/ Innovatis AG
CK2 (standard light microscope)	Olympus, Hamburg
CR 422 (low speed centrifuge for cell harvesting)	Jouan Quality System
Curix 60 processor	Agfa, Düsseldorf
Cytomics FC 500 (FACS)	Beckman Coulter, Krefeld
Eppendorf centrifuge 5415 R	Eppendorf, Hamburg
Infinite 200M (fluorescent 96-well plate reader)	Tecan, Crailsheim
MKR 13 (orbital microplate shaker)	HLC BioTech, Bovenden
NanoDrop® ND-1000 (Spectrophotometer)	peQLab, Erlangen
pipettes (1 - 20 µl / 20 - 200 µl / 200 - 1000 µl)	Gilson / Eppendorf
RoboCycler Gradient 96 (PCR cycler)	Stratagene, La Jolla, USA
Sonopuls HD 200 (sonifier)	Bandelin, Berlin
Spectramax 340PC (96-well plate spectrophotometer)	Molecular Devices, Sunnyvale, USA
TCS SL (confocal laser scanning microscope)	Leica, Wetzlar
Transferpette® 5-50 µl and 20-200 µl (multichannel pipette)	BRAND, Wertheim
Vortex Genie 2 (vortex mixer)	Scientific Industries, Bohemia, USA

2.1.16 Consumables

Table 15: List of consumables that were used in this work

Consumables	Company
0.2 µm filter for sterile filtration	Sarstedt, Nümbrecht
21-gauge needle	Sterican
black 96-well microplate	R&D Systems, Minneapolis, USA
blotting paper, 3 mm Whatman	Schleicher Schuell, Dassel
cell culture dishes (6 cm and 10 cm diameter)	Greiner, Frickenhausen
cell culture flasks (75 cm ² and 175 cm ²)	Greiner, Frickenhausen
cell culture plates (6-well, 24-well, 96-well)	Greiner, Frickenhausen
Cryo vials 1ml	Greiner, Frickenhausen
CultureCoat™ BME-coated Cell Invasion Assay (24-well plate plus inserts)	Cultrex®/Trevigen, Gaithersburg, USA
glass coverslips 18 mm x 18 mm	Carl Roth GmbH & Co, Karlsruhe
glutathione beads	Pierce / Thermo, Rockford, USA
pipette tips (1 - 20 µl; 20 - 200 µl; 200 - 1000 µl)	Greiner, Frickenhausen

Materials and Methods

pipettes (5 ml, 10 ml and 25 ml)	Corning Incorporated, Costar®
PVDF blotting membrane	Carl Roth GmbH & Co, Karlsruhe
reaction tubes 1.5 ml (standard and safe-lock)	Eppendorf, Hamburg
syringe 1 ml	BRAUN, Wertheim
Transwells (24-well plate plus inserts) for cell migration assays	Costar/Vitaris AG, Baar, Germany
tubes (15 ml and 50 ml)	Greiner, Frickenhausen
white 96-well microplate	R&D Systems, Minneapolis, USA
X-ray films	CEA, Strangnas, Sweden

2.2 Methods

2.2.1 DNA cloning

The full-length DLC1 cDNA was amplified by PCR using pCS2+MT-DLC1 as a template with primers containing *Bam*HI restriction sites (DLC1-minusATG-F: 5'-CGC GGA TCC TGC AGA AAG AAG CCG GAC CC-3' and DLC1-STOP-R: 5'- CGC GGA TCC TCA CCT AGA TTT GGT GTC TTT GG-3') and (DLC1-ATG-F: 5'-CGC GGA TCC ACC ATG TGC AGA AAG AAG CCG GAC ACC-3' and DLC1-minusSTOP-R: 5'-CGC GGA TCC CTA GAT TTG GTG TCT TTG GTT TC -3'), and cloned into pEGFPC1 and pEGFPN1 vectors, respectively (Clontech). The full-length DLC1 cDNA was subcloned from the pEGFPN1 vector by *Bam*HI restriction into the pmCherryN1 vector (Clontech), and from the pEGFPC1 vector as a *Bam*HI fragment into the pmCherryC1 vector (Clontech) digested with *Bgl*II. DLC2 was subcloned from the pEGFPC1-DLC2alpha plasmid by *Hind*III restriction into the pmCherryC1 vector. The human DLC3 beta cDNA was amplified by PCR using clone IRATp970E0455D (ImaGenes, Germany) as a template with forward primer 5'-CCG GAA TTC TAC CTT GAA TAA TTG TGC CTC GAT G-3' and reverse primer 5'-CCG GAA TTC TTC ACA GCT TTG TCT CAG GGC-3' and cloned into the pEGFPC1 vector as an *Eco*RI fragment. The 5' region encoding the SAM domain present in DLC3 alpha was amplified by PCR using cDNA derived from HeLa cells as a template with the forward primer 5'-CCG GAA TTC TCC TCT GCT GGA CGT TTT CTG-3' and reverse primer 5'-TTC TGA GTC TTC ATT CTG CTT GC-3'. The PCR product and pEGFPC1-DLC3beta were digested with *Eco*RI and *Bp*I, and the DLC3 fragments were ligated with *Eco*RI-digested pEGFPC1, generating pEGFPC1-DLC3alpha. Full-length DLC3 alpha and DLC3 beta were subcloned from the pEGFPC1 vectors by *Eco*RI restriction into the pmCherryC1 vector. The DLC1-K714E, DLC2-K736E and DLC3beta-K645E GAP-inactive mutants were generated by QuikChange site-directed PCR mutagenesis (Stratagene) using pEGFPC1-DLC1, pEGFPC1-DLC2 and pEGFPC1-DLC3beta as templates. The forward primers used were: DLC1-K714E-for (5'-CGT GGC AGA CAT GCT GGA GCA GTA TTT TCG AG-3'); DLC2-K736E-for (5'-GTG GCG GAT ATG GTG GAA CAG TTC TTC CGG GAC-3'); DLC3-K645E-for (5'-GTG GCT GAC CTG CTA GAG CAG TAT TTC CGG GAC-3'). To generate pEGFPC1-DLC3alpha-K725E, pEGFPC1-DLC3alpha was digested with *Hind*III and *Bp*I and the fragment corresponding to the DLC3alpha 5' region was ligated with pEGFP-C1-DLC3beta digested with *Hind*III and *Bp*I. All amplified cDNAs were verified by sequencing. Oligonucleotides were purchased from MWG Biotech AG (Ebersberg, Germany).

Materials and Methods

The pCS2+MT-DLC1 and pEGFPC1-DLC2alpha plasmids were kindly provided by Irene Ng (University of Hong Kong, Hong Kong, People's Republic of China).

2.2.2 Cell culture

All low-passage cell lines used in this work were kindly provided by the Institute of Clinical Pharmacology (Robert Bosch Hospital, Stuttgart, Germany). HEK293T cells were obtained from Dr. Angelika Hausser (IZI, University of Stuttgart, Germany). Cells were cultured under sterile conditions in DMEM or RPMI 1640 media supplemented with 10% heat-inactivated fetal calf serum (FCS) and incubated in a humidified atmosphere of 5% CO₂ at 37°C. Before reaching confluency, cells were passaged using trypsin-EDTA for cell detachment and maintained in culture for not longer than three months. New cultures of the cell lines were established from frozen stocks stored in liquid nitrogen. The cell number per ml was determined by using the CASY® cell counter.

2.2.3 Preparation of collagen-coated glass coverslips

For immunofluorescence microscopic experiments cells were seeded onto collagen-coated glass coverslips coated with 25 µg/ml collagen R solution (diluted in sterile PBS) for 2 h at 37°C. Coverslips were rinsed with sterile PBS prior to use.

2.2.4 Transient transfection of HEK293T cells using TransIt® 293

For luciferase assays and Raichu experiments, HEK293T cells were seeded in RPMI 1640 medium supplemented with 10% FCS (in the case of Raichu assays phenol red-free medium was used) into collagen-coated (2,5 µg/µl) 24-well plates. After adhesion overnight, cells were transfected at 50-70% confluency with plasmid DNA using TransIT® 293 reagent. Briefly, 100 µl OptiMEM® medium were mixed with TransIT® 293 (2 µl TransIT per 1 µg DNA), vortexed and incubated for 15 min at room temperature (RT). Next, plasmid DNA was added to the transfection mixture, incubated for further 20 min and then added drop-wise to the cells. One day post transfection, cells were prepared for luciferase assays and Raichu experiments (see section 2.2.16 and 2.2.17).

2.2.5 Transient transfection of MCF7 cells using Lipofectamine™ 2000

For subcellular localization studies, MCF7 cells were seeded in RPMI 1640 medium (+ 10% FCS) onto collagen-coated (25 µg/ml) glass coverslips and cultivated overnight. The next

Materials and Methods

day, the medium was exchanged and cells were transiently transfected at 70-90% confluency with plasmid DNA encoding GFP-tagged DLC constructs using Lipofectamine™ 2000. The transfection was performed according to the manufacturer's instructions using a ratio (w/v) of DNA to Lipofectamine™ 2000 of 1:2.5. Briefly, 50 µl OptiMEM® medium were mixed with Lipofectamine™ 2000, vortexed and incubated for 5 min at RT. Next, plasmid DNA (DLC1, DLC2, DLC3 alpha-K725E and DLC3 beta-K645E constructs: 250 ng; DLC3 alpha/beta constructs: 100 ng) in 50 µl OptiMEM® was added to the transfection mixture, incubated for further 20 min and then the transfection mixture (100 µl in total) was added drop-wise to the cells. After one day, cells were fixed and stained as described in section 2.2.23.

2.2.6 Transient transfection of breast cancer cell lines using Oligofectamine™

DLC family members and other targets were silenced by transfecting cells with short interfering RNAs (siRNAs; listed in Table 11). The unrelated siRNA LacZ was used as control. Transfection was performed using Oligofectamine™ reagent according to the manufacturer's instructions. Cells were transfected at 30-40% confluency in serum-free medium. Oligofectamine™ was diluted in OptiMEM® and after 5 min incubation at RT, mixed with siRNAs (ratio 2.5:1 of a 20 µM siRNA stock and Oligofectamine; siRNA end concentration was 100 pM). 20 min later, the mixture was added to the cells. After 4 h, medium containing 30% FCS was added to the cells, yielding a final concentration of 10% FCS. Cells were typically analyzed after cultivation for 2-3 days at 37°C and 5% CO₂.

2.2.7 RNA isolation

Using the PureLink™ Micro-to-Midi Total RNA Purification System, total RNA was either isolated from breast cancer cell (BCC) pellets or cells were lysed directly in cell culture plates. The RNA was extracted following the manufacturer's instructions. In brief, cells were lysed and the genomic DNA was sheared using a syringe with a 21-gauge needle. The lysate was transferred to a column and after binding of the RNA to the matrix, the RNA was washed several times and finally eluted with RNase-free water. Total RNA was quantified with a NanoDrop® ND-1000 spectrophotometer and used for complementary DNA (cDNA) synthesis (see section 2.2.8). All steps described above were performed with RNase-free solutions, reaction tubes and pipette tips.

Materials and Methods

2.2.8 Complementary DNA (cDNA) synthesis

RNA was reverse transcribed into cDNA using a First Strand cDNA Synthesis Kit with random hexamer primers. Total RNA (2 µg) was mixed with 0.2 µg random hexamer primers and incubated for 5 min at 70°C. Next, the dNTP mix (20 µmol) together with the reaction buffer and ribonuclease inhibitor (20 units) were added and incubated at 25°C for 5 min. Finally, the M-MuLV reverse transcriptase (40 units) was added to the mixture (final volume: 20 µl) and incubated at 25°C for 10 min, followed by incubation at 37°C for 60 min. To stop the reaction, the reverse transcriptase was heat-inactivated (70°C for 10 min). The cDNA was used for subsequent semi-quantitative reverse-transcriptase polymerase chain reactions (RT-PCR; see section 2.2.8).

2.2.9 Semi-quantitative RT-PCR

RT-PCR was performed to evaluate the expression levels of the individual DLC family members. Therefore, 2 µl of the cDNA together with specific primers for each DLC family member were mixed with REDTaq PCR Master Mix, yielding a total volume of 25 µl. The housekeeping gene glyceraldehyde-3-phosphate dehydrogenase (GAPDH) was amplified as internal control. The primers used are listed in Table 10. The amplification was performed by using the PCR program listed in Table 16 and the RoboCycler Gradient 96 (Stratagene).

Table 16: PRC-Program used for amplification

Temp.	min	cycles
94°C	2 min	1
94°C	30 sec	depending on cell line and primer pair
X	1 min	
72°C	1 min	

X = in case of
DLC1: 50°C
DLC2: 52°C
DLC3: 58°C
GAPDH: 53°C

10 µl of each PCR mixture was loaded onto a 1.5 % agarose gel containing ethidium bromide (EtBr) and separated by electrophoresis in TAE buffer at 70 Volt.

2.2.10 Generation of antibodies against human DLC2 and human DLC3

The anti-DLC2 and anti-DLC3 antisera were raised by immunizing rabbits with DLC2- (³⁷³TALPDAGDQSRMHEFH³⁸⁸) and DLC3-specific (¹⁹⁸WEAWPVASFRHPQWTHRGDC²¹⁷) peptides coupled to keyhole limpet hemocyanin (Pineda, Germany). Antibodies were affinity purified with the SulfoLink Immobilization kit for Peptides. Elution was with 100 mM glycine buffer (pH 2.7), and neutralized antibody fractions were pooled and dialyzed against PBS.

2.2.11 Protein extraction for immunoblotting

Cells grown on cell culture plates were washed with PBS and lysed at 4°C with radioimmunoprecipitation assay (RiPA) buffer (composition: see Table 6) plus Complete Protease Inhibitors Mixture (Roche). Whole cell lysates were clarified by centrifugation at 16,000 x *g* and 4°C for 10 min. Supernatants were either mixed with Laemmli protein sample buffer (see Table 6), boiled for 5 min at 95°C and separated by SDS polyacrylamide gel electrophoresis (SDS-PAGE; see section 2.2.13) or stored at -20°C until use.

2.2.12 Quantification of protein amounts in RiPA lysates

RiPA lysates are incompatible with the Bradford Protein Assay. Therefore, total protein amounts of RiPA cell lysates were determined by using the DC Protein Assay (Bio-Rad). The standard assay protocol was as follows: 5 µl of cell lysates were transferred to 96-well plates and incubated with 25 µl provided Reagent A' and 200 µl of Reagent B. After 15 min, the color development due to the amino acids tyrosine and tryptophan was read at 750 nm. By comparing the absorbance with a BSA standard curve, the protein concentration was determined.

2.2.13 SDS polyacrylamide gel electrophoresis (SDS-PAGE)

Equal protein amounts (usually 50 µg; quantified as described in 2.2.12) of RiPA cell lysates were denatured in Laemmli sample buffer for 5 min at 95°C and loaded onto SDS polyacrylamide gels. The gels consisted of an 8% or 15% polyacrylamide running gel for high and low molecular weight proteins, respectively, and a stacking gel (4% polyacrylamide). Electrophoresis was carried out in 1 x SDS running buffer (see Table 6) at 40 mA. After electrophoretic protein separation Western blotting (see section 2.2.14) was performed.

2.2.14 Western blotting

Proteins of the SDS polyacrylamide gels were transferred to polyvinylidene difluoride (PVDF) membrane by semi-dry blotting at 1.5 mA per cm² for 2 h. After protein transfer, the PVDF membrane was blocked for 30 min at RT with 0.5% blocking reagent in PBS containing 0.1% Tween 20 and then incubated with primary antibodies diluted in 0.5% blocking reagent containing 0.05% azide. After incubation overnight at 4°C, the membrane was washed with PBS-Tween followed by incubation with HRP-conjugated secondary antibodies for 1 h. The membranes were washed again with PBS-Tween and proteins were visualized using the enhanced chemiluminescence (ECL) detection system according to the manufacturer's instruction. X-ray films were developed with a Curix 60 processor (AGFA).

2.2.15 Rho binding domain (RBD) pull-downs

BL21 bacteria were transformed with a pGEX vector encoding the Rho binding domain (RBD) of rhotekin and expression was induced with 0.1 mM isopropyl- β -D-1-thiogalactopyranoside (IPTG) for 4 h at 37°C. Bacteria were harvested, resuspended in PBS containing Complete Protease Inhibitor Mixture, and sonicated. Triton X-100 was added (1% final) and the lysate was centrifuged for 10 min at 8,000 x *g*. GST-RBD was purified with glutathione resin (GE Healthcare). For pull-downs, cells were lysed in RBD extraction buffer (see Table 6) plus Complete Protease Inhibitor Mixture without EDTA (Roche). Equal amounts of cleared lysates were incubated with GST-RBD beads for 45 min at 4°C. Beads were washed with RBD extraction buffer, bound proteins were separated by SDS-PAGE (see 2.2.13), and RhoA was analyzed by immunoblotting (see section 2.2.14).

2.2.16 RhoA and Cdc42 biosensor assays (Raichu assays)

HEK293T cells were seeded in phenol red-free RPMI 1640 (+ 10% FCS) into collagen-coated (2.5 μ g/ml) 24-well plates and, the next day, transiently transfected with 0.5 μ g plasmid DNA encoding for the Raichu sensor together with 1 μ g pcDNA3 vector (control) or 1 μ g expression vectors encoding different mCherry-DLC variants using TransIT® 293 (see section 2.2.4). Cells were lysed one day post transfection with Raichu lysis buffer (see Table 6). After removing the debris by centrifugation at 16,000 x *g* for 10 min, the supernatants were transferred to 96-well plates and cyan fluorescent protein (CFP) and yellow fluorescent protein (YFP) fluorescence was measured after background subtraction at 475 nm and 530 nm, respectively, using a Tecan Infinite 200M plate reader (excitation, 433 nm). Expression of the DLC proteins was controlled by measuring mCherry emission at 615 nm (excitation:

575 nm). For quantification, ratios of fluorescence resonance energy transfer (FRET) / CFP were determined.

2.2.17 Luciferase reporter assays

HEK293T cells were grown on collagen-coated (2.5 µg/ml) 24-well dishes and transfected with 50 ng p3DA-Luc firefly luciferase reporter containing three SRF (serum response factor) binding elements, 50 ng of *Renilla* luciferase plasmid and 25 ng of the respective DLC plasmids (see section 2.2.4). After serum starvation overnight, cells were stimulated with 15% serum for 6 h. Cells were lysed with 300 µl passive lysis buffer (Promega) and luciferase activities in 10 µl lysate were measured by addition of 50 µl firefly substrate (see Table 6). Luminescence was measured with a Tecan Infinite 200M plate reader. DLC protein expression was verified by measuring green fluorescent protein (GFP) fluorescence of the lysates.

2.2.18 Transwell cell migration assays

The bottom side of a polycarbonate (PC) transwell membrane (8.0 µm pore size) was coated with 2.5 µg/ml collagen R and 1×10^5 cells were added to the top chamber. After allowing the cells to migrate overnight (MCF7), for 4 h (MDA-MB 436) or 3h (MDA-MB 468) cells on the upper side of the membranes were removed using a cotton swab. Cells on the underside were fixed in 4% paraformaldehyde (PFA) and stained with 0.1% crystal violet. Cells in five independent microscopic fields per membrane were counted at a 20-fold magnification.

Experiments were performed in different settings to analyze chemotaxis, haptotaxis or random migration. In case of chemotactic transwell assays, the top chamber contained medium with 0.5% FCS and the bottom chamber was supplemented with 10% FCS. For haptotactic transwell assays, both chambers contained the same medium (RPMI 1640 with 0.5% FCS) and therefore the collagen layer on the underside of the membrane was the stimulus for migration. To analyze random migration of cells, both membrane sides were coated with 2.5 µg/ml collagen and both chambers contained medium supplemented with 10% FCS. In the case of Rho kinase inhibition, transwell migration assays were performed as described for chemotaxis, but 10 µM Y27632 or 1 µM H1152 were added to the cells in the top chamber.

2.2.19 Wound-healing assays

MCF7 or MDA-MB 468 cells were seeded into collagen-coated (25 µg/ml) 12-well dishes. The next day, confluent cell monolayers were wounded with a white pipette tip, washed several times with PBS to remove detached cells and fresh medium was added. To monitor the wound closure, three regions of the scratch were marked at the bottom of the plate and images were taken at the beginning and after incubation of cells for 14 h and 24 h (MCF7 cells) or 14h and 38 h (MDA-MB 468 cells), respectively. For quantification, the wound width in the three images was measured at 10 different positions per image.

2.2.20 Invasion assays

Cell invasion assays were performed with the CultreCoat™ 24 Well BME-Coated Cell Invasion Assay Kit following the manufacturer's instructions. The set-up was similar to that described for chemotactic transwell assays in section 2.2.18, but here transwells were precoated with PathClear™ basement membrane extract (BME). 1×10^5 cells in medium containing 0.5 % FCS were seeded into the upper chamber, the lower chamber contained medium supplemented with 10% FCS. Cells that had reached the underside of the membrane after overnight (MDA-MB 231 cells) or after 24h incubation (MCF7 and MDA-MB 436 cells) were washed and incubated with a mixture of detachment solution and Calcein AM. Calcein AM is a non-fluorescent, hydrophobic compound that permeates cells. Once in the cell, it is hydrolyzed by intracellular esterases to produce calcein, a hydrophilic, strongly fluorescent compound. For quantification, the relative fluorescence unit (RU) of duplicate wells was determined by excitation at 485 nm and emission at 520 nm. Invasion assays shown in Figure 23 were performed as described above, but cells on the bottom side were stained and quantified as mentioned for transwell migration assays in section 2.2.18.

2.2.21 G-LISA Rho GTPase activation assays

We used G-LISA Rho GTPase activation assay kits following the manufacturer's instructions to determine the level of active RhoA, Rac1 and Cdc42 in MDA-MB 468 cells. Briefly, MDA-MB 468 cells were transfected with siRNA using Oligofectamine™ (see section 2.2.6) and lysed three days later with the provided lysis buffer. Lysates were cleared by centrifugation and supernatants were shock frozen in liquid nitrogen and stored until use at -80°C. Equal protein amounts of cell lysates were added to 96 well plates coated with Rho-GTP-binding protein specific for active RhoA, Rac1 or Cdc42 and incubated for 30-45 min at 4°C. Inactive GDP-bound proteins were removed by washing, whereas RhoA-, Rac1- or Cdc42-GTP

Materials and Methods

bound to the plate and were detected with specific primary antibodies and HRP-conjugated secondary antibodies. After addition of provided HRP substrate solution, the level of active RhoA, Rac1, or Cdc42 was determined by measuring the absorbance at 490 nm. Recombinant RhoA-GTP, Rac1-GTP and Cdc42-GTP proteins (contained in the G-LISA kits) were used as positive controls.

2.2.22 Cell cycle analysis

MCF7 cells were transfected with siRNA using Oligofectamine™ (see section 2.2.6), harvested three days later, washed and resuspended in 400 µl cold PBS. Cells were fixed and permeabilized by adding 1 ml ethanol at -20°C under constant vortexing. After incubation at 4°C overnight, cells were washed with PBS, resuspended in 500 µl propidium iodide (PI)-staining solution containing RNaseA (see Table 6) and incubated for 30 min at 37°C. Subsequently, flow cytometric analysis was performed using a Cytomics FC-500 FACS. To quantify the percentage of cells in the individual cell cycle phases, FACS data were analyzed with the cell cycle software Cylchred.

2.2.23 Immunofluorescence microscopy

Cells grown on glass coverslips coated with 25 µg/ml collagen were fixed with 4% paraformaldehyde (PFA) for 10 min, permeabilized with PBS containing 0.1% Triton X-100 for 5 min, and unspecific binding sites were blocked with 5% goat serum in PBS containing 0.1% Tween 20 for 30 min. Cells were incubated with primary antibody in blocking buffer for 2 h followed by incubation with secondary antibody in blocking buffer for 1 h. To analyze cytoskeletal structures in cells lacking DLC1 or DLC2 (see Figure 10), cells were simultaneously fixed and permeabilized with 4% PFA in PBS containing 0.1% Triton X-100 for 10 min. Filamentous actin was stained with Alexa Fluor® 546-conjugated phalloidin for 20 min before mounting of coverslips in Fluoromount-G (Southern Biotechnology). Staining of GFP-DLC2 expressing MCF7 cells with the mitochondrion-selective probe MitoTracker® (MitoTracker® Red CMXRos) was performed as follows. Cells were incubated with 200 nM MitoTracker® in growth medium (RPMI 1640 + 10% FCS) for 30 min at 37°C, washed with fresh growth medium and fixed with 4% PFA. After washing with PBS, coverslips were mounted in Fluoromount-G. All cells were analyzed on a confocal laser scanning microscope (TCS SL, Leica) using 488, 543, and 561 nm excitation and a 40.0/1.25 HCX PL APO oil objective lens.

3 Results

3.1 Chapter 1

3.1.1 DLC1 and DLC2 inhibit Rho signaling in intact cells

DLC1 and DLC2 have been reported to possess the same substrate selectivity *in vitro*, with GAP activity being most pronounced for RhoA and lower activity towards Cdc42 (82; 83). In intact cells, substrate specificity of these GAP proteins may depend on additional factors and has not been compared thus far.

To do so, we made use of a genetically encoded fluorescence resonance energy transfer (FRET)-based RhoA biosensor, termed Raichu-RhoA (79). This sensor consists of RhoA, the Rho binding domain (RBD) of the effector PKN (protein kinase N) and the fluorescence donor-acceptor pair CFP (cyan fluorescent protein) and YFP (yellow fluorescent protein). Upon activation by GTP loading, the RBD binds RhoA, modifying the orientation of the fusion protein and allowing FRET to occur. Since RhoA activation is approximated to be proportional to the ratio of FRET/CFP emission, the activity of GAP proteins expressed along with the biosensor can be measured. As shown in Figure 7A, cotransfection of Raichu-RhoA with expression plasmids encoding DLC1 and DLC2 into HEK293T cells led to a decrease in the emission ratio, indicating that both proteins increase RhoA-GTP hydrolysis *in vivo* (Figure 7A). This can be attributed to the GAP activity of the proteins because an inactive DLC1 variant harboring a point mutation in its GAP domain (DLC1-K714E) only had a minimal effect on the emission ratio of the biosensor (Figure 7A), as did a DLC2 GAP-inactive mutant (data not shown). Although DLC1 and DLC2 displayed activity for Cdc42 *in vitro* (82; 83), we did not observe an effect on the emission ratio of a Raichu-Cdc42 biosensor coexpressed in HEK293T cells (Figure 7B).

Results

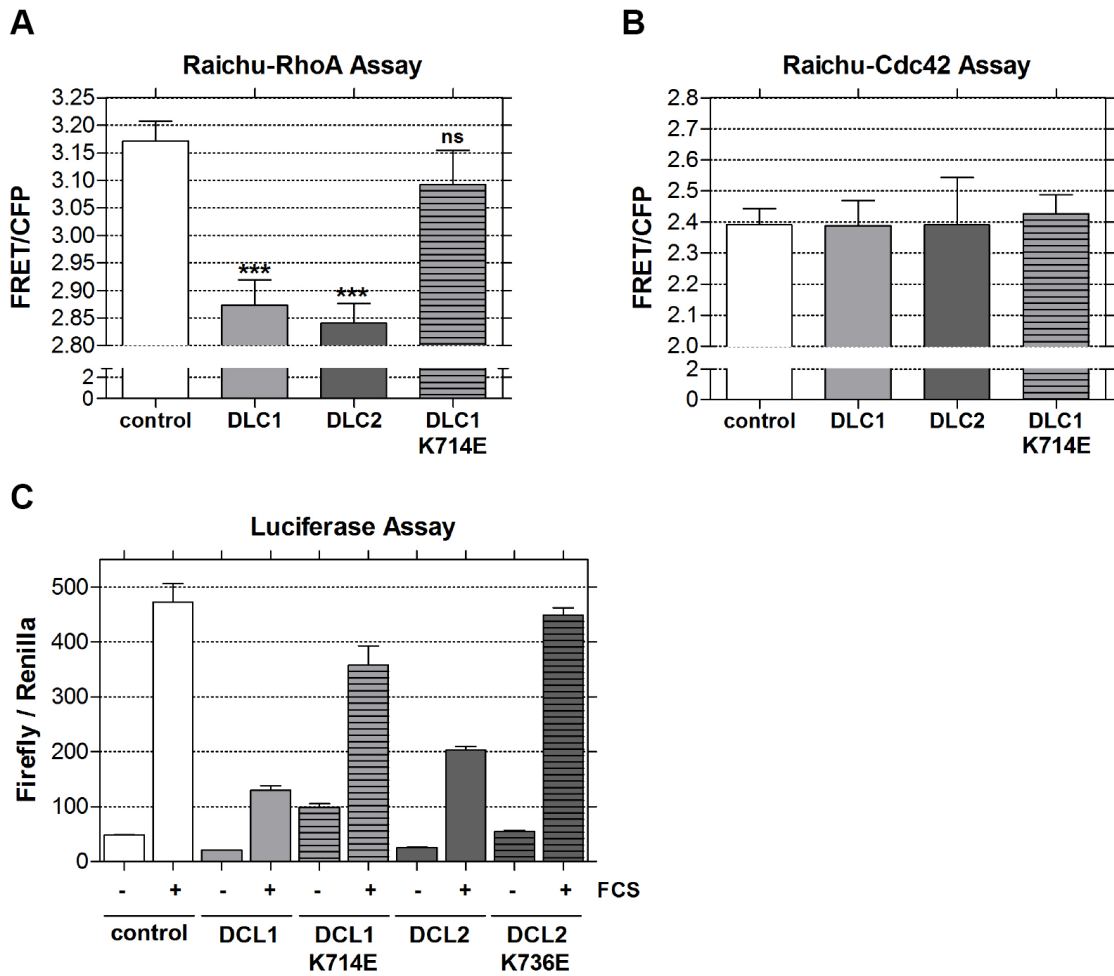


Figure 7: DLC1 and DLC2 inhibit Rho but not Cdc42 signaling in intact cells. HEK293T cells were cotransfected with plasmids encoding the Raichu-RhoA (A) or Raichu-Cdc42 (B) biosensor and mCherry-DLC1, mCherry-DLC1-K714E, Cherry-DLC2, or empty vector (control). The next day, the emission ratio of Raichu-RhoA (A) or Raichu-Cdc42 (B) was determined by measuring YFP (FRET) and CFP fluorescence (excitation, 433 nm) in cell lysates. In (A) columns represent the mean of four independent experiments performed with triplicate samples; bars, SEM. The values for DLC1 and DLC2 versus the control were statistically significant (two-tailed unpaired t test, $P < 0.0001$), whereas those for DLC1-K714E were not significantly different (ns, $P = 0.287$). In (B) one representative result out of two is shown. Bars, SEM. In both experiments the values for DLC1, DLC2 and DLC1-K714E versus the control were not significantly different (two-tailed unpaired t test, $P > 0.05$). (C) HEK293T cells were transfected with the SRF-responsive 3DA-Luc firefly luciferase reporter along with plasmids encoding *Renilla* luciferase and GFP-DLC1, GFP-DLC1-K714E, GFP-DLC2, GFP-DLC2-K736E or empty vector (control), starved overnight, and then either left untreated (-) or stimulated with FCS (+) for 6 h. Firefly luciferase activity in cell lysates of triplicate samples was determined and normalized by *Renilla* luciferase activity. The data correspond to one representative experiment out of three and are the mean of triplicate samples; bars, SEM.

Results

To address the question how the two DLC proteins modulate endogenous RhoA signaling we further analyzed their ability to block serum response factor (SRF)-dependent transcription, which is known to require functional RhoA (84). HEK293T cells were transfected with a SRF-responsive luciferase reporter along with DLC1 or DLC2 expression plasmids, starved overnight and then restimulated with serum. As shown in Figure 7C, both DLC1 and DLC2 wild type proteins suppressed SRF-dependent transcription in a similar fashion. In contrast, DLC1-K714E and DLC2-K736E only slightly reduced serum-induced luciferase reporter levels. These results are in accordance with those obtained with the RhoA biosensor and demonstrate that both DLC1 and DLC2 target RhoA in intact cells.

3.1.2 Selective and efficient silencing of DLC1 and DLC2

To investigate the molecular and cellular impact of endogenous DLC1 and DLC2 on Rho-mediated cellular events we mimicked their loss in cancer cells by using a RNA interference (RNAi) approach. To first select appropriate cell lines, we examined expression of the DLC1 and DLC2 genes in a panel of breast cancer cell lines by semi-quantitative RT-PCR (Figure 8A). In most of the cell lines, transcripts specific for both DLC genes could be detected. While DLC1 was absent in a subset of the cell lines, DLC2 was more uniformly expressed. The MCF7 cell line was chosen for further studies, since these cells express both genes and can be transfected at high efficiency with siRNAs as tested with a fluorescently labeled control siRNA (data not shown). Specific siRNAs were designed for DLC1 and DLC2 and silencing efficiency was verified by semi-quantitative RT-PCR (Figure 8B). Down-regulation of the individual transcripts was observed 48 h post transfection and persisted for at least 96 h. The siRNAs were found to be selective as knock-down of DLC1 did not affect DLC2 transcript levels and vice versa, in comparison to the siLacZ control (Figure 8B). Specific down-regulation of the DLC1 protein was further verified by immunoblotting (Figure 8C). Due to the lack of a commercially available antibody for DLC2, we raised a polyclonal DLC2 peptide antibody, which specifically detected the overexpressed protein in Western blots (data not shown). Due to the presence of non-specific bands, the DLC2 protein could not be visualized in MCF7 cells, but specific siRNA-mediated DLC2 down-regulation could be observed in MDA-MB 436 cells (see Figure 14G).

Results

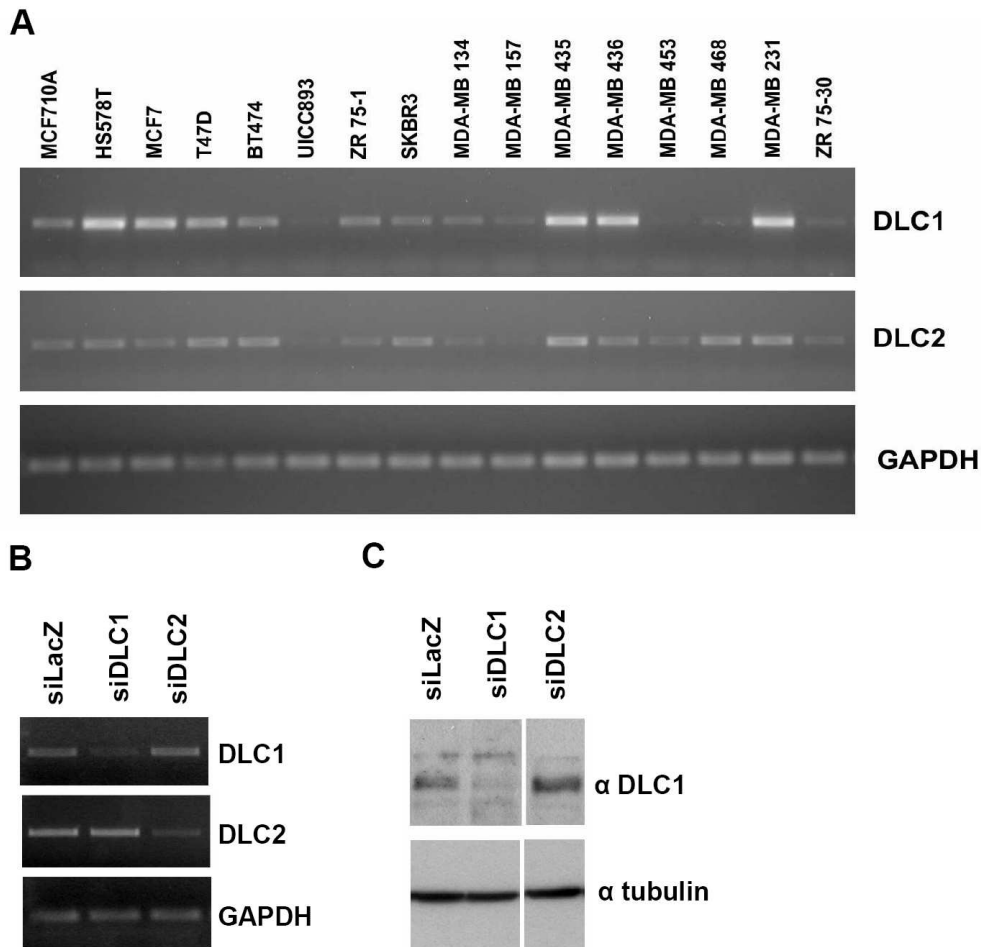


Figure 8: Expression profile of endogenous DLC1 and DLC2 and their knock-down by RNAi. (A) Semi-quantitative RT-PCR analysis of DLC1 and DLC2 genes. cDNA from the breast epithelial cell lines indicated was amplified using specific primers that span introns in the genomic sequence. GAPDH was amplified as a loading control. (B and C) MCF7 cells were transiently transfected with DLC1- or DLC2-specific siRNAs, and three days after transfection, DLC expression was evaluated by semi-quantitative RT-PCR (B) or by Western blotting (C). Cells transfected with a LacZ-specific siRNA were used as a negative control. (C) Equal amounts of total cell lysates were subjected to SDS-PAGE and transferred to a membrane. DLC1 expression was analyzed by immunoblotting using a DLC1-specific antibody (top). Equal loading was verified by reprobating the membrane with tubulin-specific antibody (bottom). The lanes shown are from the same membrane.

3.1.3 DLC1 and DLC2 knock-down increases cellular RhoA-GTP levels

DLC1 and DLC2 are thought to act as tumor suppressors by attenuating Rho signaling based on the fact that ectopic expression in carcinoma cell lines lacking these proteins reduces RhoA-GTP levels and RhoA-mediated cellular processes, such as cell migration and invasion (82; 85). However, whether the absence of DLC1 and DLC2 really have an impact on RhoA activity and associated cellular events has not been investigated in detail, nor is it

Results

clear whether these GAP proteins have redundant functions. To answer these questions, we analyzed RhoA-GTP levels in MCF7 cells lacking DLC1 or DLC2 by GST pulldown assays with the RBD of rhotekin. Cells were transfected with DLC1- and DLC2-specific siRNAs, respectively, starved and then restimulated with serum for 5 min (Figure 9). Down-regulation of both DLC1 and DLC2 enhanced serum-induced RhoA-GTP levels compared to the control, indicating that endogenous DLC1 and DLC2 indeed reduce the amount of active RhoA. This is consistent with the fact that overexpression of DLC1 and DLC2 targets RhoA in intact cells (see Figure 7).

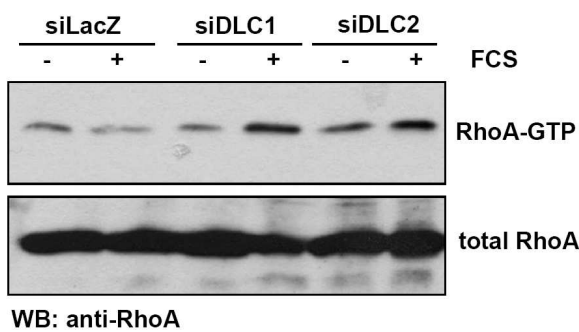


Figure 9: DLC1 and DLC2 knock-down increase cellular RhoA-GTP levels. MCF7 cells were transiently transfected with siRNAs specific for DLC1 and DLC2 or with LacZ-specific control siRNA. Three days after transfection, cells were starved in serum-free medium for 24 h and then either left untreated (-) or restimulated with 20% FCS for 5 min (+). RhoA-GTP was precipitated by incubation of total cell lysates with GST-RBD coupled to glutathione beads. Bound proteins were separated by SDS-PAGE and analyzed by Western blotting with RhoA-specific mAb (top); total RhoA levels were determined by immunoblotting of cell lysates with RhoA-specific antibody (bottom).

3.1.4 DLC1 depletion enhances stress fiber formation and focal adhesion assembly

Overexpression of DLC1 and DLC2 has been shown to cause cell detachment associated with the disassembly of stress fibers and focal adhesions (82; 85). To investigate whether the loss of endogenous DLC proteins influences the architecture of the actin cytoskeleton, we analyzed the structure of focal adhesions and stress fibers in siRNA-transfected MCF7 cells. Therefore, cells lacking DLC1 and DLC2 were stained with a paxillin-specific antibody and phalloidin to visualize focal adhesions and F-actin structures, respectively. Analysis by confocal microscopy revealed that silencing of DLC1 stabilized actin stress fibers and promoted an accumulation of focal adhesions located at the tips of these actin-myosin bundles (Figure 10). This was verified with a second independent siRNA for DLC1, proving that the effect was specific (data not shown). Surprisingly, cells lacking DLC2 demonstrated no obvious morphological changes and looked similar to siLacZ control cells (Figure 10).

Results

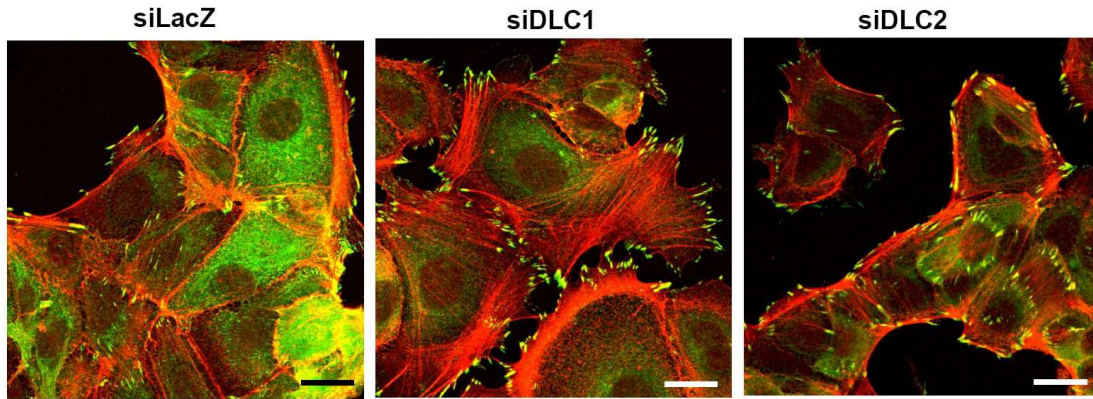


Figure 10: Loss of DLC1 enhances stress fiber formation and focal contact assembly. MCF7 cells were transiently transfected with siRNAs specific for DLC1 and DLC2 or with LacZ-specific control siRNA and replated onto collagen-coated glass coverslips three days after transfection. The next day, cells were fixed and stained with paxillin-specific primary and Alexa Fluor® 488-labeled secondary antibody (green). F-actin was visualized by costaining with Alexa Fluor® 546-labeled phalloidin (red). The confocal images shown are stacks of three to four sections taken from the bottom of the cell. Scale bars represent 20 μm .

3.1.5 Subcellular distribution of DLC1 and DLC2 in MCF7 cells

DLC1 has been reported to localize to focal adhesions, as shown by colocalization with the focal adhesion protein vinculin (70). Yeast-two-hybrid screenings identified DLC1 as a binding partner for members of the tensin family of focal adhesion proteins and this interaction has been proposed to be associated with biological activity (70-72). Since low expression levels and/or the quality of specific antibodies precluded visualization of the endogenous proteins we thus examined the subcellular distribution of DLC1 and DLC2 in MCF7 cells by transiently expressing GFP-tagged variants of the two proteins. Indirect immunostaining revealed that DLC1 colocalized with paxillin, whereas DLC2 failed to do so (Figure 11A). These distinct subcellular localizations are likely to provide an explanation for the effect of DLC1 silencing, and not that of DLC2, on stress fiber formation and focal adhesion assembly.

The DLC2 protein has been reported to localize to mitochondria in the hepatocellular carcinoma cell line Huh-7 as shown by colocalization and biochemical fractionation studies (67). To verify this finding, MCF7 cells transiently expressing GFP-DLC2 were labeled with MitoTracker®. As presented in Figure 11B, the GFP-DLC2 signal failed to colocalize with that of the MitoTracker® and was mainly detectable in the cytoplasm without any accumulation in a specific compartment. It is therefore possible that the targeting of DLC2 to mitochondria in Huh-7 cells is dependent on cell type-specific cofactors.

Results

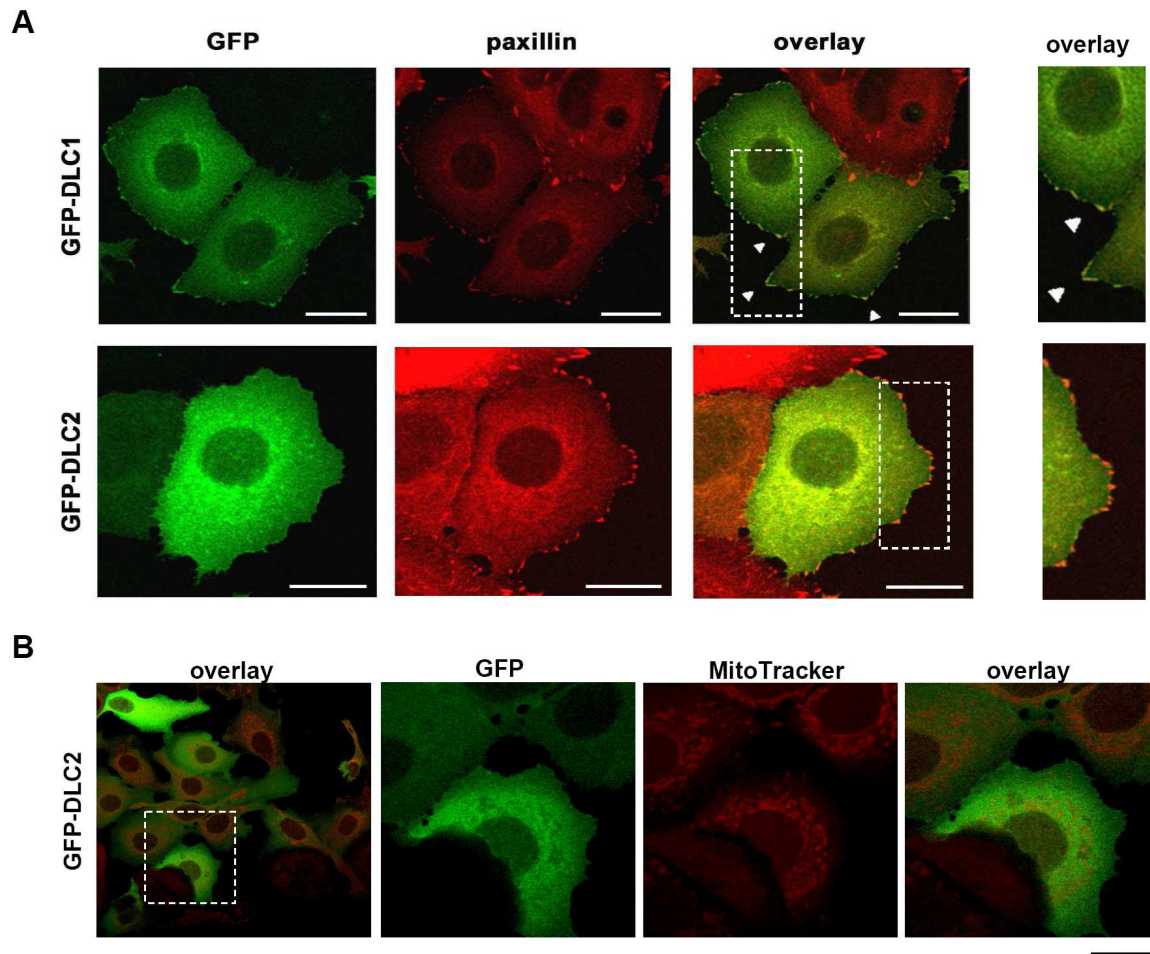


Figure 11: DLC1 localizes to focal adhesions whereas DLC2 neither targets to mitochondria nor to focal adhesions in MCF7 cells. (A) For subcellular localization studies, MCF7 cells were transiently transfected with expression vectors encoding GFP-DLC1 or GFP-DLC2. The next day, cells were fixed and stained with paxillin-specific primary and Alexa Fluor® 546–labeled secondary antibody (red). DLC1-positive focal adhesions are marked with arrowheads in the overlay. (B) To verify whether DLC2 localizes to mitochondria, MCF7 cells were transiently transfected with expression vectors encoding GFP-DLC2. The next day, cells were stained with Alexa Fluor® 546-coupled MitoTracker (red). (A and B) The confocal images shown are stacks of three to four sections. Scale bars represent 20 μm .

3.1.6 Down-regulation of DLC1 enhances cell migration

Rho proteins are important players in the regulation of cell motility [reviewed in (15; 14)]. To study the effect of DLC1 and DLC2 down-regulation on directed cell migration we performed scratch assays by wounding confluent monolayers of siRNA-transfected MCF7 cells. Compared to the siLacZ control, cells lacking DLC1 closed the wound more rapidly, whereas silencing of DLC2 had a slight inhibitory effect on the speed of wound closure (Figure 12A). This is quantified in Figure 12B: Cells lacking DLC1 closed 53% of the gap after 14 h and 67% after 24 h, compared to 27% and 38%, respectively, in the case of the siLacZ control.

Results

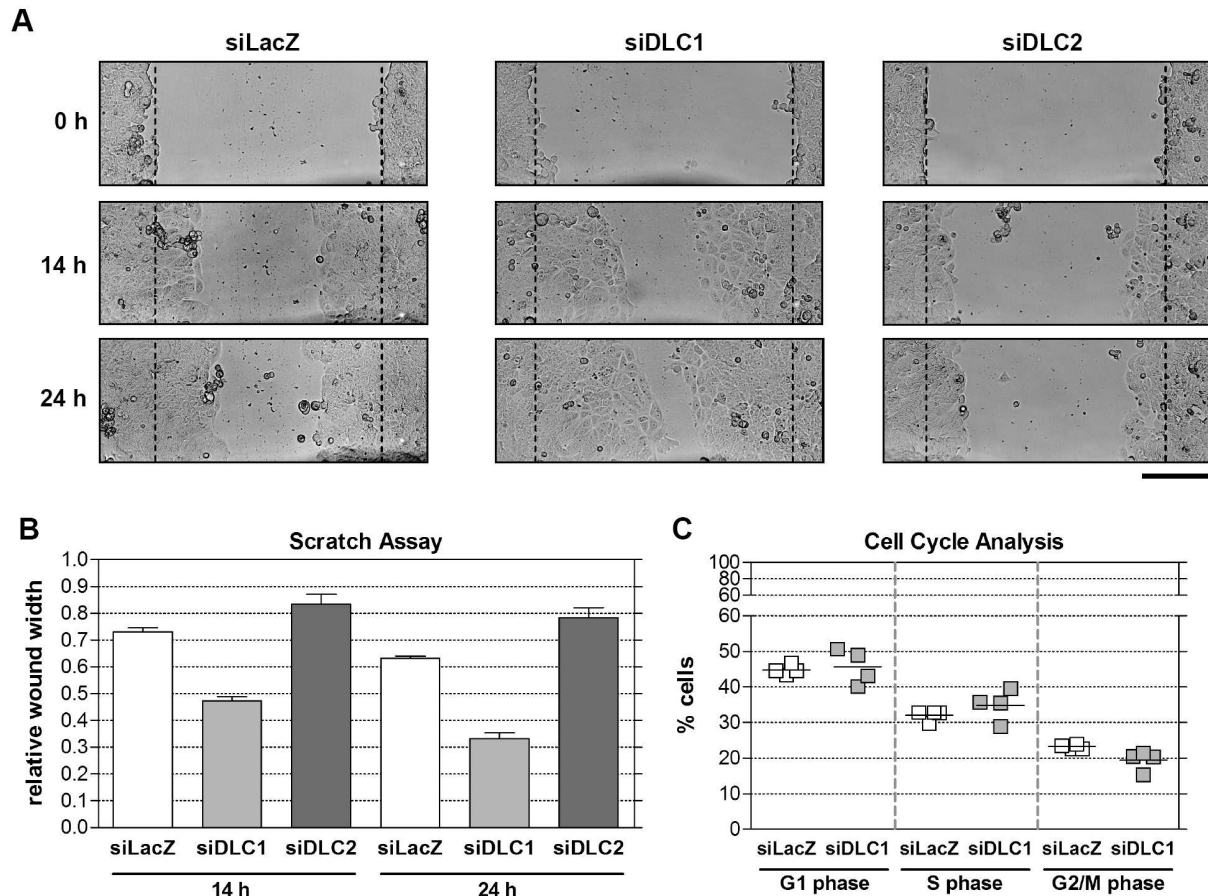


Figure 12: Knock-down of DLC1 enhances wound closure. (A) MCF7 cells were transiently transfected with siRNAs specific for DLC1 and DLC2 or with LacZ-specific control siRNA and replated onto collagen-coated dishes two days after transfection. The next day, confluent monolayers were scratched with a white pipette tip. Pictures were taken at a 10-fold magnification to document the scratch at time point zero (dashed line) and after incubation for 14 h and 24 h. The scale bar represents 200 μm . (B) Quantification of wound closure in MCF7 cells transfected with DLC1-, DLC2- and LacZ-specific siRNAs. Three independent positions of the wounded cell monolayers were photographed at time point zero, after incubation for 14 h, and 24 h and the width of the scratch was determined at 10 different positions per picture. The wound width after 14 h and 24 h were normalized to the width at time point zero. Bars, SEM. (C) Cell cycle analysis of MCF7 cells transiently transfected with siRNA specific for DLC1 or with LacZ-specific control siRNA. Three days post transfection cells were fixed and stained with propidium iodide. The distribution of G1-, S- and G2/M-phases of the cell population was determined by flow cytometry. The shown data points represent the results of four independent experiments.

Results

Given the proposed importance of Rho GTPases in cell cycle progression (86), we wanted to rule out the influence of DLC1 depletion on cell proliferation, which could also lead to enhanced wound closure. Therefore, we performed cell cycle analysis with siRNA-transfected MCF7 cells. Comparison of DLC1 knock-down with siLacZ control cells did not reveal any significant differences in the percentages of cells in G1, S and G2/M phases of the cell cycle (Figure 12C). MTT proliferation assays performed by Johanna Heering further confirmed that DLC1-depleted cells displayed growth properties resembling those of siLacZ control cells (data not shown). These data suggest that the enhanced wound closure ability of DLC1-deficient cells is indeed due to an accelerated migratory capacity of the cells.

To address the question how DLC proteins affect chemotaxis in the presence of a serum gradient we measured cell motility in transwell assays with 0.5% serum in the upper and 10% serum in the lower chamber. In MCF7 cells, the loss of DLC1 typically stimulated migration 3-fold compared to the siLacZ control (Figure 13A,B). A second DLC1-specific siRNA (see Western blot in Figure 14D) equally enhanced cell migration, confirming that the effect was due to the knock-down of DLC1 (Figure 14A). In line with the wounding experiments, silencing of DLC2 had no effect on serum-induced chemotaxis (Figure 13A,B). The failure of DLC2 knock-down to enhance cell motility in wounding and transwell assays was verified with an independent siRNA (Figure 14B,C and E).

To confirm these data with a second cell line, we performed transwell assays with MDA-MB 436 cells that also express both DLC genes (see Figure 8A). Consistent with the results in MCF7 cells, down-regulation of DLC1 enhanced cell migration, whereas depletion of DLC2 had no effect on the migratory behavior of the cells (Figure 13C,D). Efficient silencing of the DLC proteins in MDA-MB 436 cells is demonstrated by semi-quantitative RT-PCR and by Western blotting (Figure 13 E to G).

Results

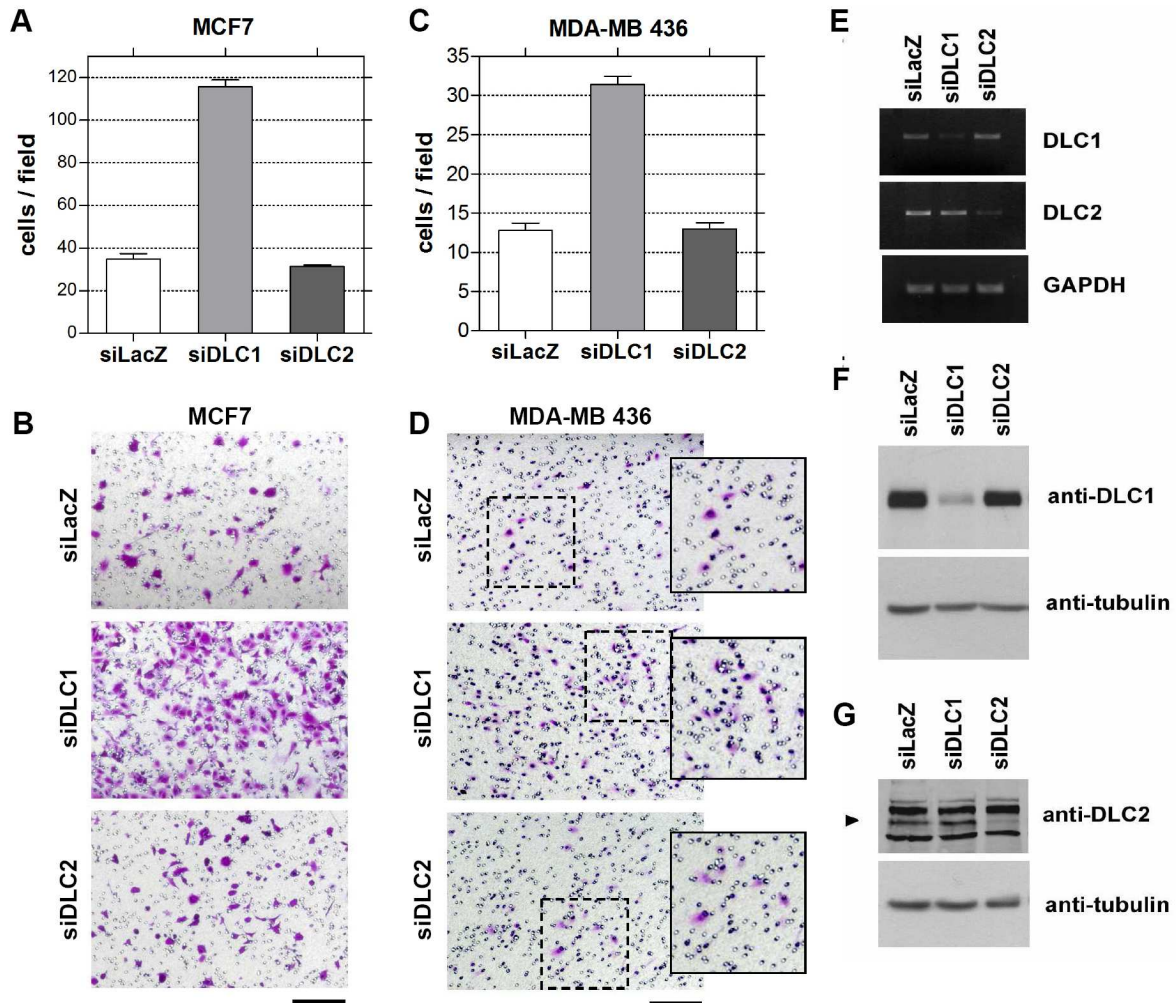


Figure 13: Down-regulation of DLC1 but not DLC2 stimulates migration of MCF7 and MDA-MB 436 cells. MCF7 (A and B) and MDA-MB 436 cells (C and D) were transiently transfected with siRNAs specific for DLC1 and DLC2 or with LacZ-specific control siRNA. Three days after transfection, 1×10^5 cells were seeded in medium containing 0.5% FCS into the upper chamber of a transwell. The lower well contained medium supplemented with 10% FCS. Cells that had migrated across the filter after overnight incubation (MCF7 cells) and after 4 h (MDA-MB 436 cells) were fixed and stained with crystal violet (B and D). The number of migrated cells was determined by counting five independent microscopic fields (20-fold magnification). Columns correspond to the mean of duplicate wells and are representative of at least three independent experiments; bars represent SEM. In the individual experiments, the fold increase of migration for siDLC1 versus control cells was 3.31, 3.23, 2.00, and 2.83, respectively, for MCF7 cells and 2.45, 1.92 and 1.88, respectively, for MDA-MB 436 cells. (E to G) Silencing efficiency in siRNA-transfected MDA-MB 436 cells was verified three days after transfection by semi-quantitative RT-PCR (E) as described in Figure 8. (F and G) Equal amounts of total cell lysates were subjected to SDS-PAGE and transferred to membrane. DLC expression was analyzed by immunoblotting using a DLC1- and DLC2-specific antibody (top). Reprobing the membrane with tubulin-specific antibody verified equal loading (bottom).

Results

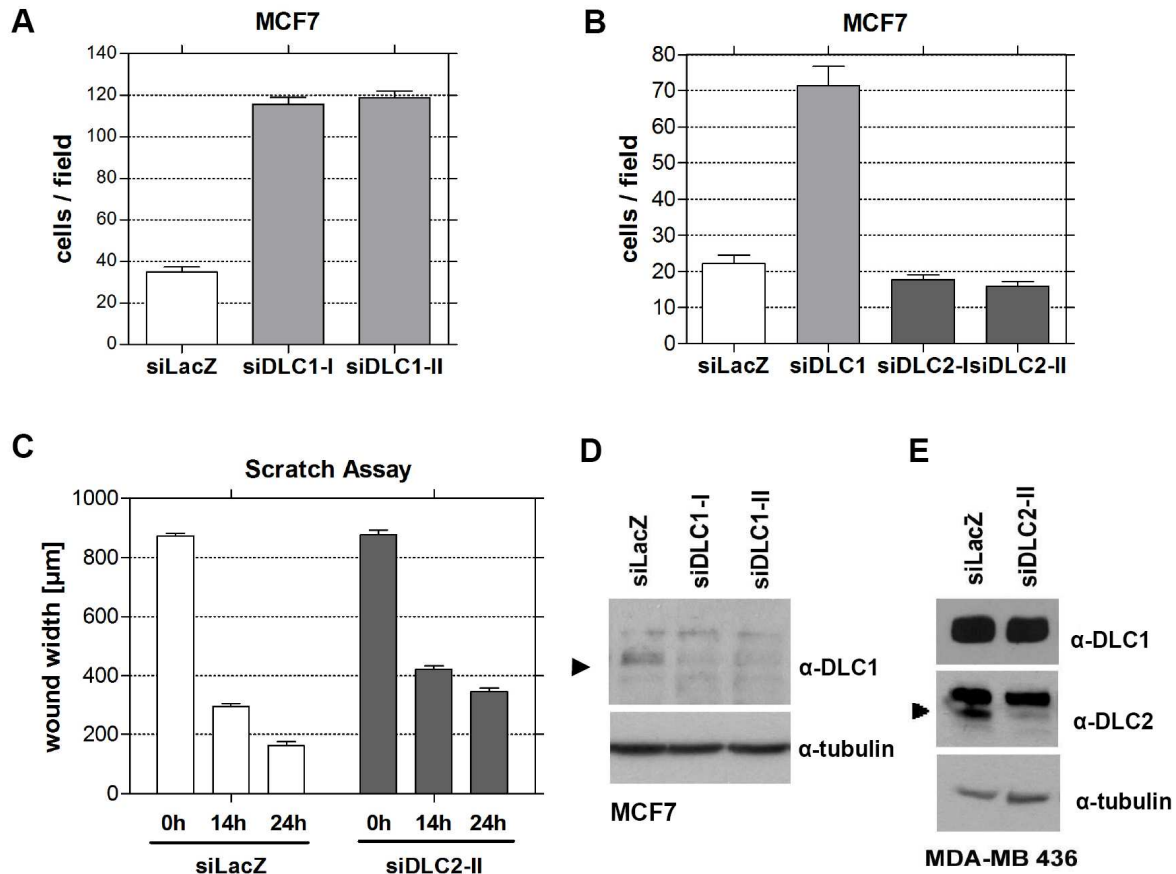


Figure 14: Verification of migration assay results with independent siRNAs for DLC1 and DLC2. MCF7 (A-D) and MDA-MB436 (E) cells were transiently transfected with the indicated siRNAs. (A and B) Cells were harvested three days post transfection and 1×10^5 cells were seeded in medium containing 0.5% FCS into the upper chamber of a transwell. The lower well contained medium supplemented with 10% FCS. Cells that had migrated across the filter after overnight incubation were fixed and stained with crystal violet. The number of migrated cells was determined by counting five independent microscopic fields (20-fold magnification). Data shown are the mean of duplicate wells; error bars represent SEM. The mean fold induction of three independent experiments for siDLC1-II versus siLacZ cells was 2.597 ± 0.0523 SEM. (C) MCF7 cells were harvested two days after transfection and wounding assays were performed and quantified as described in Figure 12. (D and E) DLC1 and DLC2 expression (top panels) were evaluated by Western blotting three days post transfection as described in Figure 8 and 13. The blot in D corresponds to the full blot shown in Figure 8C. Reprobing of the membrane with tubulin-specific antibody verified equal loading (bottom).

3.1.7 DLC1 knock-down cells does not increase the invasive behavior of breast cancer cells

Given the role of DLC1 in cell migration, it is possible that it also plays a role in regulating cell invasion. To answer this question, we performed invasion assays using basement membrane extract (BME)-coated transwells. As shown in Figure 15, DLC1 depletion neither enhanced the invasive behavior of the breast cancer cell lines MCF7 (A) and MDA-MB 436 (B), which

Results

are poorly invasive, nor that of the highly invasive MDA-MB 231 (C) cell line, compared to the control siLacZ.

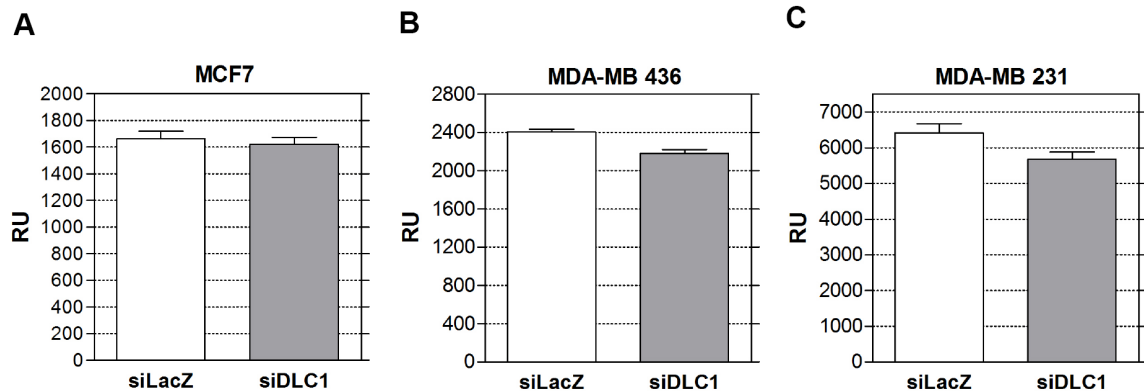


Figure 15: DLC1 knock-down does not enhance invasiveness of breast cancer cell lines. Low-invasive MCF7 (A) and MDA-MB 436 (B) cells as well as invasive MDA-MB 231 (C) cells were transiently transfected with siRNAs specific for DLC1, or with LacZ-specific siRNA as a control. Three days post transfection, 1×10^5 cells were seeded in medium containing 0.5% FCS into the upper chamber of a basement membrane extract (BME)-coated transwell. The lower well contained medium supplemented with 10% FCS. After incubation for one day, cells that had migrated across the filter were incubated in cell dissociation solution and Calcein AM. Cellular esterases hydrolyze Calcein AM into the fluorescent calcein. The plate was read at 520 nm (excitation, 485 nm). Data shown are the mean of the relative fluorescence units (RU) \pm SEM of duplicate wells and are representative of two independent experiments.

3.1.8 DLC1 controls cell migration by modulation of Dia1 signaling

The multiple functions of RhoA are mediated by its downstream effectors, the major ones being the Rho kinase (ROCK) and Dia1, the mammalian ortholog of *Drosophila* diaphanous 1. Rho stimulates actin polymerization through activation of Dia1, which promotes addition of actin monomers to the barbed end of actin filaments (87). Dia1 acts together with ROCK to mediate Rho-induced stress fiber formation (88). ROCK phosphorylates and activates LIM kinase, leading to the inhibition of the actin-depolymerizing factor cofilin (23). In addition, ROCK induces actomyosin-based contractility through phosphorylation-induced inactivation of myosin light chain phosphatase (89).

To identify the molecular pathway underlying DLC1 inhibition of cell migration, we utilized the pharmacological inhibitors Y27632 and H1152 to specifically inactivate ROCK. These inhibitors were added to siRNA-transfected MCF7 cells in the upper chamber of the transwells and the number of migrated cells was then quantified. As shown in Figure 16A, migration of cells lacking DLC1 was not affected by the presence of either ROCK inhibitor. We next depleted Dia1 using a siRNA that was used previously to show that Dia1 is crucial for stroma cell-derived factor 1 α -induced migration of rat glioma cells (25). Efficient silencing

Results

of Dia1 in MCF7 cells was confirmed by Western blot analysis (Figure 16C). Interestingly, simultaneous down-regulation of Dia1 and DLC1 completely abrogated cell migration resulting from DLC1 knock-down, while knock-down of Dia1 alone did not affect basal cell migration (Figure 16B). A second Dia1-specific siRNA (siDia1-II) confirmed these results (Figure 16B).

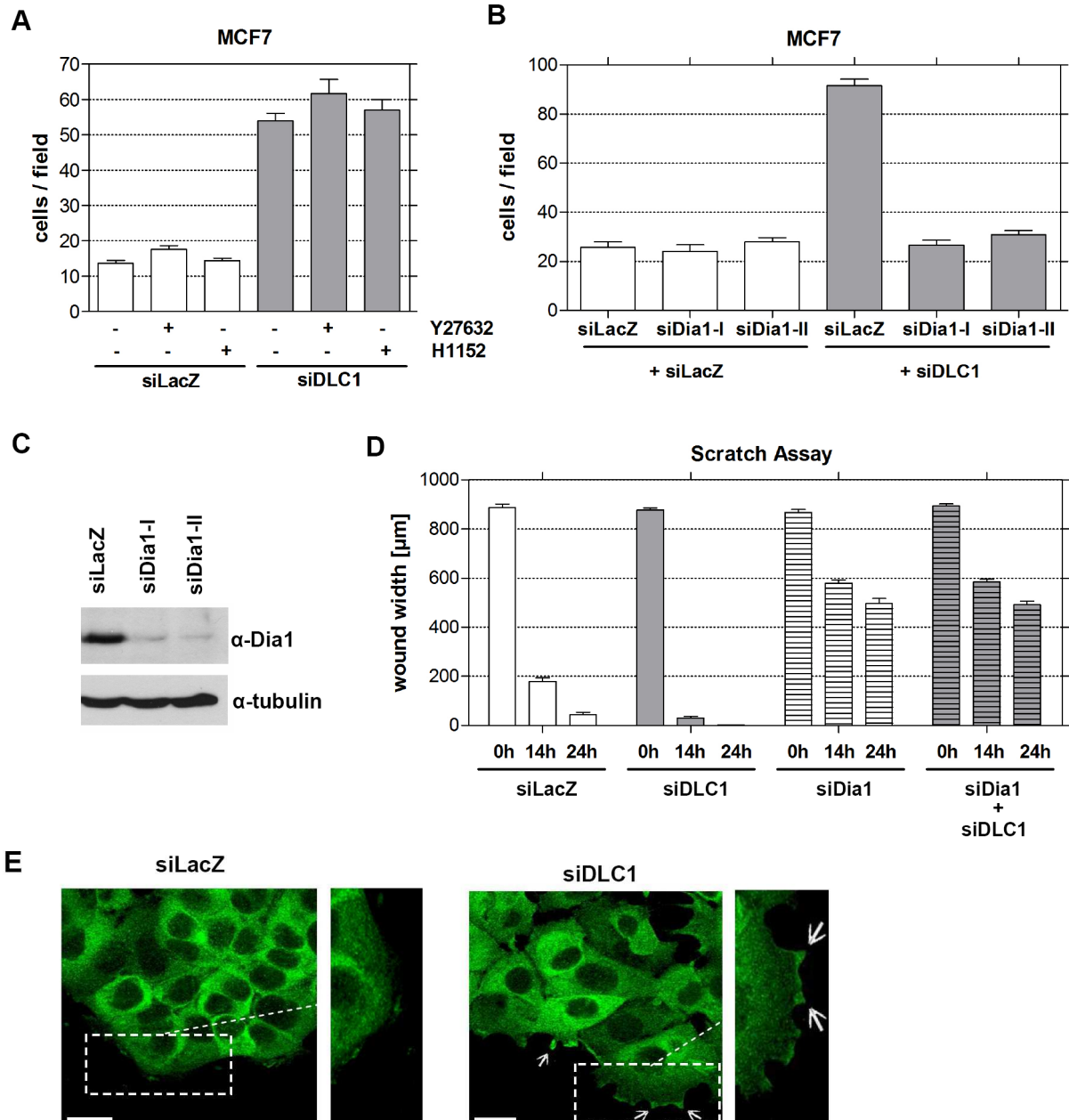


Figure 16: Migration of DLC1-depleted cells requires Dia1. Figure legend: see next page.

Results

Figure 16: Migration of DLC1-depleted cells requires Dia1. (A) MCF7 cells were transiently transfected with siRNAs specific for DLC1 or LacZ. Three days after transfection, 1×10^5 cells were seeded into the upper chamber of a transwell in medium containing 0.5% FCS (-) plus 10 μ M Y27632 or 1 μ M H1152, respectively. The lower well contained medium supplemented with 10% FCS. The number of migrated cells after overnight incubation was determined by counting five independent microscopic fields (20-fold magnification). Columns correspond to the mean of duplicate wells; bars represent SEM. A representative experiment out of two is shown. (B) MCF7 cells were transiently transfected with siRNAs specific for LacZ, DLC1, Dia1, and DLC1 plus Dia1 at a 1:1 ratio. The siRNA amount in each transfection mix was adjusted with LacZ siRNA. Two different siRNAs targeting Dia1 were used (siDia1-I and siDia1-II). MCF7 cells were harvested three days after transfection and subjected to migration assays as described in Figure 12. A representative experiment out of three is shown. Columns correspond to the mean of duplicate wells; bars represent SEM. The mean fold induction of three independent experiments for siDLC1 versus siLacZ cells was 2.902 ± 0.063 SEM. Values for siDLC1 versus siDLC1 + siDia1-I were statistically different (two tailed unpaired t test, $P < 0.0001$) and were confirmed with a second independent siRNA targeting Dia1 (siDia1-II). (C) MCF7 cells were transiently transfected with the indicated siRNAs. Silencing efficiency of the independent Dia1-specific siRNAs (siDia1-I and siDia1-II) was verified three days post transfection by immunoblotting of cell lysates using Dia1-specific polyclonal antibody (top panel). Equal loading was verified by reprobing the membrane with tubulin-specific antibody (bottom panel). (D) MCF7 cells were harvested two days after transfection and wounding assays were performed and quantified as described in Figure 12. (E) MCF7 cells transfected with siLacZ and siDLC1 were replated onto collagen-coated coverslips and confluent monolayers were wounded with a pipette tip. Cells were fixed 6 h later and stained with a Dia1-specific mAb and Alexa Fluor® 488–conjugated secondary antibody. Arrows indicate Dia1-positive membrane protrusions. Images are stacks of three to four confocal sections. Scale bar, 20 μ m.

We also tested whether silencing of Dia1 prevents the increased migration of cells lacking DLC1 in scratch assays. Dia1 knock-down reduced basal cell motility under these conditions, and in line with the transwell migration assays, completely blocked increased motility of DLC1-depleted cells (Figure 16D).

It has been reported, that Dia1 mediates actin polymerization at the leading edge of migrating cells. To further demonstrate an involvement of Dia1 we analyzed its localization in siRNA-transfected MCF7 cells. Immunostaining of a wounded monolayer with anti-Dia1 antibody revealed that Dia1 accumulated in membrane protrusions of migratory cells at the wound edge, which were especially prominent in cells lacking DLC1 (Figure 16E). Accordingly, our data indicate a dominant role of Dia1 rather than ROCK in promoting migration of breast carcinoma cells.

Next, we wanted to identify the Rho isoform which drives the migration of DLC1-depleted cells. We performed transwell migration assays with cells simultaneously lacking DLC1 and RhoA, RhoC or Cdc42, respectively. Surprisingly, knock-down of both RhoA and RhoC increased cell migration and did not prevent migration of cells lacking DLC1 (Figure 17B), suggesting that these Rho isoforms are not the main mediators of cell migration in the absence of DLC1. However, silencing of RhoA/C also reduced DLC1 expression levels,

Results

making interpretation of results difficult (Figure 17A). Because it is unlikely that both siRNAs have the same non-specific effect, this observation may indicate that DLC1 protein levels are regulated by RhoA/C expression in a feedback manner. Interestingly, down-regulation of Cdc42 partially inhibited migration of cells lacking DLC1 (Figure 17B). Although ectopic DLC1 expression did not lead to measurable GTP hydrolysis of the Raichu-Cdc42 biosensor, regulation of endogenous Cdc42 by DLC1 cannot be ruled out. It is also possible that the effect of Cdc42 down-regulation on migration of cells lacking DLC1 is indirect, as Dia1 has been reported to contribute to localization of Cdc42 to the leading edge of migrating cells (25). Unlike Dia2 and Dia3, Dia1 is not a characterized Cdc42 effector, making future studies necessary to address which Rho protein is responsible for promoting cell migration in DLC1-depleted cells.

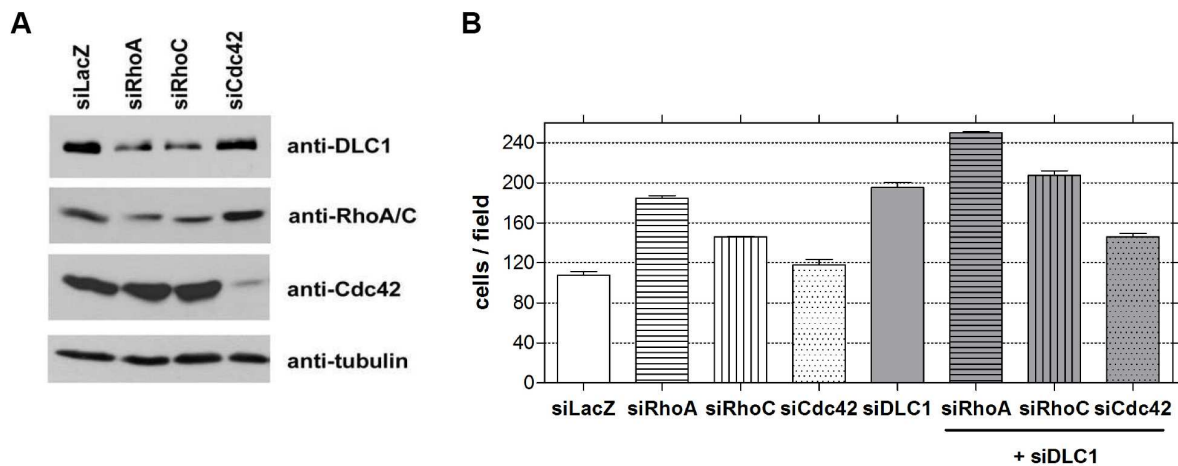


Figure 17: The role of RhoA, RhoC and Cdc42 in DLC1 signaling. (A) MCF7 cells were transiently transfected with the indicated siRNAs. Silencing efficiency and specificity was verified three days post transfection by immunoblotting of cell lysates using DLC1-specific antibody (top panel), and RhoA- and Cdc42-specific antibodies (middle panels). The RhoA-specific polyclonal antibody used recognizes mainly RhoA and RhoC, which do not migrate as distinct bands due to their similar molecular weight. When RhoA is silenced, RhoC can be visualized as the faster migrating band and vice versa. Equal loading was verified by immunoblotting with tubulin-specific antibody (bottom panel). (B) MCF7 cells were transiently transfected with the indicated siRNAs. The siRNA amount in each transfection mix was adjusted with LacZ siRNA. Cells were harvested three days post transfection and 1×10^5 cells were seeded in medium containing 0.5% FCS into the upper chamber of a transwell. The lower well contained medium supplemented with 10% FCS. Cells that had migrated across the filter were fixed and stained. The number of migrated cells was determined by counting five independent microscopic fields (20-fold magnification). Data shown are the mean of duplicate wells and are representative of two independent experiments; error bars: SEM.

3.2 Chapter 2

3.2.1 Exogenously expressed DLC3 shows GAP activity for RhoA

The structurally conserved DLC3 gene is the most recently cloned DLC family member. According to *in vitro* GAP assays performed with purified bacterial protein, the GAP specificity of DLC3 is similar to that of DLC1 and DLC2, with highest activity observed for RhoA, moderate activity for Cdc42 and none for Rac1 (90).

To investigate DLC3 GAP activity in intact cells, we performed experiments in HEK293T cells using the FRET-based RhoA biosensor (see section 3.1.1) and compared the substrate specificity of DLC3 with that of DLC1. Cells were transfected with expression vectors for DLC1 and the two DLC3 isoforms alpha and beta, respectively, along with the Raichu-RhoA biosensor. As presented in Figure 18A, DLC3 alpha as well as beta strongly attenuated the emission ratio of the biosensor (FRET/CFP), which is proportional to RhoA activity. Both proteins accelerated GTP hydrolysis of RhoA stronger than DLC1 did. As a negative control, inactive DLC1 (DLC1-K714E) was used, which only had a minimal effect on the FRET/CFP ratio compared to cells transfected with the vector control. This experiment thus shows that both exogenously expressed DLC3 variants possess *in vivo* GAP activity for RhoA.

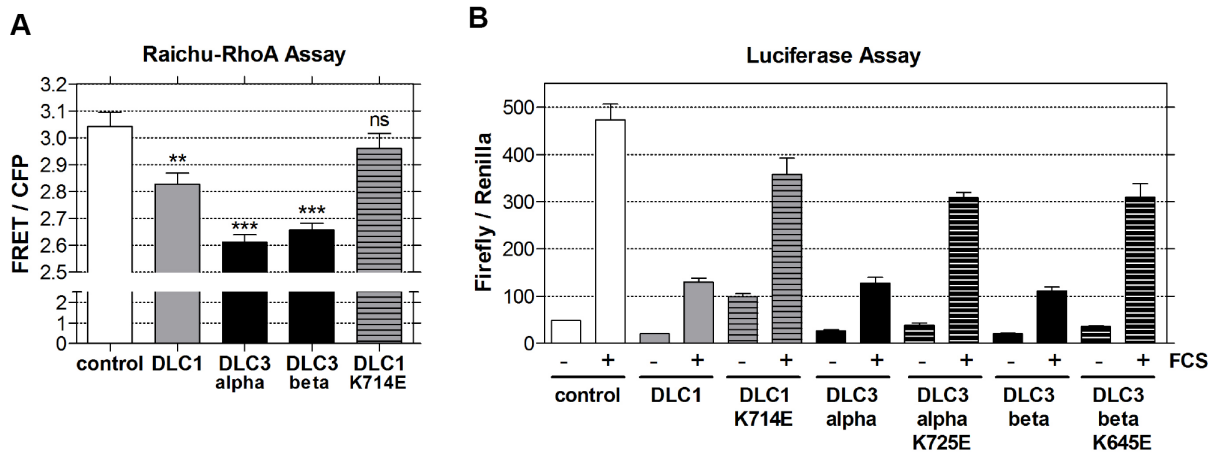


Figure 18: DLC1 and DLC3 alpha/beta inhibit Rho signaling in intact cells. (A) For RhoA activity measurements HEK293T cells were cotransfected with plasmids encoding the Raichu-RhoA biosensor and DLC1, DLC1-K714E or DLC3 alpha/beta isoforms. The next day, cells were lysed and the ratio of FRET/CFP emission was determined by measuring CFP and YFP fluorescence. Data shown represent the mean of three independent experiments performed with triplicate samples; bars, SEM. The values for DLC1, DLC3 alpha and DLC3 beta versus the control were statistically significant (two-tailed unpaired t test, DLC3 alpha/beta: $P < 0.0001$; DLC1: $P < 0.05$), whereas those for DLC1-K714E were not (ns, $P = 2.899$). (B) HEK293T cells were transfected with a SRF-responsive firefly

Results

luciferase reporter along with plasmids encoding *Renilla* luciferase and DLC1, DLC3 alpha/beta or their GAP-inactive mutants DLC1-K714E, DLC3 alpha-K725E, DLC3 beta-K645E, respectively, starved overnight and then either left untreated (-) or stimulated with serum (+) for 6 h. The firefly and *Renilla* luciferase activity were assayed in cell lysates of triplicate samples. SRF activity corresponds to the ratio of firefly luciferase and *Renilla* activity. One representative experiment out of three is shown; bars, SEM.

To examine the impact of DLC3 alpha and beta on endogenous RhoA activity, we determined their ability to block serum response factor (SRF)-mediated transcription (84). HEK293T cells were transfected with DLC3 alpha, beta or DLC1 expression plasmids along with a SRF-responsive luciferase reporter. Next, cells were starved overnight and restimulated with serum. As shown in Figure 18B, DLC3 alpha, beta as well as DLC1 wild type proteins suppressed SRF-dependent transcription in a similar fashion. This can be attributed to the GAP activity of the proteins since the inactive protein variants harboring a point mutation in their GAP domain (DLC1-K714E, DLC3 alpha-K725E and DLC3 beta-K645E) only had a minimal reducing effect on luciferase reporter levels compared to the control. These results support the data obtained with the Raichu-RhoA biosensor (Figure 18A) and demonstrate that both DLC3 proteins target endogenous RhoA.

3.2.2 DLC3 is located in focal adhesions and disrupts actin stress fibers

To determine the subcellular compartment to which the DLC3 proteins localize in breast epithelial cells, MCF7 cells were transiently transfected with expression plasmids encoding GFP-tagged DLC3 alpha and beta, fixed the next day and microscopically analyzed. Ectopic expression of both DLC3 isoforms had dramatic effects on cell morphology (Figure 19, left): It decreased the number of stress fibers, the cells became more rounded and formed long actin-based extensions, making localization analyses impossible. Such morphological changes have been reported previously and were shown to be due to the GAP activity of DLC3 (90). In accordance with this report cells expressing inactive variants of DLC3 alpha and beta (K725E and K645E, respectively) did not show these morphological alterations (Figure 19, right). Here, besides some cytoplasmic staining, an extensive accumulation to punctuate spots in the cell periphery became obvious, which indicated localization to focal adhesions (Figure 19, top). Paxillin staining revealed a complete overlap with the dot-like pattern of the GFP-DLC3 alpha and beta signals, indicating that both DLC3 isoforms are indeed targeted to these cellular structures in breast cancer cells (Figure 19).

Results

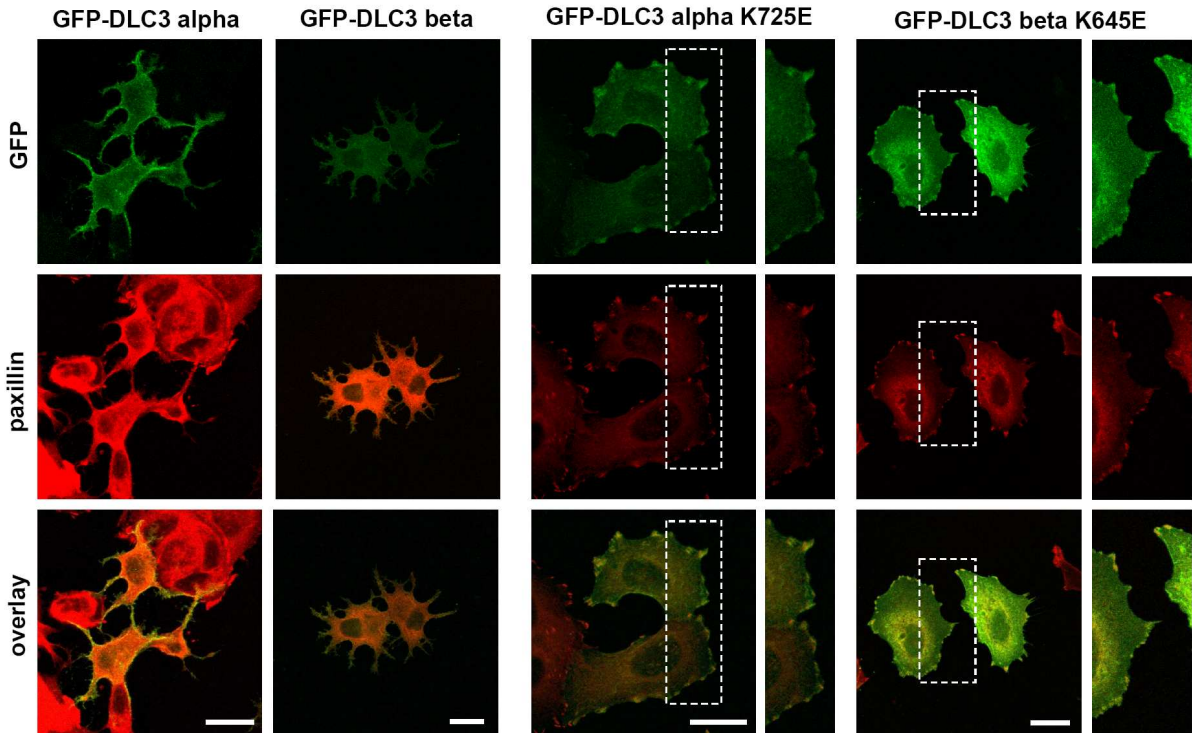


Figure 19: The DLC3 isoforms alpha and beta are located to focal adhesions. For subcellular localization studies, MCF7 cells, grown on collagen-coated glass coverslips, were transiently transfected with expression vectors encoding GFP-DLC3 alpha/beta or their GAP-inactive mutants DLC3 alpha-K725E and DLC3 beta-K645E (green). The next day, cells were fixed and stained with paxillin-specific antibody and Alexa Fluor® 546-labeled secondary antibody (red). Images of the cells were obtained using a confocal laser scanning microscope and represent stacks of three to four sections taken from the bottom of the cell. Scale bars represent 20 μm .

Due to the lack of commercially available DLC3 antibodies, we raised a polyclonal DLC3 peptide antibody to validate the localization in focal adhesions for endogenous DLC3 proteins. This antibody detected overexpressed DLC3 proteins in Western blots (data not shown), but due to the presence of numerous non-specific bands we could not reliably visualize endogenous DLC3 neither by immunoblotting nor by immunostaining. Nevertheless, in agreement with our overexpression studies Kawai and coworkers, observed the presence of endogenous DLC3 alpha in focal adhesions of HeLa cells as well as in HepG2 and Swiss 3T3 cells (90). Furthermore, it has been shown that DLC3 binds both the Src homology 2 (SH2) domain and the phosphotyrosine binding (PTB) domain of tensin1, a protein that localizes to the cytoplasmic side of focal adhesions (71).

Since, DLC3 and DLC1 not only target the same intracellular compartment but further have the same substrate specificity in intact cells, this may indicate that they have similar biological functions. To test this presumption, we performed RNAi experiments to analyze the cellular functions of endogenous DLC3.

3.2.3 DLC3 expression in breast cancer cell lines

We first examined DLC3 transcription levels in a panel of breast cancer epithelial cells by semi-quantitative RT-PCR. As shown in Figure 20A, DLC3 mRNA was low or absent in a significant number of breast cancer cell lines (e.g. MCF10A, BT474, and MDA-MB 435). Of note, the DLC3-specific primers chosen amplify both alpha and beta isoforms. As a prerequisite for RNAi experiments, we selected a DLC3 expressing cell line for further analysis. We chose MCF7 cells, although they expressed only moderate levels of the DLC3 transcript, since we yielded high transfection efficiencies in former RNAi studies, the experimental setups are well-established, and using the same cell line makes the results more comparable to those obtained for DLC1.

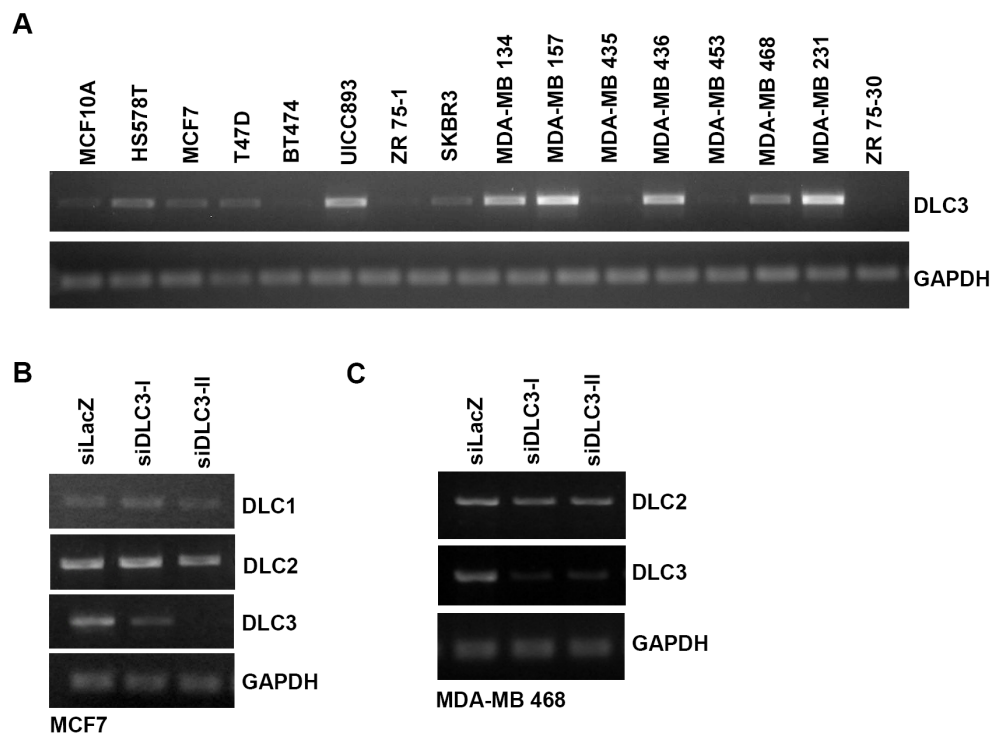


Figure 20: Expression analysis of DLC3 in breast cancer cell lines and RNAi-mediated silencing of DLC3 in MCF7 and MDA-MB 468 cells. (A) Semi-quantitative RT-PCR analysis of the DLC3 gene in a panel of breast cancer cell lines. RNA of the indicated breast epithelial cell lines was isolated, reverse transcribed into cDNA and then amplified using DLC3-specific primers that span introns in the genomic sequence (top). GAPDH was amplified as a loading control (bottom). (B and C) To verify the specificity and efficiency of two distinct siRNAs targeting DLC3 (siDLC3-I and siDLC3-II), MCF7 (B) and MDA-MB 468 cells (C) were either transiently transfected with the DLC3-specific siRNAs or siLacZ as a control. Three days post transfection, expression of the DLC genes (top panels) was evaluated by semi-quantitative RT-PCR. GAPDH was amplified as a loading control (bottom).

3.2.4 Efficient and specific silencing of DLC3

Two siRNAs targeting different regions of the DLC3 transcript (siDLC3-I and siDLC3-II) were designed and tested for their silencing efficiency and specificity. Cells were transfected with these siRNAs and the expression levels of the three DLC family members were analyzed by semi-quantitative RT-PCR three days later (Figure 20B). Both siRNAs were efficient and selective, since knock-down of DLC3 decreased the DLC3 gene transcription level but neither influenced DLC1 nor DLC2 transcript levels, in comparison to the siLacZ control (Figure 20B). In addition, we obtained the same results in the breast cancer cell lines MDA-MB 436 (data not shown) and the DLC1-negative MDA-MB 468 (Figure 20C). Since the polyclonal DLC3 peptide antibody detected numerous non-specific proteins on immunoblots (data not shown), it was not possible to demonstrate DLC3 silencing on the protein level.

3.2.5 DLC3 depletion increases chemotactic migration but not migration in wounding assays

The GAP-dependent effect of ectopically expressed DLC3 on the actin cytoskeleton together with its localization in focal adhesions suggest a possible role for DLC3 in regulating cellular motility via the control of Rho GTPase activity. To prove this assumption, we performed two different assays to analyze the migratory behavior of DLC3-depleted cells, scratch assays and transwell assays.

In scratch assays, a confluent monolayer of siRNA-transfected cells was wounded and the efficiency of wound closure was monitored at different time points. As Figure 21A shows, DLC1-deficient cells closed the wound more rapidly than the siLacZ control, whereas MCF7 cells lacking DLC3 failed to do so. To confirm these data with a second cell line, we performed wounding experiments with the DLC1-negative cell line MDA-MB 468. In contrast to MCF7 cells, wounding of cell monolayers did not induce a synchronized movement of the cells as a sheet. Rather, the cells migrated as loosely associated clusters, making the precise determination of the wound width difficult. However, comparing the pictures in Figure 21B, it is apparent that cells lacking DLC3 closed the wound to a similar extent as the control cells.

Results

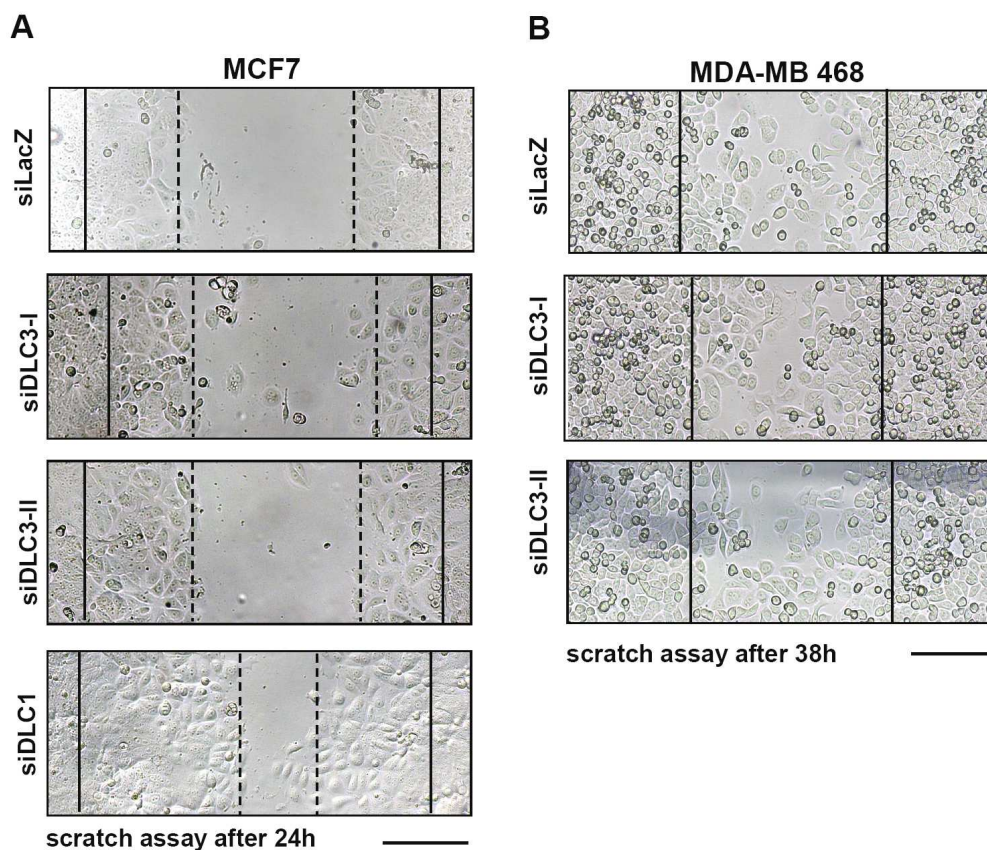


Figure 21: Loss of DLC3 does not enhance wound closure in MCF7 and MDA-MB 468 cells. MCF7 (A) and MDA-MB 468 cells (B) were transiently transfected with two distinct siRNAs specific for DLC3 (siDLC3-I and siDLC3-II) or with LacZ-specific siRNA as a control. In addition, siDLC1-transfected cells were used as a positive control for enhanced wound closure in MCF7 cells (A). Two days post transfection cells were replated onto collagen-coated dishes. The next day, confluent monolayers were scratched with a pipette tip and washed three times with growth medium to remove detached cells. Pictures were taken at a 10-fold magnification the scratch at time point zero (solid lines in A and B) and after incubation for 24 h (MCF7 cells; dashed lines) or 38h (MDA-MB 468 cells; dashed lines), respectively. Scale bars, 200 μ m. Data shown correspond to one representative experiment out of two.

A different approach to study directed cell migration are chemotactic transwell assays, where cells are seeded into an upper chamber and are required to migrate as single cells through membrane pores to reach a bottom chamber containing a soluble attractant (10% serum). In contrast to wound-healing assays, DLC3-depleted MCF7 cells displayed a significantly higher (in average: 2-fold higher) migratory behavior in these transwell assays than the siLacZ control (Figure 22A). We concluded that only in combination with a strong chemoattractant is the depletion of DLC3 sufficient to stimulate cell migration. In line with the experiments performed in MCF7 cells, the DLC1-negative MDA-MB 468 cells also displayed an increased chemotactic behavior after DLC3 knock-down (Figure 22B).

Results

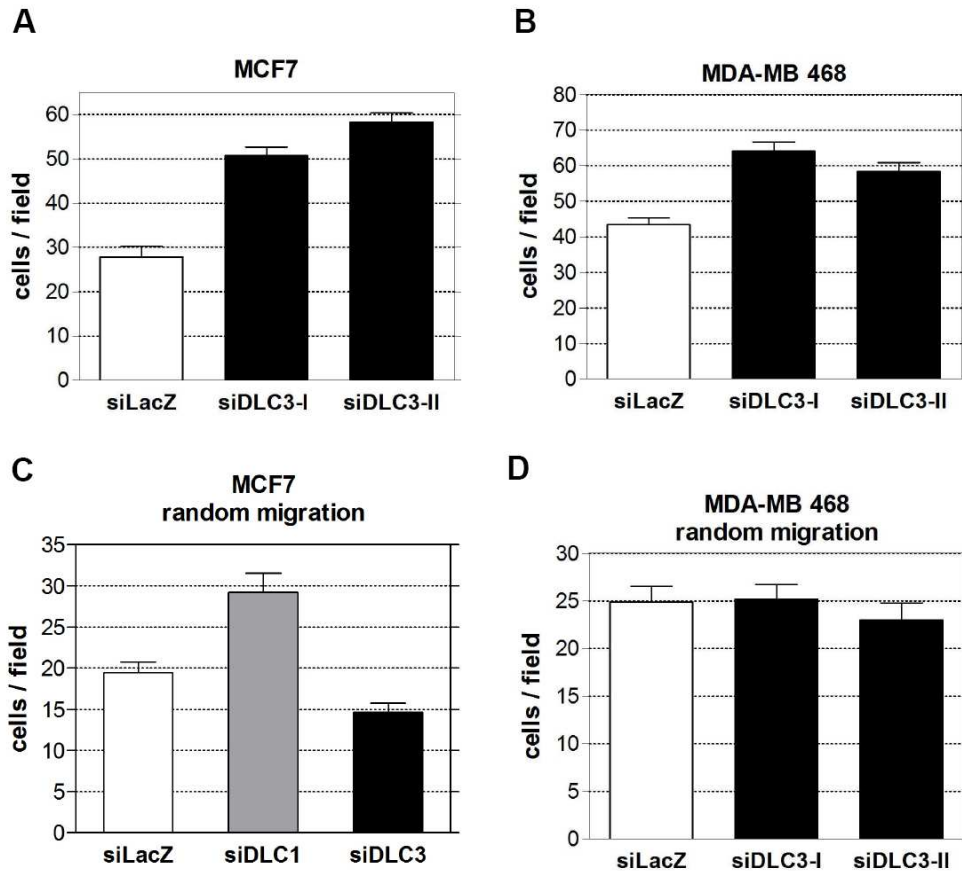


Figure 22: Down-regulation of DLC3 stimulates chemotaxis in MCF7 and MDA-MB 468 cells but does not induce random cell migration. MCF7 (A) and MDA-MB468 cells (B) were transiently transfected with siRNAs specific for DLC3 (siDLC3-I and siDLC3-II), or with siLacZ control. Three days post transfection, 1×10^5 cells were seeded in medium containing 0.5% FCS into the upper chamber of a transwell. The lower well contained medium supplemented with 10% FCS. Cells that had migrated across the filter were fixed and stained after overnight incubation (MCF7; A) or after 3 hours (MDA-MB 468; B). Data shown are the mean \pm SEM of duplicate wells and are representative of three independent experiments. The mean fold induction of three experiments was 1.684 ± 0.065 SEM (MCF7 cells) and 1.639 ± 0.042 SEM (MDA-MB 468 cells) for siDLC3-I versus siLacZ cells. Values for siDLC3-I and siDLC3-II versus the siLacZ control were statistically significant (two-tailed unpaired t test; $P < 0.001$). Random cell migration of siDLC3-transfected MCF7 (C) and MDA-MB 468 cells (D). Cells were prepared as described in (A) and (B) but migration was performed in the absence of a chemotactic agent. Upper and lower chambers contained 0.5% FCS and filters were coated with collagen on both sides. (A-D) The number of migrated cells was determined by counting five independent microscopic fields (20-fold magnification). Data shown are the mean \pm SEM of duplicate wells and are representative of at least two independent experiments.

3.2.6 DLC3 knock-down does not stimulate random migration

In contrast to wound-healing assays, where the synchronized movement of cell sheets can be monitored, transwell assays explore the migration of individual cells without consideration of cell-cell interaction. However, to distinguish between the random migration of single cells

Results

(chemokinesis) and directed migration towards a concentration gradient of extracellular matrix (haptotaxis) or a soluble factor (chemotaxis), we performed transwell assays under varying conditions. When filters were coated with collagen on the underside only and cells were left to migrate in the absence of a serum gradient, both DLC3 and DLC1 knock-down cells displayed an enhanced haptotactic migratory capacity compared to siLacZ control cells (data not shown). Secondly, we investigated cell motility in the absence of any gradient to investigate random migration. Thus, both sides of the filter were coated with collagen and equal concentrations of the agent (10% FCS) were added to the chambers. In the absence of a serum or collagen gradient, migration of DLC3-depleted MCF7 cells was very poor and comparable to that of control cells (Figure 22C), whereas the loss of DLC1 stimulated cell migration under this condition. This indicates that DLC1 but not DLC3 is involved in the regulation of random cell migration. We repeated these studies with MDA-MB 468 cells and obtained the same results (Figure 22D). Without a chemotactic or haptotactic stimulus, random migration of DLC3-deficient cells was similar to siLacZ controls. We concluded from these experiments that the single cell condition is not sufficient to enhance cell migration, but rather the strong stimuli of a soluble attractant or ECM protein is required to stimulate cell migration of DLC3 knock-down cells.

3.2.7 DLC3 down-regulation does not increase cell invasion

Next, we examined the invasive properties of cells lacking DLC3 by seeding them into using basement membrane extract (BME)-coated transwells. Because MCF7 cells are poorly invasive, we performed these assays with the highly invasive MDA-MB 231 cell line. As shown in Figure 23, DLC3-deficient MDA-MB 231 cells failed to show enhanced invasive properties compared to the siLacZ control. This result is similar to the one obtained for DLC1 knock-down cells (see section 3.1.7, Figure 15).

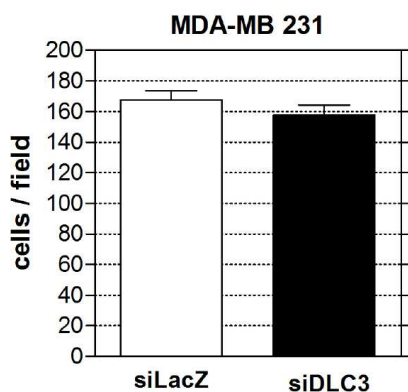


Figure 23: DLC3 knock-down cells do not increase the invasiveness of MDA-MB 231 cells. MDA-MB 231 cells were transiently transfected with siRNAs specific for DLC3, or with LacZ-specific siRNA as a control. Three days post transfection, 1×10^5 cells were seeded in medium containing 0.5% FCS into the upper chamber of a BME-coated transwell. The lower well contained medium supplemented with 10% FCS. After incubation overnight, cells that had migrated across the filter were fixed and stained with crystal violet. The number of migrated cells was determined by counting five independent microscopic fields (20-fold magnification). Data shown is the mean \pm SEM of duplicate wells and is representative of two independent experiments.

Results

3.2.8 DLC3 knock-down attenuates RhoA activity

Since DLC3 has GAP activity for RhoA in *in vitro* studies (90) and intact cells (see Figure 18), we tested whether DLC3 knock-down, like DLC1 depletion, increases RhoA-GTP levels. MCF7 cells were transfected with DLC3-specific siRNAs, starved and then restimulated with serum (Figure 24A). Surprisingly, RhoA-GTP levels were undetectable in serum-starved DLC3-depleted cells and failed to increase upon serum stimulation, although total RhoA levels were not altered (Figure 24A), which is in contrast to the results obtained with DLC1- and DLC2-downregulated cells (see section 3.1.3, Figure 9).

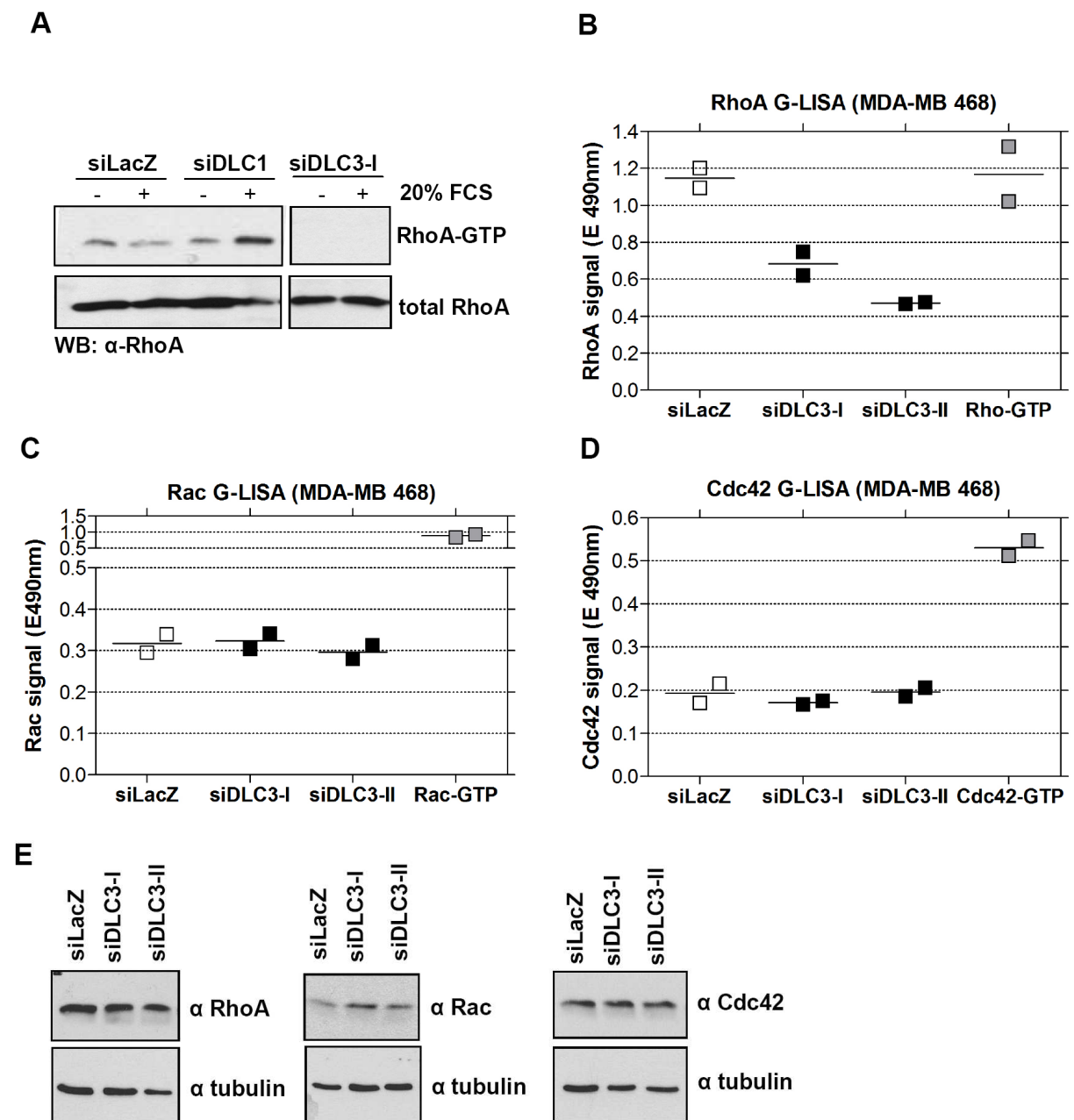


Figure 24: Depletion of DLC3 decreases cellular RhoA-GTP levels but does not influence Rac-GTP and Cdc42-GTP levels. Figure legend: see next page.

Results

Figure 24: Depletion of DLC3 decreases cellular RhoA-GTP levels but does not influence Rac-GTP and Cdc42-GTP levels. MCF7 (A) and MDA-MB 468 cells (B-E) were transiently transfected with siRNA specific for DLC3 (siDLC3-I and siDLC3-II) or with siLacZ control and either used for RBD pulldown (A) or G-LISA assays (B-D), respectively. (A) Three days after transfection, cells were starved in serum-free medium for 24h and then either left untreated (-) or restimulated with 20% FCS for 5 min (+). RhoA-GTP was precipitated and analyzed as described in Figure 9. MCF7 cells transfected with siDLC1 were used as a positive control. The lanes shown are from the same membrane. (B-D) Three days post transfection, cells were lysed and equal amounts of total cell lysate were subjected to a G-LISA specific for RhoA-GTP (B), Rac-GTP (C) or Cdc42-GTP (D). The active (GTP-loaded) level of RhoA (B), Rac (C) and Cdc42 (D) is proportional to the absorbance measured at 490 nm. Recombinant constitutively active Rho proteins (included in the G-LISA kits) were used as positive control. Values correspond to the mean of duplicate samples and are representative of two independent experiments. (E) Equal amounts of total cell lysates were subjected to SDS-PAGE, transferred to membrane and total RhoA, Rac1, and Cdc42 levels were analyzed by immunoblotting using RhoA-, Rac1- and Cdc42-specific antibodies, respectively (top panels). Equal loading was verified by reprobing the membrane with tubulin-specific antibody (bottom panels).

We repeated our experiments with MDA-MB 468 cells and in addition made use of the highly sensitive and quantitative RhoA G-LISA assay where a RhoA GTP-binding protein is linked to the wells of a 96 well plate. Active, GTP-bound RhoA in cell lysates will bind to the wells while inactive GDP-bound RhoA is removed during washing steps. The bound active RhoA is detected with a RhoA specific antibody. The data of the G-LISA confirmed the RBD pulldown results. Again, DLC3-deficient cells displayed a lower level of GTP-bound RhoA than the control cells (Figure 24B). Since RhoA activity is attenuated in both cell lines upon DLC3 knock-down using two specific siRNAs we are convinced that this is indeed due to DLC3 depletion.

To address the question which DLC3-dependent mechanism leads to the low RhoA-GTP level, we performed G-LISA assays for Rac1 and Cdc42. Previous studies showed that RhoA activity can be altered by the impact of other Rho GTPases (91). If endogenous DLC3 has a distinct GAP activity *in vivo* compared to the one observed *in vitro*, its depletion could hyperactivate a Rho GTPases which in a second step diminishes RhoA activity. We therefore determined the GTP-bound levels of the other two classical RhoGTPases, Rac1 and Cdc42, in MDA-MB 468 cells by performing G-LISA assays (Figure 24 C,D). However, neither the basal levels of active Rac1 (Figure 24C) and Cdc42 (Figure 24D) nor their overall expression, as determined in immunoblots (Figure 24E), were significantly changed in cells lacking DLC3. Therefore, further experiments are necessary to answer the question why the loss of DLC3 leads to diminished RhoA activity.

3.2.9 DLC3 depletion impacts on cell morphology

Exogenous expression of DLC3 alpha and beta has been shown to cause cell rounding associated with the disassembly of stress fibers and focal adhesions [(90); Figure 19], which are thought to be RhoA-dependent. However, the data obtained with RBD pulldowns and G-LISAs clearly showed that DLC3 depletion leads to decreased RhoA activity. Therefore, we explored the influence of DLC3 silencing on the actin cytoskeleton. MDA-MB 468 cells lacking DLC3 were stained with a paxillin-specific antibody and phalloidin to visualize focal adhesions and F-actin structures, respectively. In contrast to DLC1-depleted cells (Figure 10), there was no obvious increase in the stress fiber content and the number or size of focal adhesions in cells lacking DLC3 (Figure 25). Instead, these cells showed a highly flat and outspread phenotype in comparison to the siLacZ control cells. FACS analysis revealed that the general size of cells in suspension was not influenced by DLC3 knock-down, since forward scatter profiles were similar to the control (data not shown). RhoA is known to be important for contractility of the cell body (92; 93). Therefore, DLC3-depleted cells are most likely more relaxed and outspread due to their low RhoA-GTP level.

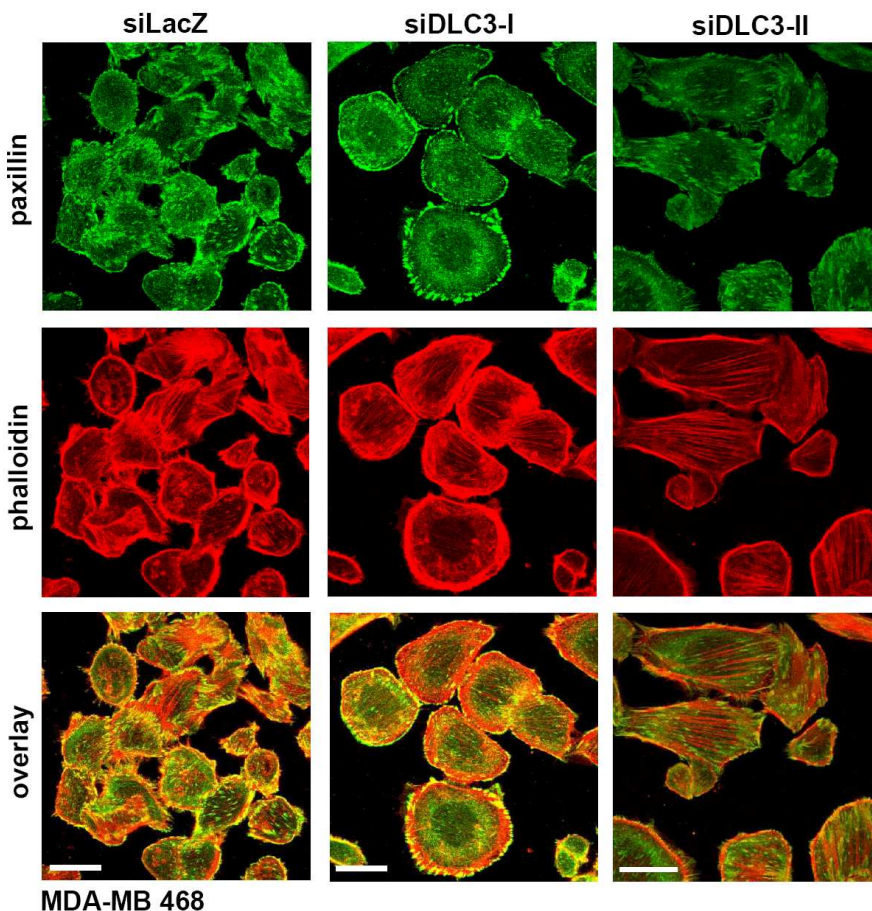


Figure 25: Depletion of DLC3 leads to morphological changes in MDA-MB 468 cells. MDA-MB 468 cells were transiently transfected with siRNAs targeting DLC3 (siDL3-I and siDLC3-II) or with siLacZ control and replated onto collagen-coated glass coverslips after three days. The next day, cells were fixed and stained with paxillin-specific antibody and Alexa Fluor 488-labeled secondary antibody (green). Filamentous actin was visualized by staining with Alexa Fluor 546-tagged phalloidin (red). Images of the cells were obtained using a confocal laser scanning microscopy system and represent stacks of 3 sections. Scale bars represent 20 μm .

4 Discussion

Rho GTPases are proteins with pleiotropic cellular functions that include the regulation of actin cytoskeletal and microtubule dynamics. Deregulation of Rho activity is known to be involved in oncogenic transformation of cells since these cellular structures are necessary for cellular events like morphology, migration and proliferation. The DLC family genes are deleted or underexpressed in a variety of human cancers, including breast cancer, and have been proposed to act as tumor suppressors by antagonizing Rho signaling. DLC proteins are structurally related and represent multimotif proteins, which beside their GAP domain also contain two further conserved modules (SAM and START domain) and an unstructured region with potential phosphorylation sites. It is not clear whether the three DLC family members have the same cellular functions and therefore behave redundantly or whether they have individual non-cooperative actions and function independently of each other. Here we demonstrate that all three proteins are capable of inactivating RhoA when expressed in intact cells, based on results obtained with a RhoA biosensor and SRF luciferase assays. These data suggested that all three DLC family members share the same substrate specificity. Interestingly, the consequences of DLC protein loss revealed prominent differences in cell behavior of human breast cancer cell lines, indicating individual functions of each family member.

4.1 Investigating DLC1 and DLC3 functions by RNA interference

When expressed in HEK293T cells, both DLC1 and DLC3 led to decreased RhoA-GTP levels. In the case of DLC3 alpha and beta, RhoGAP activity was even higher than that of DLC1 and DLC2. This provides an explanation why the transfection of MCF7 cells with even low doses of an expression plasmid encoding wild type DLC3 promoted such drastic morphological changes and, as a consequence, a GAP-inactive mutant was required to determine DLC3 subcellular localization. In MCF7 cells, DLC1 and DLC3 were localized to focal adhesions. This, together with their common RhoA specificity suggests that the two proteins may have overlapping biological functions. Indeed, chemotactic transwell assays revealed that ablation of DLC1 and DLC3 favored directed migration of MCF7 cells and of a second human breast cancer cell line (DLC1: MDA-MB 436 cells; DLC3: MDA-MB 468 cells). In contrast to these results, wounding experiments led to a distinct behavior of DLC1 and DLC3 knock-down cells. DLC1- but not DLC3-depleted cells closed the wound more rapidly than the control did. Of note, we can exclude an off-targeting effect via the transfected DLC1

Discussion

siRNA as a reason for enhanced cell locomotion, since DLC1 depletion in DLC1-negative MDA-MB 468 cells failed to affect cell migration in wounding as well as in chemotactic transwell assays.

It has been reported that expression of DLC1 leads to inhibition of tumor cell growth (85). This has been attributed to down-regulation of active Rho protein levels, since DLC1 GAP-deficient mutants were less active in suppressing cell growth (85). To exclude that the accelerated wound closure in DLC1 deficient cells was due to enhanced cell proliferation, we performed cell cycle analysis of MCF7 cells transfected either with siRNA targeting DLC1 or a siLacZ control. DLC1 knock-down cells showed no significant difference to control cells. This is in accordance with data of Xue and coworkers (94), showing that DLC1 knock-down had only a modest impact on the colony forming ability of hepatoma cells, although DLC1 overexpression efficiently suppressed colony formation. Interestingly, when they used p53-deficient liver progenitor cells that were coinfecting with Myc and DLC1 shRNAs and subsequently transplanted into recipient mice, DLC1 loss significantly accelerated tumor onset *in vivo*. Therefore, DLC1 may need to cooperate with other oncogenic lesions to influence cell growth.

Of note, although both transwell and scratch assays monitor directed cell migration, the stimuli that initiate cell locomotion differ a lot. In case of transwell assays single cells are attracted by a chemotactic agent, such as serum, located on the other side of a porous membrane. In wounding experiments, however, confluent cell monolayers are scratched and the cells at the wound edge start to move to close the gap. Furthermore, the influence of cell-cell contact on cell migration differs in the two assays and therefore may impact on cell locomotion. Obviously, the two DLC family members seem to influence cell movement by distinct mechanisms. This can also be seen by their different impact on random cell migration. DLC3 knock-down cells failed to induce cell motility in the absence of a chemotactic agent in transwell assays, whereas DLC1 deficient cells did.

In our hands, RNAi experiments revealed a different impact of DLC1 and DLC3 knock-down on RhoA activity, although published data (90; 95) as well as our studies with cells expressing DLC1 and DLC3 proteins identified RhoA as a substrate for both GAP proteins. DLC1 deficient cells demonstrated increased active RhoA levels whereas the knock-down of DLC3 led to a decreased level of GTP-bound RhoA, shown by RBD-pulldown assays and RhoA G-LISA assays. The difference in active RhoA levels was also reflected by morphological alterations of the cells. Active RhoA is known to stabilize focal adhesions and

Discussion

promote stress fiber formation. In agreement with the divergent influence of DLC1 and DLC3 on the RhoA-GTP level, hyperactivation of RhoA in cells lacking DLC1 promoted an increase in stress fiber formation whereas cells deficient in DLC3 showed a more relaxed, outspread morphology, likely due to diminished RhoA activity. The phenotype of DLC1 deficient cells is inconsistent with findings made with fibroblasts from 9.5 day DLC1^{-/-} mice embryos. Durkin and coworkers reported that these cells were able to proliferate in culture, but display reduced actin stress fiber and vinculin-containing focal adhesion formation (96). However, the effect of focal adhesion disassembly and stress fiber disruption in cultured cells overexpressing DLC1 confirm our data (97; 98) .

In agreement with the DLC1 property to accelerate hydrolysis of RhoA-GTP, DLC1-depleted cells exhibited enhanced RhoA-GTP levels. In this regard, the diminished RhoA activity in DLC3 deficient cells was quite unexpected. Given that Sander and colleagues reported an inactivation of RhoA by the action of active Rac1 (91), we performed G-LISA assays to measure the level of Rac1-GTP in DLC3-depleted MDA-MB 468 cells. The assays revealed no difference in GTP-bound Rac1 levels between DLC3 knock-down cells and control cells. So far, we could not find an explanation why the absence of DLC3 failed to increase active RhoA levels in our experimental setup. It is possible that DLC3 possesses GAP-independent functions, which are predominant and counteract the activation of RhoA upon DLC3 down-regulation. Since it has been reported that DLC3, like the other family members, has some limited GAP activity towards Cdc42 (90), we performed G-LISA assays for Cdc42. However, DLC3 knock-down cells did not increase the level of active Cdc42 in MDA-MB 468 cells.

Interestingly, the depletion of both DLC1, which led to an increased RhoA-GTP level, as well as the knock-down of DLC3, which diminished RhoA activity, facilitated migration of breast epithelial cells in chemotactic transwell assays. This reflects quite well the controversial discussion on the contribution of RhoA to the complex process of cell migration. Rho GTPases regulate actin cytoskeleton rearrangements and microtubule (MT) stabilization, which are both critically involved in cell migration. Actin polymerization at the leading edge drives membrane protrusion, association of the actin cytoskeleton with integrins regulates their binding to the ECM (extracellular matrix), and actin bundles within the body generate tension to pull the cell body forward and retract the tail. Elevated levels of active RhoA were shown to negatively modulate cell migration due to excessive stress fiber formation and adhesion forces (99; 100). But on the other hand, loss of Rho activation results in migration defects and impaired stabilization of MTs directed to the front (87). Even the well-studied Rho effector proteins ROCK and Dia1 have both been implicated in negative and positive

Discussion

regulation of cell migration depending on the cell type and condition. Further experiments are needed to answer the question, how cells deficient in DLC3 acquire the property to migrate in chemotactic transwell but not in wounding experiments. In general, the molecular function of DLC3 is not well understood. In fact, the few existing reports on DLC3 have not identified any specific functions that are not shared by DLC1.

In contrast to DLC3, we were able to more clearly identify and exclude signaling pathways, by which DLC1 contributes to cell locomotion. Since DLC1-depleted cells displayed an enhanced RhoA level, we assumed that an effector protein downstream of RhoA mediated the accelerated cell motility. RhoA interacts with two major effector proteins, ROCK and Dia1, which cooperate in the case of stress fiber formation (88) and oppose another in other signaling events, such as in cell-cell contact regulation (26). Furthermore, Rho-ROCK signaling is involved in tail retraction and attenuates integrin-mediated adhesion in the tail. Dia1 is required for the de novo nucleation of actin filaments in order to facilitate temporal and spatial remodeling of the actin cytoskeleton needed for establishment of cell shape, cytokinesis, and cell motility (93). The decision which of the several effector proteins becomes activated by GTP-loaded Rho proteins seems to depend partly on the amount of active RhoA. A high level of Rho-GTP activates both ROCK and Dia1 to induce retraction, whereas a lower level of Rho preferentially activates Dia1 (24). This view is consistent with the reported K_d values of the Rho-binding domains of ROCK and Dia1 for the GTP-bound form of Rho, 130 nM and 6 nM, respectively (101; 102). This concept provides a useful way to interpret Rho actions at different time points and different locations in a single cell.

In order to find out which RhoA effector protein is responsible for enhanced cell migration in DLC1-depleted MCF7 cells, we performed transwell migration assays, in which we added ROCK inhibitors to the cells in the top chamber. Interestingly, pharmacological suppression of ROCK activity did not impede cell migration. Therefore, we excluded ROCK as the effector protein mediating enhanced cell migration of DLC1 knock-down cells. In contrast to this, Dia1 depletion completely abrogated increased migration of DLC1-deficient cells in transwell assays as well as in wounding experiments. This is in accordance with two recent studies, in which Dia1 was identified as a critical component in directed migration of MEFs (mouse embryonic fibroblasts) and glioma cells, respectively (103; 104). Interestingly, the impact of Dia1 depletion on cell locomotion per se was different when we either performed transwell assays or wounding experiments. Knock-down of Dia1 dramatically reduced cell migration in wounding experiments compared to the siLacZ control, whereas in transwell migration

Discussion

assays cells behaved similarly as the siLacZ control. It has been reported, that Dia1 depletion interferes with several signaling pathways, including microtubule stabilization, cell polarization and focal adhesion turnover (25). Microtubules are polarized in migrating cells and are essential for the directed migration of many cell types, possibly by delivery of signaling molecules and membrane components (105). As a consequence of Dia1 knock-down, both directionality and locomotion were impaired in glioma cells (25). Furthermore, Dia1 is important for proper localization of adherence junction components to the cell periphery and therefore has been implicated in the regulation of cell-cell contacts (26). Knowing that in transwell migration assays and wounding experiments the experimental settings differ as well as the way how cell locomotion is initiated, it is not surprising that the same cells behave differently in the two assays. Therefore, the loss of directionality or cell-cell integrity for instance may or may not have impact on cell locomotion. Nevertheless, since Dia1 depletion completely abrogated the increased migration of MCF7 cells lacking DLC1 in both assays, this strongly suggests that DLC1 controls cell movement through Dia1.

RhoA has always been assumed to act at the back of migrating cells to induce tail retraction via activation of ROCK. More recent studies using biosensors combined with live cell microscopy have provided proof that RhoA activity is not restricted to the rear but also present at the leading edge of migrating cells (106; 107; 104). Consistent with these reports, active Rho was found to colocalize with Dia1 at the front edge of migrating cells (104). Dia1-staining of the wound edge of MCF7 cells lacking DLC1 revealed enhanced accumulation of Dia1 at membrane protrusions, compared to cells transfected with siLacZ control, confirming the role of Dia1 as a downstream target of DLC1. We therefore conclude that the loss of DLC1 leads to a strong local enrichment of Dia1 at the leading edge, which then mediates enhanced cell migration. Such a proposed role for DLC1 at sites of membrane protrusion is supported by findings of Healy and colleagues who observed local inactivation of a RhoA biosensor in MEFs ectopically expressing DLC1 (108). Accumulating data suggest that in migrating cells the Rho-Dia1 pathway is activated at the front and facilitates migration by two possible mechanisms. On the one hand, microtubule-dependent recruitment of Cdc42 in the front ensures cell polarization needed for directed cell migration and/or on the other hand actin-dependent translocation of c-Src to focal adhesions can stimulate adhesion turnover necessary for enhanced migratory velocity [reviewed in (93)]. Which of the mentioned Rho-Dia1 pathways leads to accelerated cell movement in DLC1-depleted cells remains to be investigated in future studies.

Discussion

Members of the Rho GTPase family not only regulate cell migration, they are also good candidate molecules involved in cell invasion [reviewed in (109)]. For instance, RhoC has been implicated in tumorigenesis since increased expression of RhoC is linked to an enhanced metastatic potential of tumor cells. Furthermore, knockdown of RhoC inhibited angiogenesis induced by tumor cells through affecting the release of vascular endothelial growth factor (VEGF), inhibiting endothelial cell migration and altering endothelial cell organization (110). DLC1 may also be involved in cell invasion, since several reports exist which connect DLC1 depletion to an enhanced ability of the cells to invade and to form metastasis to bone and lung (78). Although we could clearly demonstrate an enhanced migratory behavior of DLC1 knock-down cells, in our hands, the depletion of DLC1 failed to enhance the invasiveness of non-invasive MCF7 cells, low-invasive MDA-MB 436 cells and highly invasive MDA-MB 231 cells. When tumor cells invade into the three dimensional (3D) space cell movement is strongly restricted by an extensive network of extracellular matrix (ECM) fibrils such as collagen. The classic concept for cell invasion therefore postulates the requirement of coordinated cell adhesion, motility and proteolytic degradation of ECM substrates. Cells adhere to the collagen matrix in an integrin-dependent manner, produce tube-like defects in the matrix by proteolysis and migrate into the formed tubes. Therefore, DLC1-deficient cells, although able to enhance cell motility in the 2D model, may not produce ECM-degrading proteases, particularly matrix metalloproteases (MMP). The proteolysis-dependent mesenchymal movement can be converted to an amoeboid-like movement. In that case, cells adapt a round shape and pass through the fibrillar ECM network by constantly changing their shape and squeezing the cell bodies along preformed fiber strands. It has been reported that the activity of ROCK is essential for adapting a round amoeboid morphology (111). Since DLC1-deficient cells seem to activate the Rho-Dia1 pathway, and not Rho-ROCK, this might provide an explanation why DLC1 knock-down cells do not succeed in mediating cell invasion.

When we investigated the involvement of the different Rho isoforms in mediating cell migration of DLC1-depleted cells, we observed that knock-down of both RhoA and RhoC led to increased cell locomotion. Furthermore RhoA/C depletion did not prevent migration of cells lacking DLC1. However, silencing of RhoA/C also reduced DLC1 expression levels, making interpretation of the results difficult. Because it is unlikely that both siRNAs have the same non-specific effect, this observation may indicate that DLC1 protein levels are regulated by RhoA/C expression in a feedback manner. Interestingly, down-regulation of Cdc42 partially inhibited migration of cells lacking DLC1. Although ectopic DLC1 expression did not lead to measurable GTP hydrolysis of the Raichu-Cdc42 biosensor, negative regulation of

Discussion

endogenous Cdc42 by DLC1 cannot be ruled out and should be investigated in more detail. Possibly, the impact of DLC1 on Cdc42 is restricted to a highly local region within the cell that is not detectable in the cell lysates used in Raichu assays. It is also possible that the effect of Cdc42 deletion on migration of DLC1 deficient cells is indirect. As described above, Dia1 has been reported to contribute to localization of Cdc42 to the leading edge of migrating cells (103).

Very few, if any, RhoGAPs consist of only a singly GAP domain, most are large proteins that contain additional functional modules. The RhoGAP multidomain proteins are thought to integrate signals from a number of regulatory pathways. Therefore, DLC proteins may have GAP-dependent as well as GAP-independent mechanisms to interfere with cell migration. For instance, the rat ortholog of DLC1 (p122RhoGAP) binds PLC-delta1 and stimulates the hydrolysis of PIP₂ (phosphatidylinositol 4,5-bisphosphate) *in vitro* (44). PIP₂ serves as a precursor for other lipid second messengers but in addition has an important role in regulating cytoskeleton assembly by inducing conformational changes in actin-binding proteins, such as vinculin and talin (112). Thus DLC proteins may also influence cytoskeletal dynamics by altering local PIP₂ levels as well as by regulating Rho GTPase activity. Several other binding partners of DLC family members have been identified in the past years, but in most cases the physiological significance of the interaction is not known. In our group, we identified by yeast-two-hybrid screening and coimmunoprecipitations PTEN as an interaction partner of DLC1 (Heering, submitted). Although the precise functional dependence is not understood thus far, a DLC1-PTEN complex at the plasma membrane may be involved in the local regulation of cell migration.

4.2 Investigating DLC2 functions by RNA interference

We identified GFP-DLC2 as a mainly cytosolic protein in MCF7 cells without any obvious accumulation to cellular compartments. Unlike our findings, it has been reported for Huh-7 hepatoma cells that DLC2 targets to mitochondria via its START domain (67). At these organelles, DLC2 could serve as a binding partner of HMG-CoA (hydroxymethylglutaryl (HMG) coenzyme A) reductase, since yeast-two-hybrid screenings identified this protein as an interaction candidate (113). The HMG-CoA reductase is involved in the energy pathway found in mitochondria and is the rate limiting enzyme in cholesterol biosynthesis (114). Furthermore, Ng and coworkers speculate that DLC2 might fulfill its growth suppressive function, reported by Ching et al. (82), by regulating mitochondrial membrane permeability and the mitochondrial pathway of apoptosis (67). In addition to these possible roles of DLC2,

Discussion

Hatch et al. claim that DLC2 mediates activation of mitochondrial phosphatidyl-glycerol-phosphate (PGP) synthase in CHO cells after ceramide supplementation (115). Nevertheless, in our cellular system DLC2 failed to localize to mitochondria, as demonstrated by costaining with the mitochondria-selective probe MitoTracker®.

In MCF7 cells, GFP-tagged DLC1 and DLC3 were distributed within the cytoplasm and further showed dominant targeting to focal adhesions. This recruitment is mediated by their interaction with tensin proteins, as reported in several publications (70-72; 74). Interestingly, DLC2 also contains a potential tensin-SH2 domain-binding motif (457-SIYDNV-462). Although we did not observe focal adhesion targeting in MCF7 cells, Kawai and coworkers (116) showed colocalization of DLC2 with the FA marker vinculin in HeLa cells and further demonstrated an interaction of endogenous DLC2 with tensin 2 by GST pull-down assay using the C-terminal part of tensin2 as bait. Responsible for the localization to FAs is a focal adhesion targeting (FAT) region in the N-terminal half of DLC2 that directly interacts with the C-terminus of tensin 2 (116). Since we neither observed DLC2 targeting to mitochondria nor to focal adhesions in MCF7 cells it seems reasonable that in addition to the START domain and FAT region cell type-specific cofactors, which are absent in our experimental model, mediate subcellular targeting of DLC2. Nevertheless, DLC2 acts as a RhoGAP protein in this breast cancer cell line. In accordance with its GAP specificity for RhoA in intact cells, shown by Raichu and luciferase assays, knock-down of DLC2 increased active RhoA levels in MCF7 cells.

Chemotactic transwell assays revealed that cells lacking DLC1 or DLC3 acquired enhanced cell locomotion, whereas DLC2 knock-down cells failed to do so. Given that DLC2, but not DLC1 and DLC3, is excluded from focal adhesions in MCF7 cells we assume that the absence from FAs could provide an explanation for the inability of DLC2 to regulate cell migration. That the proper localization of DLC family members is important to fulfill a certain biological function is confirmed by the results of Qian and colleagues. They described that the mutation of the tensin-binding site of DLC1 not only prevented targeting to focal adhesions but also reduced growth inhibition by DLC1, without affecting its overall RhoGAP activity *in vivo* (71). This indicates that the tumor suppressor function of DLC family members requires precise targeting of the RhoGAP activity and/or that DLC family members may perhaps have GAP-independent functions.

The fact that DLC2 depletion did not facilitate migration of MCF7 and MDA-MB 436 cells conflicts with a previous study, in which DLC2 was silenced with a set of four siRNA

Discussion

duplexes and demonstrated enhanced motility of HepG2 cells (69). It is important to note that in our hands such a commercially available siRNA pool for DLC2 also down-regulated DLC1 transcript levels. It thus cannot be ruled out that the reported enhanced migratory potential of HepG2 cells, which also express DLC1 (117; 118), was in fact due to an off-target effect involving the knock-down of DLC1. Currently there is an ongoing discussion concerning the reason for off-targeting. It was believed that the biological machinery of RNA interference is highly specific due to Watson-Crick base pairing interactions which discriminates targeted versus non-target mRNA. But the almost ideal specificity of RNAi has shown not to hold entirely true in reality, since monitoring of gene activity by microarray technology has demonstrated that siRNA-treated cells show off-target silencing of numerous genes (119). The majority of experimentally verified off-targets have a 6-7 nucleotide match to the siRNA in the so-called 'seed' region, a motif located within the untranslated region at the 3' end [3' UTR; (120)]. Alternatively, the cellular consequences of DLC gene silencing may be cell type specific, possibly depending on DLC2 subcellular targeting, Rho expression levels and/or on the balance of GEF and other GAP proteins that keep Rho in check. From the DLC2 RNAi experiments we thus conclude that it is not the overall level of active RhoA that mediates cell migration, but rather its precise spatio-temporal activation. Since DLC2-deleted cells behaved similarly to control cells in the different assays performed, the precise biological function of DLC2 in breast epithelial cells still remains to be resolved.

4.3 Conclusions and future directions

DLC proteins are frequently lost in a variety of human cancers and seem to have tumor suppressor properties. The three family members are structurally related and beside two other conserved motifs they contain a GAP domain to accelerate GTPase activity of Rho proteins. The predominant view was that DLC family members have overlapping cellular functions and impact on cell behavior by controlling the level of GTP-bound Rho proteins. Our RNA interference studies strongly suggest that DLC proteins impact on the complex multistep processes of cell migration by regulating actin cytoskeleton dynamics. The proper localization of DLC family members is important to fulfill their biological functions. In MCF7 cells, DLC1 and DLC3 are recruited to focal adhesions, most likely due to their interaction with tensin proteins. In contrast to this, we identified DLC2 as a mainly cytosolic protein in MCF7 cells without any obvious accumulation to cellular compartments such as mitochondria. Although DLC2 contains a potential tensin-SH2 domain-binding motif it failed to target to focal adhesions in MCF7 cells. This is probably the reason why DLC2 proteins are unable to regulate migration in MCF7 cells although their silencing led to an enhanced

Discussion

RhoA activity. Therefore, not the overall level of active RhoA mediates cell migration, but rather its precise spatio-temporal activation. The precise biological function of DLC2 in breast epithelial cells still remains to be resolved. In contrast to DLC2, the deletion of both DLC1 as well as DLC3 had impact on the migratory behavior of the cells. Interestingly, RNAi experiments revealed that the two DLC family members regulate cell movement by distinct mechanisms. For instance, DLC1 knock-down cells are able to induce random cell motility but DLC3 deletion failed to do so. For reasons we do not understand so far, the knock-down of DLC3 led to a decreased level of GTP-bound RhoA. This can also be seen by the more relaxed and outspread phenotype of the cells. We could rule out the possibility that cells deficient in DLC3 increase the overall level of the other two classical Rho GTPases Rac1 and Cdc42, which then might have a negative impact on RhoA activity. The explicit mechanism by which DLC3 impacts on cell movement needs to be investigated in more detail. In case of DLC1 we could connect the enhanced migratory behavior of DLC1 deficient cells to a Dia1-dependent signaling pathway. Presumably, the loss of DLC1 leads to a local activation of RhoA at the leading edge of migrating cells and as a consequence to an accumulation of its effector protein Dia1. Dia1 then might accelerate actin polymerization in order to form membrane protrusions, which are known to facilitate cell locomotion.

It is important to realize, that cellular signaling pathways are not isolated from each other but are rather interconnected to form complex signaling networks. Therefore, the same signaling molecule can control different processes within different signaling complexes or at different intracellular locations. Depending on the cell type, the interconnection of the pathways and the set of signaling molecules differ. It is therefore not surprising, that the activation of a signaling molecule may have distinct consequences, depending on the cellular context. Cell migration is a multistep process which involves the action of various signaling pathways. To understand how DLC proteins regulate such a complex cellular event *in vivo* represents a major challenge. Further efforts using mass-spectrometry-based proteomic analyses and yeast-two-hybrid screening will reveal additional interaction partners of the DLC family proteins. This might help to elucidate the precise mechanism by which DLC proteins interfere with cell locomotion and potentially identify GAP-independent functions of the DLC family members. Since the accurate spatio-temporal activation of signaling proteins as well as adaptor proteins are needed for cell locomotion, future work should further focus on FRET-based microscopic techniques together with live cell imaging to investigate local changes within migrating cells.

5 Reference List

1. Jemal A, Siegel R, Ward E, Hao Y, Xu J, Murray T, Thun MJ. Cancer statistics, 2008. *CA Cancer J Clin.* 2008 ;58(2):71-96.
2. Association of Epidemiological Cancer Registries. *Cancer in Germany 2003-2004 Incidence and Trends.*
3. Ratsch SB, Gao Q, Srinivasan S, Wazer DE, Band V. Multiple genetic changes are required for efficient immortalization of different subtypes of normal human mammary epithelial cells. *Radiat Res.* 2001 ;155(1 Pt 2):143-150.
4. Hanahan D, Weinberg RA. The hallmarks of cancer. *Cell.* 2000 Jan 7;100(1):57-70.
5. Farber E. The multistep nature of cancer development. *Cancer Res.* 1984 Okt ;44(10):4217-23.
6. Lauffenburger DA, Horwitz AF. Cell migration: a physically integrated molecular process. *Cell.* 1996 Feb 9;84(3):359-69.
7. Adams JC. Cell-matrix contact structures. *Cell Mol Life Sci.* 2001 März ;58(3):371-92.
8. Cramer LP. Organization and polarity of actin filament networks in cells: implications for the mechanism of myosin-based cell motility. *Biochem Soc Symp.* 1999 ;65:173-205.
9. Hynes RO. Integrins: bidirectional, allosteric signaling machines. *Cell.* 2002 ;110(6):673-687.
10. Burridge K, Chrzanowska-Wodnicka M. Focal adhesions, contractility, and signaling. *Annu Rev Cell Dev Biol.* 1996 ;12:463-518.
11. Bresnick AR. Molecular mechanisms of nonmuscle myosin-II regulation. *Curr Opin Cell Biol.* 1999 ;11(1):26-33.
12. Sellers JR. Myosins: a diverse superfamily. *Biochim Biophys Acta.* 2000 März 17;1496(1):3-22.
13. Broussard JA, Webb DJ, Kaverina I. Asymmetric focal adhesion disassembly in motile cells. *Curr Opin Cell Biol.* 2008 ;20(1):85-90.
14. Raftopoulou M, Hall A. Cell migration: Rho GTPases lead the way. *Dev Biol.* 2004 Jan 1;265(1):23-32.
15. Ladwein M, Rottner K. On the Rho'd: the regulation of membrane protrusions by Rho-GTPases. *FEBS Lett.* 2008 Juni 18;582(14):2066-74.
16. Heasman SJ, Ridley AJ. Mammalian Rho GTPases: new insights into their functions from in vivo studies. *Nat Rev Mol Cell Biol.* 2008 Sep ;9(9):690-701.

Reference list

17. Rossman KL, Der CJ, Sondek J. GEF means go: turning on RHO GTPases with guanine nucleotide-exchange factors. *Nat Rev Mol Cell Biol.* 2005 Feb ;6(2):167-80.
18. Tcherkezian J, Lamarche-Vane N. Current knowledge of the large RhoGAP family of proteins. *Biol Cell.* 2007 Feb ;99(2):67-86.
19. Dransart E, Olofsson B, Cherfils J. RhoGDI revisited: novel roles in Rho regulation. *Traffic.* 2005 Nov ;6(11):957-66.
20. Bishop AL, Hall A. Rho GTPases and their effector proteins. *Biochem J.* 2000 Jun 1;348 Pt 2:241-55.
21. Goode BL, Eck MJ. Mechanism and function of formins in the control of actin assembly. *Annu Rev Biochem.* 2007 ;76:593-627.
22. Amano M, Ito M, Kimura K, Fukata Y, Chihara K, Nakano T, Matsuura Y, Kaibuchi K. Phosphorylation and activation of myosin by Rho-associated kinase (Rho-kinase). *J Biol Chem.* 1996 Aug 23;271(34):20246-9.
23. Maekawa M, Ishizaki T, Boku S, Watanabe N, Fujita A, Iwamatsu A, Obinata T, Ohashi K, Mizuno K, Narumiya S. Signaling from Rho to the actin cytoskeleton through protein kinases ROCK and LIM-kinase. *Science.* 1999 Aug 6;285(5429):895-8.
24. Tsuji T, Ishizaki T, Okamoto M, Higashida C, Kimura K, Furuyashiki T, Arakawa Y, Birge RB, Nakamoto T, Hirai H, Narumiya S. ROCK and mDial antagonize in Rho-dependent Rac activation in Swiss 3T3 fibroblasts. *J. Cell Biol.* 2002 May 28;157(5):819-830.
25. Yamana N, Arakawa Y, Nishino T, Kurokawa K, Tanji M, Itoh RE, Monypenny J, Ishizaki T, Bito H, Nozaki K, Hashimoto N, Matsuda M, Narumiya S. The Rho-mDial pathway regulates cell polarity and focal adhesion turnover in migrating cells through mobilizing Apc and c-Src. *Mol Cell Biol.* 2006 Sep ;26(18):6844-58.
26. Sahai E, Marshall CJ. ROCK and Dia have opposing effects on adherens junctions downstream of Rho. *Nat Cell Biol.* 2002 Jun ;4(6):408-15.
27. Fukata M, Kaibuchi K. Rho-family GTPases in cadherin-mediated cell-cell adhesion. *Nat Rev Mol Cell Biol.* 2001 Dec ;2(12):887-97.
28. Fritz G, Just I, Kaina B. Rho GTPases are over-expressed in human tumors. *Int J Cancer.* 1999 ;81(5):682-687.
29. Fritz G, Brachetti C, Bahlmann F, Schmidt M, Kaina B. Rho GTPases in human breast tumours: expression and mutation analyses and correlation with clinical parameters. *Br J Cancer.* 2002 ;87(6):635-644.

Reference list

30. Khosravi-Far R, Solski PA, Clark GJ, Kinch MS, Der CJ. Activation of Rac1, RhoA, and mitogen-activated protein kinases is required for Ras transformation. *Mol Cell Biol.* 1995 ;15(11):6443-6453.
31. del Peso L, Hernández-Alcoceba R, Embade N, Carnero A, Esteve P, Paje C, Lacal JC. Rho proteins induce metastatic properties in vivo. *Oncogene.* 1997 Dez 18;15(25):3047-57.
32. Vega FM, Ridley AJ. Rho GTPases in cancer cell biology. *FEBS Lett.* 2008 Juni 18;582(14):2093-101.
33. Clark EA, Golub TR, Lander ES, Hynes RO. Genomic analysis of metastasis reveals an essential role for RhoC. *Nature.* 2000 ;406(6795):532-535.
34. Boettner B, Van Aelst L. The role of Rho GTPases in disease development. *Gene.* 2002 März 20;286(2):155-74.
35. Olson MF. Guanine nucleotide exchange factors for the Rho GTPases: a role in human disease? *J Mol Med.* 1996 ;74(10):563-571.
36. Peck J, Douglas G, Wu CH, Burbelo PD. Human RhoGAP domain-containing proteins: structure, function and evolutionary relationships. *FEBS Lett.* 2002 Sep 25;528(1-3):27-34.
37. Gamblin SJ, Smerdon SJ. GTPase-activating proteins and their complexes. *Curr Opin Struct Biol.* 1998 Apr ;8(2):195-201.
38. Moon SY, Zheng Y. Rho GTPase-activating proteins in cell regulation. *Trends Cell Biol.* 2003 Jan ;13(1):13-22.
39. Li R, Zhang B, Zheng Y. Structural determinants required for the interaction between Rho GTPase and the GTPase-activating domain of p190. *J Biol Chem.* 1997 Dez 26;272(52):32830-5.
40. Bernards A, Settleman J. GAP control: regulating the regulators of small GTPases. *Trends Cell Biol.* 2004 ;14(7):377-385.
41. Kozma R, Ahmed S, Best A, Lim L. The GTPase-activating protein n-chimaerin cooperates with Rac1 and Cdc42Hs to induce the formation of lamellipodia and filopodia. *Mol Cell Biol.* 1996 Sep ;16(9):5069-80.
42. Durkin ME, Yuan B, Zhou X, Zimonjic DB, Lowy DR, Thorgeirsson SS, Popescu NC. DLC-1: a Rho GTPase-activating protein and tumour suppressor. *J Cell Mol Med.* 11(5):1185-207.
43. Yuan BZ, Miller MJ, Keck CL, Zimonjic DB, Thorgeirsson SS, Popescu NC. Cloning, characterization, and chromosomal localization of a gene frequently deleted in human liver cancer (DLC-1) homologous to rat RhoGAP. *Cancer Res.* 1998 ;58(10):2196-2199.

Reference list

44. Homma Y, Emori Y. A dual functional signal mediator showing RhoGAP and phospholipase C-delta stimulating activities. *EMBO J.* 1995 Jan 16;14(2):286-91.
45. Plaumann M, Seitz S, Frege R, Estevez-Schwarz L, Scherneck S. Analysis of DLC-1 expression in human breast cancer. *J Cancer Res Clin Oncol.* 2003 ;129(6):349-354.
46. Spatz A, Borg C, Feunteun J. X-chromosome genetics and human cancer. *Nat Rev Cancer.* 2004 Aug ;4(8):617-29.
47. Yuan B, Durkin ME, Popescu NC. Promoter hypermethylation of DLC-1, a candidate tumor suppressor gene, in several common human cancers. *Cancer Genet Cytogenet.* 2003 ;140(2):113-117.
48. Marks P, Rifkind RA, Richon VM, Breslow R, Miller T, Kelly WK. Histone deacetylases and cancer: causes and therapies. *Nat Rev Cancer.* 2001 ;1(3):194-202.
49. Guan M, Zhou X, Soultz N, Spandidos DA, Popescu NC. Aberrant methylation and deacetylation of deleted in liver cancer-1 gene in prostate cancer: potential clinical applications. *Clin Cancer Res.* 2006 ;12(5):1412-1419.
50. Kim TY, Jong H, Song S, Dimtchev A, Jeong S, Lee JW, Kim T, Kim NK, Jung M, Bang Y. Transcriptional silencing of the DLC-1 tumor suppressor gene by epigenetic mechanism in gastric cancer cells. *Oncogene.* 2003 Jun 19;22(25):3943-51.
51. Ponting CP. SAM: a novel motif in yeast sterile and Drosophila polyhomeotic proteins. *Protein Sci.* 1995 ;4(9):1928-1930.
52. Kwan JJ, Donaldson LW. The NMR structure of the murine DLC2 SAM domain reveals a variant fold that is similar to a four-helix bundle. *BMC Struct Biol.* 2007 ;734.
53. Li H, Fung K, Jin D, Chung SSM, Ching Y, Ng IO, Sze K, Ko BCB, Sun H. Solution structures, dynamics, and lipid-binding of the sterile alpha-motif domain of the deleted in liver cancer 2. *Proteins.* 2007 ;67(4):1154-1166.
54. Zhong D, Zhang J, Yang S, Soh UJK, Buschdorf JP, Zhou YT, Yang D, Low BC. The SAM domain of the RhoGAP DLC1 binds EF1A1 to regulate cell migration. *J Cell Sci.* 2009 ;122(Pt 3):414-424.
55. Qiao F, Bowie JU. The many faces of SAM. *Sci STKE.* 2005 ;2005(286):re7.
56. Tompa P. Intrinsically unstructured proteins evolve by repeat expansion. *Bioessays.* 2003 ;25(9):847-855.
57. Scholz R, Regner J, Theil A, Erlmann P, Holeiter G, Jahne R, Schmid S, Hausser A, Olayioye MA. DLC1 interacts with 14-3-3 proteins to inhibit RhoGAP activity and block nucleocytoplasmic shuttling. *J Cell Sci.* 2009 ;122(Pt 1):92-102.
58. Bridges D, Moorhead GBG. 14-3-3 proteins: a number of functions for a numbered protein. *Sci STKE.* 2005 Aug 9;2005(296):re10.

Reference list

59. Dougherty MK, Morrison DK. Unlocking the code of 14-3-3. *J Cell Sci.* 2004 Apr 15;117(Pt 10):1875-84.
60. Li SS. Specificity and versatility of SH3 and other proline-recognition domains: structural basis and implications for cellular signal transduction. *Biochem J.* 2005 ;390(Pt 3):641 EP -.
61. Iyer LM, Koonin EV, Aravind L. Adaptations of the helix-grip fold for ligand binding and catalysis in the START domain superfamily. *Proteins.* 2001 ;43(2):134-144.
62. Ponting CP, Aravind L. START: a lipid-binding domain in StAR, HD-ZIP and signalling proteins. *Trends Biochem Sci.* 1999 ;24(4):130-132.
63. Soccio RE, Breslow JL. StAR-related lipid transfer (START) proteins: mediators of intracellular lipid metabolism. *J Biol Chem.* 2003 Jun 20;278(25):22183-6.
64. Alpy F, Tomasetto C. Give lipids a START: the StAR-related lipid transfer (START) domain in mammals. *J Cell Sci.* 2005 ;118(Pt 13):2791-2801.
65. Hanada K, Kumagai K, Tomishige N, Kawano M. CERT and intracellular trafficking of ceramide. *Biochim Biophys Acta.* 2007 Jun ;1771(6):644-53.
66. Miller WL. Steroidogenic acute regulatory protein (StAR), a novel mitochondrial cholesterol transporter. *Biochim Biophys Acta.* 2007 Jun ;1771(6):663-76.
67. Ng DC, Chan S, Kok KH, Yam JWP, Ching Y, Ng IO, Jin D. Mitochondrial targeting of growth suppressor protein DLC2 through the START domain. *FEBS Lett.* 2006 Jan 9;580(1):191-8.
68. Nagase T, Kikuno R, Hattori A, Kondo Y, Okumura K, Ohara O. Prediction of the coding sequences of unidentified human genes. XIX. The complete sequences of 100 new cDNA clones from brain which code for large proteins in vitro. *DNA Res.* 2000 ;7(6):347-355.
69. Leung TH, Ching Y, Yam JWP, Wong C, Yau T, Jin D, Ng IO. Deleted in liver cancer 2 (DLC2) suppresses cell transformation by means of inhibition of RhoA activity. *Proc Natl Acad Sci U S A.* 2005 Okt 18;102(42):15207-12.
70. Yam JWP, Ko FCF, Chan C, Jin D, Ng IO. Interaction of Deleted in Liver Cancer 1 with Tensin2 in Caveolae and Implications in Tumor Suppression. *Cancer Res.* 2006 Sep 1;66(17):8367-8372.
71. Qian X, Li G, Asmussen HK, Asnaghi L, Vass WC, Braverman R, Yamada KM, Popescu NC, Papageorge AG, Lowy DR. Oncogenic inhibition by a deleted in liver cancer gene requires cooperation between tensin binding and Rho-specific GTPase-activating protein activities. *Proc Natl Acad Sci U S A.* 2007 Mai 22;104(21):9012-7.

Reference list

72. Liao Y, Si L, deVere White RW, Lo SH. The phosphotyrosine-independent interaction of DLC-1 and the SH2 domain of cten regulates focal adhesion localization and growth suppression activity of DLC-1. *J Cell Biol.* 2007 Jan 1;176(1):43-9.
73. Kawai K, Iwamae Y, Yamaga M, Kiyota M, Ishii H, Hirata H, Homma Y, Yagisawa H. Focal adhesion-localization of START-GAP1/DLC1 is essential for cell motility and morphology. *Genes Cells.* 2009 ;14(2):227-241.
74. Kawai K, Kiyota M, Seike J, Deki Y, Yagisawa H. START-GAP3/DLC3 is a GAP for RhoA and Cdc42 and is localized in focal adhesions regulating cell morphology. *Biochem Biophys Res Commun.* 2007 ;364(4):783-789.
75. Kim TY, Lee JW, Kim H, Jong H, Kim T, Jung M, Bang Y. DLC-1, a GTPase-activating protein for Rho, is associated with cell proliferation, morphology, and migration in human hepatocellular carcinoma. *Biochem Biophys Res Commun.* 2007 ;355(1):72-77.
76. Yuan B, Zhou X, Durkin ME, Zimonjic DB, Gumundsdottir K, Eyfjord JE, Thorgeirsson SS, Popescu NC. DLC-1 gene inhibits human breast cancer cell growth and in vivo tumorigenicity. *Oncogene.* 2003 ;22(3):445-450.
77. Wong C, Yam JW, Ching Y, Yau T, Leung TH, Jin D, Ng IO. Rho GTPase-activating protein deleted in liver cancer suppresses cell proliferation and invasion in hepatocellular carcinoma. *Cancer Res.* 2005 ;65(19):8861-8868.
78. Goodison S, Yuan J, Sloan D, Kim R, Li C, Popescu NC, Urquidi V. The RhoGAP Protein DLC-1 Functions as a Metastasis Suppressor in Breast Cancer Cells. *Cancer Res.* . 2005 Juli 15;65(14):6042-6053.
79. Yoshizaki H, Ohba Y, Kurokawa K, Itoh RE, Nakamura T, Mochizuki N, Nagashima K, Matsuda M. Activity of Rho-family GTPases during cell division as visualized with FRET-based probes. *J Cell Biol.* 2003 Juli 21;162(2):223-32.
80. Simpson KJ, Dugan AS, Mercurio AM. Functional analysis of the contribution of RhoA and RhoC GTPases to invasive breast carcinoma. *Cancer Res.* 2004 Dez 1;64(23):8694-701.
81. Yamaguchi H, Lorenz M, Kempiak S, Sarmiento C, Coniglio S, Symons M, Segall J, Eddy R, Miki H, Takenawa T, Condeelis J. Molecular mechanisms of invadopodium formation: the role of the N-WASP-Arp2/3 complex pathway and cofilin. *J. Cell Biol.* 2005 Jan 31;168(3):441-452.
82. Ching Y, Wong C, Chan S, Leung TH, Ng DC, Jin D, Ng IO. Deleted in liver cancer (DLC) 2 encodes a RhoGAP protein with growth suppressor function and is underexpressed in hepatocellular carcinoma. *J Biol Chem.* 2003 März 21;278(12):10824-30.
83. Wong C, Lee JM, Ching Y, Jin D, Ng IO. Genetic and Epigenetic Alterations of DLC-1 Gene in Hepatocellular Carcinoma. *Cancer Res.* 2003 Nov 15;63(22):7646-7651.

Reference list

84. Posern G, Treisman R. Actin' together: serum response factor, its cofactors and the link to signal transduction. *Trends Cell Biol.* 2006 Nov ;16(11):588-96.
85. Wong C, Yam JW, Ching Y, Yau T, Leung TH, Jin D, Ng IO. Rho GTPase-Activating Protein Deleted in Liver Cancer Suppresses Cell Proliferation and Invasion in Hepatocellular Carcinoma. *Cancer Res.* 2005 Okt 1;65(19):8861-8868.
86. Narumiya S, Yasuda S. Rho GTPases in animal cell mitosis. *Curr Opin Cell Biol.* 2006 Apr ;18(2):199-205.
87. Ishizaki T, Morishima Y, Okamoto M, Furuyashiki T, Kato T, Narumiya S. Coordination of microtubules and the actin cytoskeleton by the Rho effector mDia1. *Nat Cell Biol.* 2001 Jan ;3(1):8-14.
88. Watanabe N, Kato T, Fujita A, Ishizaki T, Narumiya S. Cooperation between mDia1 and ROCK in Rho-induced actin reorganization. *Nat Cell Biol.* 1999 Juli ;1(3):136-43.
89. Kimura K, Ito M, Amano M, Chihara K, Fukata Y, Nakafuku M, Yamamori B, Feng J, Nakano T, Okawa K, Iwamatsu A, Kaibuchi K. Regulation of myosin phosphatase by Rho and Rho-associated kinase (Rho-kinase). *Science.* 1996 Juli 12;273(5272):245-8.
90. Kawai K, Kiyota M, Seike J, Deki Y, Yagisawa H. START-GAP3/DLC3 is a GAP for RhoA and Cdc42 and is localized in focal adhesions regulating cell morphology. *Biochem Biophys Res Commun.* 2007 Dez 28;364(4):783-9.
91. Sander EE, ten Klooster JP, van Delft S, van der Kammen RA, Collard JG. Rac Downregulates Rho Activity: Reciprocal Balance between Both GTPases Determines Cellular Morphology and Migratory Behavior. *J. Cell Biol.* 1999 Nov 29;147(5):1009-1022.
92. Bi D, Nishimura J, Niino N, Hirano K, Kanaide H. Contractile properties of the cultured vascular smooth muscle cells: the crucial role played by RhoA in the regulation of contractility. *Circ Res.* 2005 Apr 29;96(8):890-7.
93. Narumiya S, Tanji M, Ishizaki T. Rho signaling, ROCK and mDia1, in transformation, metastasis and invasion. *Cancer Metastasis Rev.* 2009 Juni ;28(1-2):65-76.
94. Xue W, Krasnitz A, Lucito R, Sordella R, Vanaelst L, Cordon-Cardo C, Singer S, Kuehnel F, Wigler M, Powers S, Zender L, Lowe SW. DLC1 is a chromosome 8p tumor suppressor whose loss promotes hepatocellular carcinoma. *Genes Dev.* 2008 ;22(11):1439-1444.
95. Kim TY, Healy KD, Der CJ, Sciaky N, Bang Y, Juliano RL. Effects of Structure of Rho GTPase-activating Protein DLC-1 on Cell Morphology and Migration. *J Biol Chem.* . 2008 Nov 21;283(47):32762–32770.
96. Durkin ME, Avner MR, Huh C, Yuan B, Thorgeirsson SS, Popescu NC. DLC-1, a Rho GTPase-activating protein with tumor suppressor function, is essential for embryonic development. *FEBS Lett.* 2005 Feb 14;579(5):1191-6.

Reference list

97. Wong CC, Wong C, Ko FC, Chan L, Ching Y, Yam JW, Ng IO. Deleted in Liver Cancer 1 (DLC1) Negatively Regulates Rho/ROCK/MLC Pathway in Hepatocellular Carcinoma. *PLoS ONE*. . 2008 ;3(7):e2779.
98. Yuan B, Zhou X, Durkin ME, Zimonjic DB, Gumundsdottir K, Eyfjord JE, Thorgeirsson SS, Popescu NC. DLC-1 gene inhibits human breast cancer cell growth and in vivo tumorigenicity. *Oncogene*. 2003 Jan 23;22(3):445-50.
99. Besson A, Gurian-West M, Schmidt A, Hall A, Roberts JM. p27Kip1 modulates cell migration through the regulation of RhoA activation. *Genes Dev*. 2004 Apr 15;18(8):862-76.
100. Sahai E, Olson MF, Marshall CJ. Cross-talk between Ras and Rho signalling pathways in transformation favours proliferation and increased motility. *EMBO J*. 2001 Feb 15;20(4):755-66.
101. Blumenstein L, Ahmadian MR. Models of the Cooperative Mechanism for Rho Effector Recognition: IMPLICATIONS FOR RHOA-MEDIATED EFFECTOR ACTIVATION. *J. Biol. Chem*. 2004 Dez 17;279(51):53419-53426.
102. Rose R, Weyand M, Lammers M, Ishizaki T, Ahmadian MR, Wittinghofer A. Structural and mechanistic insights into the interaction between Rho and mammalian Dia. *Nature*. 2005 Mai 26;435(7041):513-518.
103. Yamana N, Arakawa Y, Nishino T, Kurokawa K, Tanji M, Itoh RE, Monypenny J, Ishizaki T, Bito H, Nozaki K, Hashimoto N, Matsuda M, Narumiya S. The Rho-mDia1 pathway regulates cell polarity and focal adhesion turnover in migrating cells through mobilizing Apc and c-Src. *Mol Cell Biol*. 2006 Sep ;26(18):6844-58.
104. Goulimari P, Kitzing TM, Knieling H, Brandt DT, Offermanns S, Grosse R. Galpha12/13 is essential for directed cell migration and localized Rho-Dia1 function. *J Biol Chem*. 2005 Dez 23;280(51):42242-51.
105. Ridley AJ, Schwartz MA, Burridge K, Firtel RA, Ginsberg MH, Borisy G, Parsons JT, Horwitz AR. Cell Migration: Integrating Signals from Front to Back. *Science*. 2003 Dez 5;302(5651):1704-1709.
106. Pertz O, Hodgson L, Klemke RL, Hahn KM. Spatiotemporal dynamics of RhoA activity in migrating cells. *Nature*. 2006 Apr 20;440(7087):1069-1072.
107. Kurokawa K, Matsuda M. Localized RhoA Activation as a Requirement for the Induction of Membrane Ruffling. *Mol. Biol. Cell*. 2005 Sep 1;16(9):4294-4303.
108. Healy KD, Hodgson L, Kim T, Shutes A, Maddileti S, Juliano RL, Hahn KM, Harden TK, Bang Y, Der CJ. DLC-1 suppresses non-small cell lung cancer growth and invasion by RhoGAP-dependent and independent mechanisms. *Mol Carcinog*. 2008 Mai ;47(5):326-37.

Reference list

109. Sahai E, Marshall CJ. RHO-GTPases and cancer. *Nat Rev Cancer*. 2002 Feb ;2(2):133-42.
110. Wang W, Wu F, Fang F, Tao Y, Yang L. RhoC is essential for angiogenesis induced by hepatocellular carcinoma cells via regulation of endothelial cell organization. *Cancer Sci*. 2008 Okt ;99(10):2012-8.
111. Gadea G, de Toledo M, Anguille C, Roux P. Loss of p53 promotes RhoA-ROCK-dependent cell migration and invasion in 3D matrices. *J Cell Biol*. 2007 Juli 2;178(1):23-30.
112. Gilmore AP, Burridge K. Regulation of vinculin binding to talin and actin by phosphatidylinositol-4-5-bisphosphate. *Nature*. 1996 Juni 6;381(6582):531-5.
113. Nagaraja GM, Kandpal RP. Chromosome 13q12 encoded Rho GTPase activating protein suppresses growth of breast carcinoma cells, and yeast two-hybrid screen shows its interaction with several proteins. *Biochem Biophys Res Commun*. 2004 Jan 16;313(3):654-65.
114. Danesh FR, Kanwar YS. Modulatory effects of HMG-CoA reductase inhibitors in diabetic microangiopathy. *FASEB J*. 2004 Mai ;18(7):805-15.
115. Hatch GM, Gu Y, Xu FY, Cizeau J, Neumann S, Park J, Loewen S, Mowat MRA. StARD13(Dlc-2) RhoGap mediates ceramide activation of phosphatidylglycerolphosphate synthase and drug response in Chinese hamster ovary cells. *Mol Biol Cell*. 2008 März ;19(3):1083-92.
116. Kawai K, Seike J, Iino T, Kiyota M, Iwamae Y, Nishitani H, Yagisawa H. START-GAP2/DLC2 is localized in focal adhesions via its N-terminal region. *Biochem Biophys Res Commun*. 2009 März 20;380(4):736-41.
117. Yuan BZ, Miller MJ, Keck CL, Zimonjic DB, Thorgeirsson SS, Popescu NC. Cloning, characterization, and chromosomal localization of a gene frequently deleted in human liver cancer (DLC-1) homologous to rat RhoGAP. *Cancer Res*. 1998 Mai 15;58(10):2196-9.
118. Ng IO, Liang ZD, Cao L, Lee TK. DLC-1 is deleted in primary hepatocellular carcinoma and exerts inhibitory effects on the proliferation of hepatoma cell lines with deleted DLC-1. *Cancer Res*. 2000 Dez 1;60(23):6581-4.
119. Jackson AL, Bartz SR, Schelter J, Kobayashi SV, Burchard J, Mao M, Li B, Cavet G, Linsley PS. Expression profiling reveals off-target gene regulation by RNAi. *Nat Biotech*. 2003 Juni ;21(6):635-637.
120. Jackson AL, Burchard J, Schelter J, Chau BN, Cleary M, Lim L, Linsley PS. Widespread siRNA "off-target" transcript silencing mediated by seed region sequence complementarity. *RNA*. . 2006 Juli ;12(7):1179–1187.

6 Acknowledgements

First of all, I would like to thank Prof. Klaus Pfizenmaier for giving me the opportunity to realize this thesis within the Institute of Cell Biology and Immunology at the University of Stuttgart.

I wish to express my special gratitude to Dr. Monilola Olayioye for offering me such a manifold and interesting project, her excellent supervision and for all her efforts regarding this thesis.

I would also like to thank all lab members in M. Olayioye's group, especially Johanna Heering, Patrik Erlmann, Ruth Jähne, Simone Schmid, and Rolf Scholz for all their thoughts and help in the lab.

I am also thankful to all the other staff and students for the cheerful and supportive atmosphere at the IZI.

Most importantly, I would like to give the biggest thanks to my beloved Micha and my dear family for all their support and care over the years.

I hereby assure that I performed this work independently without further help or other materials than stated.

Gerlinde Holeiter

Stuttgart, 15th of April 2009

Lebenslauf

Name Gerlinde Holeiter

Anschrift Allmandstraße 41
70569 Stuttgart

Geburtsdatum 19.02.1980

Geburtsort Sathmar (Rumänien)

Promotion **Promotion** am Institut für Zellbiologie und Immunologie,
Universität Stuttgart

The Role of the Deleted in Liver Cancer Protein Family in Breast Epithelial Cell Transformation

Hochschulstudium Studium der **Technischen Biologie** an der **Universität Stuttgart**

Diplomarbeit
Institut für Zellbiologie und Immunologie

Charakterisierung der Rezeptorchimäre TNFR1-TM2-Fas und TNFR2-TM1-Fas in stabil exprimierenden Hela-Zellen und Mausfibroblasten sowie die Analyse zur rezeptorvermittelten Signaltransduktion

Studienarbeit
Biologisches Institut,
Abteilung für Molekularbiologie und Pflanzenvirologie

Laufverhalten des geminiviralen Zell-zu-Zell-Transportproteins BC1 in SDS-Gelen und in neu etablierten Essigsäure-Harnstoff-Gelen

Ausbildung 09/1996 bis 06/1999 Naturwissenschaftlich-Technisches
Gymnasium, Kerschensteinerschule, Stuttgart-Feuerbach

Ausbildung zur staatlich geprüften **Chemisch-technischen Assistentin**

Schulausbildung **Gymnasium**

09/1996 bis 06/1999 Naturwissenschaftlich-Technisches
Gymnasium, Kerschensteinerschule in Stuttgart-Feuerbach

Realschule

09/1990 bis 02/1992 Realschule Sindelfingen - Hinterweil

03/1992 bis 07/1996 Realschule Ostfildern - Nellingen

Grundschule

09/1986 bis 02/1988 Grundschule Lembergschule Nagold

03/1988 bis 07/1990 Grundschule Sindelfingen - Hinterweil

Tätigkeiten neben dem Studium

Wissenschaftliche Hilfskraft:

- am Biologischen Institut, Universität Stuttgart
Abteilung für Molekularbiologie und Pflanzenvirologie
- am Institut für Zellbiologie und Immunologie, Universität Stuttgart

Praktische Erfahrungen

- Ausbildung zur staatlich geprüften **Chemisch-technischen Assistentin**
- **Praktikum in Umweltmesstechnik** am Forschungszentrum Karlsruhe

Publikationen

Holeiter G, Heering J, Erlmann P, Schmid S, Jähne R, Olayioye MA. ***Deleted in liver cancer 1 controls cell migration through a Dia1-dependent signaling pathway.*** Cancer Res. 2008 Nov 1;68(21):8743-51.

Scholz RP, Regner J, Theil A, Erlmann P, Holeiter G, Jähne R, Schmid S, Hausser A, Olayioye MA. ***DLC1 interacts with 14-3-3 proteins to inhibit RhoGAP activity and block nucleocytoplasmic shuttling.*** J Cell Sci. 2009 Jan 1;122: 92-102. Epub 2008 Dec 9.

Kleinow T, Holeiter G, Nischang M, Stein M, Karayavuz M, Wege C, Jeske H. ***Post-translational modifications of Abutilon mosaic virus movement protein (BC1) in fission yeast.*** Virus Res. 2008 Jan; 131(1): 86-94. Epub 2007 Oct 4.